UNIVERSITÉ DE SHERBROOKE

Faculté de génie

Département de génie électrique et de génie informatique

ONDULEUR QUASI-Z-SOURCE POUR UN SYSTÈME DE TRACTION DE VÉHICULES ÉLECTRIQUES À SOURCES MULTIPLES : CONTRÔLE ET GESTION

QUASI-Z-SOURCE INVERTER FOR MULTIPLE SOURCES ELECTRIC VEHICLE TRACTION SYSTEM : CONTROL AND MANAGEMENT

Thèse de doctorat

Spécialité : génie électrique

Mande Daouda

Sherbrooke (Québec) Canada

MEMBRES DU JURY

M. João Pedro F. TROVÃO, Directeur

Université de Sherbrooke (UdeS), QC, Canada

M. Minh C. TA, Codirecteur

Université de Sherbrooke (UdeS), QC, Canada

M. Ahmed KHOUMSI

Université de Sherbrooke (UdeS), QC, Canada

M. Thanh VO-DUY

Université des Sciences et Technologies de Hanoï (HUST), Vietnam

M. Sousso KELOUWANI

Université du Québec à Trois-Rivières (UQTR), QC, Canada

Acknowledgements

I would like to express my deep gratitude to my supervisor Professor João Pedro Fernandes Trovão who gave me the golden opportunity to do this wonderful project. I thank him very much for his constructive suggestions and helpful criticism throughout the duration of the project. His enthusiastic concern for the research progress kept pushing me closer and closer to my objective. His kind advice and positive thoughts have always motivated me to pursue my work more seriously.

Similarly, I would like to express my sincere gratitude to my codirector, Professor Minh Cao Ta. I thank him for his guidance in the realization of this project. His pertinent advice, his availability and his encouragement were invaluable support for me.

I would also like to express my deep gratitude to Canadian Francophonie Scholarship Program for their financial support during this study.

I would also sincerely appreciate the help from Professor Ruben Gonzalez Rubio and Professor Maude Josée Blondin.

I wish to express my sincere appreciation to the jury members, Professor Maxime Darnon, Professor Ahmed Khoumsi, Professor Thanh Vo-Duy, and Professor M. Sousso Kelouwani for their encouragement, invaluable comments, and questions.

Appreciations are also dedicated to e-TESC lab members, Chi Thi Phuong Nguyen, Thang Van Do and Pascal Messier for their kindly help on the management of the laboratory utilities and technical supports.

I am extremely grateful to my family members and my friends for their supports and encouragement. I really appreciate them for the help they have given me during these years of my studies.

Last but not least, I would like to thank my wife Guémilatou Zagré, my son Nadir, and my daughter Kenza for their unconditional love and continuous patience throughout my studies.

Résumé

L'électronique de puissance joue un rôle fondamental et contribue à atteindre les nouveaux objectifs de l'automobile en termes d'économie d'énergie et d'environnement. Les convertisseurs d’électroniques de puissance sont considérés comme les éléments clés qui interfacent leurs sources d'alimentation avec la chaîne de traction du véhicule électrique (VE). Ils contribuent à obtenir une efficacité et des performances élevées dans les systèmes électriques. Cependant, les onduleurs traditionnels tels que les onduleurs à source de tension, les onduleurs à source de courant et les onduleurs conventionnels à deux étages qui constituent les onduleurs les plus couramment utilisés, présentent certaines limitations conceptuelles. Par conséquent, de nombreux efforts de recherche se sont concentrés sur le développement de nouveaux convertisseurs d’électroniques de puissance adaptés à l'application aux véhicules électriques.

Afin de développer et d'améliorer les performances des VEs à sources multiples commerciales, cette thèse vise à sélectionner, contrôler l'onduleur à source impédante et fournit une approche de gestion pour l'application du système de traction du VE à sources multiples. Une revue concise des principales topologies existantes d'onduleur à source impédante a été présentée. Cela a permis de sélectionner la topologie de l’onduleur quasi-Z-source (QZS) comme architectures prometteuses pouvant être utilisées dans les véhicules électriques, avec de meilleures performances et de fiabilité. L'étude comparative entre l'onduleur bidirectionnel conventionnel à deux étages et de celui à QZS pour les applications du VE a été présentée. En outre, une étude comparative entre différentes topologies de groupes motopropulseurs concernant les facteurs d'indice de vieillissement des batteries pour une application du VE hors route a été explorée. Ces études ont permis de prouver que la topologie de l’onduleur QZS représente une bonne topologie candidate à utiliser dans un système de VE à sources multiples.

Pour améliorer les performances de l’onduleur QZS appliquées aux véhicules électriques, des contrôleurs PI d'ordre fractionnaire (PIOF) optimisés pour l’onduleur QZS sont conçus avec l'algorithme de colonies de fourmis afin d'obtenir des valeurs d'indice de performance de vieillissement plus appropriées pour la batterie. De plus, cette thèse propose un système de stockage d'énergie hybride

(SSEH) pour le VE afin de permettre une utilisation efficace de l'énergie de la batterie pour une couverture de distance plus longue et une extension de son autonomie. L'optimisation du contrôleur PIOF et du contrôleur par modèle prédictif d'ensemble de contrôle fini (CMP-ECF) pour l'onduleur QZS bidirectionnel a été appliqué au VE à sources multiples avec des approches de gestion appuyées par des règles. Le contrôleur d'affaiblissement de flux magnétique du moteur a été conçu pour fournir un fonctionnement correct avec le couple maximal disponible à n'importe quelle vitesse dans les limites de courant et de tension.

Des investigations et des simulations sont effectuées pour vérifier les différentes topologies étudiées et l'efficacité de la structure de contrôleur proposée avec l'onduleur QZS bidirectionnel. De plus, une simulation en temps réel basée sur Opal-RT a été mise en œuvre pour valider l'efficacité de la stratégie de contrôle SSEH proposée. Les résultats confirment l'amélioration des performances du VE avec l'ajout d'un supercondensateur utilisant la configuration du contrôle proposée, permettant une utilisation efficace de l'énergie de la batterie avec une réduction de la valeur moyenne quadratique, de la valeur moyenne et de l'écart type de 57%, 59% et 27%, respectivement, du courant de la batterie par rapport à l'onduleur connecté directement à la batterie.

Mots clés : Véhicule électrique, onduleur à quasi-Z-source, contrôle boost constant maximum, facteurs d'indice de vieillissement, contrôleur PI d'ordre fractionnaire, contrôleur par modèle prédictif d'ensemble de contrôle fini, système de stockage d'énergie hybride, batterie, supercondensateur, simulation en temps réel.

Abstract

Power electronics play a fundamental role and help to achieve the new goals of the automobiles in terms of energy economy and environment. The power electronic converters are the key elements which interface their power sources to the drivetrain of the electric vehicle (EV). They contribute to obtaining high efficiency and performance in power systems. However, traditional inverters such as voltage-source, current-source inverters and conventional two-stage inverters present some conceptual limitations. Consequently, many research efforts have been focused on developing new power electronic converters suitable for EVs application.

In order to develop and enhance the performance of commercial multiple sources EV, this dissertation aims to select and to control the impedance source inverter and to provide management approaches for multiple sources EV traction system. A concise review of the main existing topologies of impedance source inverters has been presented. That enables to select QZSI (quasi-Z-source inverter) topology as promising architectures with better performance and reliability. The comparative study between the bidirectional conventional two-stage inverter and QZSI for EV applications has been presented. Furthermore, comparative study between different powertrain topologies regarding batteries aging index factors for an off-road EV has been explored. These studies permit to prove that QZSI topology represents a good candidate to be used in multi-source EV system.

For improving the performance of QZSI applied to EVs, optimized fractional order PI (FOPI) controllers for QZSI is designed with the ant colony optimization algorithm (ACO-NM) to obtain more suitable aging performance index values for the battery. Moreover, this thesis proposes a hybrid energy storage system (HESS) for EVs to allow an efficient energy use of the battery for a longer distance coverage. Optimized FOPI controller and the finite control set model predictive controller (FCS-MPC) for HESS using bidirectional QZSI is applied for the multi-source EV. The flux-weakening controller has been designed to provide a correct operation with the maximum available torque at any speed within current and voltage limits.

Simulation investigations are performed to verify the topologies studied and the efficacity of the proposed controller structure with the bidirectional QZSI. Furthermore, Opal-RT-based real-time simulation has been implemented to validate the effectiveness of the proposed HESS control strategy. The results confirm the EV performance enhancement with the addition of supercapacitors using the proposed control configuration, allowing the efficient use of battery energy with the reduction of root-mean-square value, the mean value, and the standard deviation by 57%, 59%, and 27%, respectively, of battery current compared to the battery-only based inverter.

Keywords: Electric vehicle, quasi-Z-source inverter, maximum constant boost control, aging index factors, fractional order PI controller, finite control set model predictive controller, hybrid energy storage system, battery, supercapacitor, real-time simulation.

Table of Contents

List of Figures

List of Tables

Nomenclature/Symbols

Abbreviations

ACO-NM	Ant colony optimization algorithm combined to a constrained Nelder-Mead method
BAT	Battery
Bq-ZSI	Bidirectional quasi-Z-source inverter
CMP-ECF	Contrôleur prédictif du modèle d'ensemble de contrôle fini
DGS	Distributed generation systems
EQZSI	Embedded quasi-Z-source inverter
ESS	Energy storage system
EV	Electric vehicle
FCS-MPC	Finite control set model predictive controller
FOC	Field oriented control
FOPI	Fractional order proportional integral
FW	Flux-weakening
GA	Genetic algorithms
HEV	Hybrid electric vehicle
HESS	Hybrid energy storage system
IRHA	Iterative reduction-based heuristic algorithm
LiFeMgPO4	Lithium-iron magnesium phosphate
LPF	Low-pass filter
MCBC	Maximum constant boost control
MPC	Model predictive control
PI	Proportional-integral
PID	Proportional-integral-derivative
PSO	Particle swarm optimization
PWM	Pulse width modulation
QZSI	Quasi-Z-source inverter
QZS	Quasi-Z-source
RHP	Right-half-plane

RMS	Root-mean-square
SBC	Simple boost control method
SC	Supercapacitor
SPMSM	Surface permanent magnet synchronous motor
SPWM	Sinusoidal pulse width modulation
UPS	Uninterruptible power supply
THD	Total harmonic distortion
ZN	Ziegler-Nichols
ZSN	Z-source network
ZSI	Z-source inverter

Symbols

AC	Alternative current
B	Boost factor
C	Capacitor
C_1	Capacitor 1
C_2	Capacitor 2
$C_{batcell}$	Cell capacity
C_{sc}	Rated capacitance
$c_x A$	Aerodynamic standard
D	Shoot-through duty ratio
DC	Direct current
e_{cur}	Motor current error
e_{mot}	Motor speed error
f	Coefficient of viscous friction
f_{lim}	Hard constraint function
f_{LPF}	Cut-off frequency of low-pass filter
f_s	Switching frequency
g_1	Cost function 1
g_2	Cost function 2

G_e	Total voltage gain
G_{tr}	Motor to wheel transmission ratio
i_{abc}	Three-phase stator currents
i_{aref}	Phase a stator reference current
I_{batref}	Battery reference current
i_{bref}	Phase b stator reference current
i_{cref}	Phase c stator reference current
i_d	d-axis current
i_{dref}	Reference d-axis current
i_{load}	Load current
i_{L_1}	Inductor 1 current
i_{L_2}	Inductor 2 current
Δi_{L1}	Value of inductor current ripple
i_q	q-axis current
i_{qref}	Reference q-axis current
i_{max}	Maximal current
$I_{sc_{ref}}$	Supercapacitor reference current
I_{sc}	Supercapacitor current
J	Rotor inertia
k_{conv}	Coefficient depending on the power direction
k_p	Proportional gain
k_i	Integral gain
k_d	Derivative gain
k_{roll}	Rolling coefficient
L	Phase inductance of SPMSM
L_1	Inductor 1
L_2	Inductor 2
lb	lower bound
ub	upper bound

m_e	Inverter modulation index
$m_{S_8S_9}$	Modulation index of DC-DC converter
M_{veh}	Total mass of the EV
$n_{batcellse}$	Number of cells in series
$n_{batcellpa}$	Number of branches in parallel
$n_{sccellse}$	Number of capacitors in series
$n_{sccellpa}$	Number of capacitors in parallel
P_{in}	Input power
P_{out}	Output power
p	Number of pole pair
P_r	Rated power
$r_{batcell}$	Cell equivalent serial resistance
r_s	Phase resistance (of motor)
r_{sc}	Internal resistance of supercapacitor
R_{wh}	Wheel radius
S_7	Switches 7
S_8	Switches 8
S_9	Switches 9
T	Switching cycle
T_0	Interval of the shoot-through state
T_1	Interval of the non-shoot-through state
T_e	Developed motor torque
T_{sim}	Model simulation time
v_a	Sinusoidal waveform A for PWM
v_b	Sinusoidal waveform B for PWM
v_c	Sinusoidal waveform C for PWM
v_{bat}	Battery voltage
$v_{batcellnom}$	Cell nominal voltage
$v_{batcellmin}$	Cell minimum voltage

v_d	Voltage on the d-axis
v_{dref}	Reference voltage on the d-axis
$\hat{v}_{dc}$	DC link peak voltage
v_{c_1}	Capacitor 1 voltage
v_{c_2}	Capacitor 2 voltage
v_{in}, v_1	Input voltage
V_L	Voltage across the inductor
v_{max}	Voltage limit
v_n	Constant voltage envelope n
$\hat{v}_o$	Peak phase voltage
v_p	Constant voltage envelope p
Δv_{c1}	Value of capacitor voltage ripple
v_q	Phase voltage on the q-axis
v_{qref}	Phase voltage reference on the q-axis
v_{sc}	Supercapacitor voltage
v_{scnom}	Nominal supercapacitor voltage

Greek symbols

$\boldsymbol{\psi_f}$	Magnet flux linkage
$\boldsymbol{\Omega}$	Rotor angular speed
Ω_{base}	Base speed
ρ	Air density (at 20^{O} C)
η_{tran}	Efficiency of the transmission
λ	Weighting factor
τ_{LPF}	Time constant of low-pass filter
μ	Mean value
σ	Standard deviation
c_v	Variation coefficient
Γ_{ch}	Load torque

η	Efficiency
γ	Current ripple

Chapter 1 Introduction

1.1 Background and Context

Human emissions of greenhouse gases are a primary driver of global warming, extreme weather changes, earth pollutions, and present one of the world's most pressing challenges. Global fossil CO_2 emissions in 2021 increased by approximately 4.9% to 36.4 billion metric tons compared to 2020, pushing global emissions close to 2019 levels (36.7 Gt CO_2) according to the latest report [1]. One of the major challenges of today's global society is to reduce the negative impacts that the transport sector has on the environment regarding greenhouse gas emissions. This sector is responsible for about 24% of total CO_2 global emissions in 2019 as shown in Figure 1.1 [2]. The sale of EV has been grown rapidly over the past ten years. The global sale of EV exceeded 7.2 million in 2019, an increase of 29% over the previous years [3].

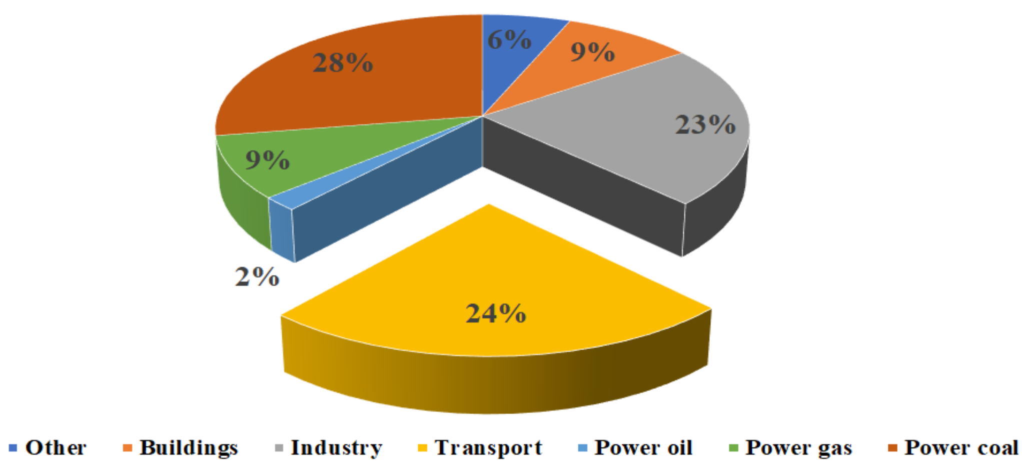

Figure 1.1: Global energy-related CO_2 emissions by sector [2].

Oil represents the primary motorized transportation fuel used in most countries. Oil high demand in the global transportation sector contributes to drive up oil prices. With the increasing of oil prices and the global warming, automobile manufacturers are producing more electric vehicles (EVs). The production of EVs becomes progressively more essential not only because they decrease greenhouse gas emission but also, they are able to decrease the dependence on oil, as the power is generated from other sources than oil [4, 5, 6].

Consequently, EVs have become the scientific research project in many countries around the world in the twenty-first century. In an EV, an electric motor, a power electronic converter and an electronic controller constitute the core of the traction system. The use of voltage source, current source inverter and conventional two-stage inverter increases not only the complexity of circuitry and control but also the cost and the space requirement. Recently, Z-source inverters have been examined and investigated by number of researchers as alternative power electronic converters with better performance in terms of efficiency, power density and manufacturability. Various modifications have been carried out by researchers with advantages as well as drawbacks for a lot of applications. One of the key challenges for electric traction system is the power electronic converter which is the vital element interfacing its power source and the drivetrain. One of the most interesting benefits of a power electronic converter is to provide a high efficiency in wide power range. It represents a principal component for improving the energy efficiency and performance of various applications. In the case of EVs, it also includes systems that provide improved safety, for example solid-state lighting and electronic stability systems.

This thesis proposes the multi-source quasi-Z-source inverter (QZSI) with enhanced performance to be applied to electric traction system. Multi-source QZSI architecture is considered a promising technology because it has several advantages. The continuous input current reduces the voltage and current stress on the switches, and the two input sources increase the flexibility of the system. Additionally, it retains the advantages of ZSI with high efficiency, such as improved power quality, increased voltage gain, enhancement of load-adaptive capability and a flexible input voltage range. Power electronic converters are needed for the processing, control, and conversion of electrical energy in electric vehicles. They are fundamental elements of EV that can contribute to achieve fuel economy, reduction of CO_2 emissions and dependence on oil. They require innovations in topologies, design of components and control. Multi-source QZSI uses magnetic windings and capacitors. There is a complexity of the design, components selection and real-time implementation of the proposed system. Furthermore, the multi-source QZSI needs suitable control techniques to enhance its performance. That adds additional challenge in the implementation of the overall control system. Therefore, the design of multi-source QZSI, the system control and the management approach for multi-source are the focus of attention of this thesis. There are many requirements imposed on electrical energy sources in order to ensure high efficiency and good motion properties for electric vehicles such as high power and energy density, long cycle-life, reliability, wide temperature range and no emission of pollutants. To address this issue the thesis purposes to use the multi-source QZSI to enhance electric vehicle traction system performance.

This thesis is completed at the electric – Transport, Energy Storage and Conversion Laboratory (e-TESC Lab.), University of Sherbrooke, Quebec, Canada. It is part of the Canada Research Chair in Efficient Electric Vehicles with Hybridized Energy Storage Systems aiming at improving the efficiency and performance of the components of EVs and Hybrid EVs (HEVs). The chair has four research axes focused on energy management, design and control of electrical machines, design, control and development of power electronic converters for EV applications and energy storage systems. This thesis is under the power electronics axis focused on development of power electronic converters and performance enhancement of QZSI for EV applications and supported in part by Grant 950-230672 from Canada Research Chairs Program, in part by Grant RGPIN-2017-05924 from the Natural Sciences and Engineering Research Council of Canada, in part by FCT-Portuguese Foundation for Science and Technology project UIDB/00308/2020, and in part by Canadian Francophonie Scholarship Program. A schematic summary is provided in Figure 1.2.

1.2 General overview of the study system

1.2.1 Electric traction systems

EV is characterised by an electric energy conversion chain upstream of the drive train [7] consisting of an electricity storage system (battery, fuel cell, etc.), power converter, and an electric motor with its control system. The schematic for illustrating electric traction systems is shown in Figure 1.3. During the propulsion mode, the voltage from the battery is converted by the bidirectional converter and the inverter into 3-phase voltage to drive the motor and produce the required torque. During the regenerative braking mode, power converter behaves as a rectifier to charge the storage systems. The motion of EV depends on the motor torque applied to overcome the motor resistant torque. In our study surface permanent magnet synchronous motor (SPMSM) is used as electric motor. The motor affords the rotational speed and torque to the mechanical load to set the EV system in motion. The mechanical load is composed of the road characteristics, the wheels, the vehicle components, and passengers' masses. The EV control system is carried out with control algorithms. It is used to control the fundamental variables of an EV such as rotational speed, torque, currents, and voltages. Ones of the key blocks inside EVs are the power converters used for motor and auxiliary power supply of electric loads. The power converter can handle the energy transfer from the DC bus of the power converter and the high voltage DC bus used for the electric traction. The power converter enables the energy transfer between the high voltage side and low voltage side giving many advantages in terms of cost, flexibility, and efficiency.

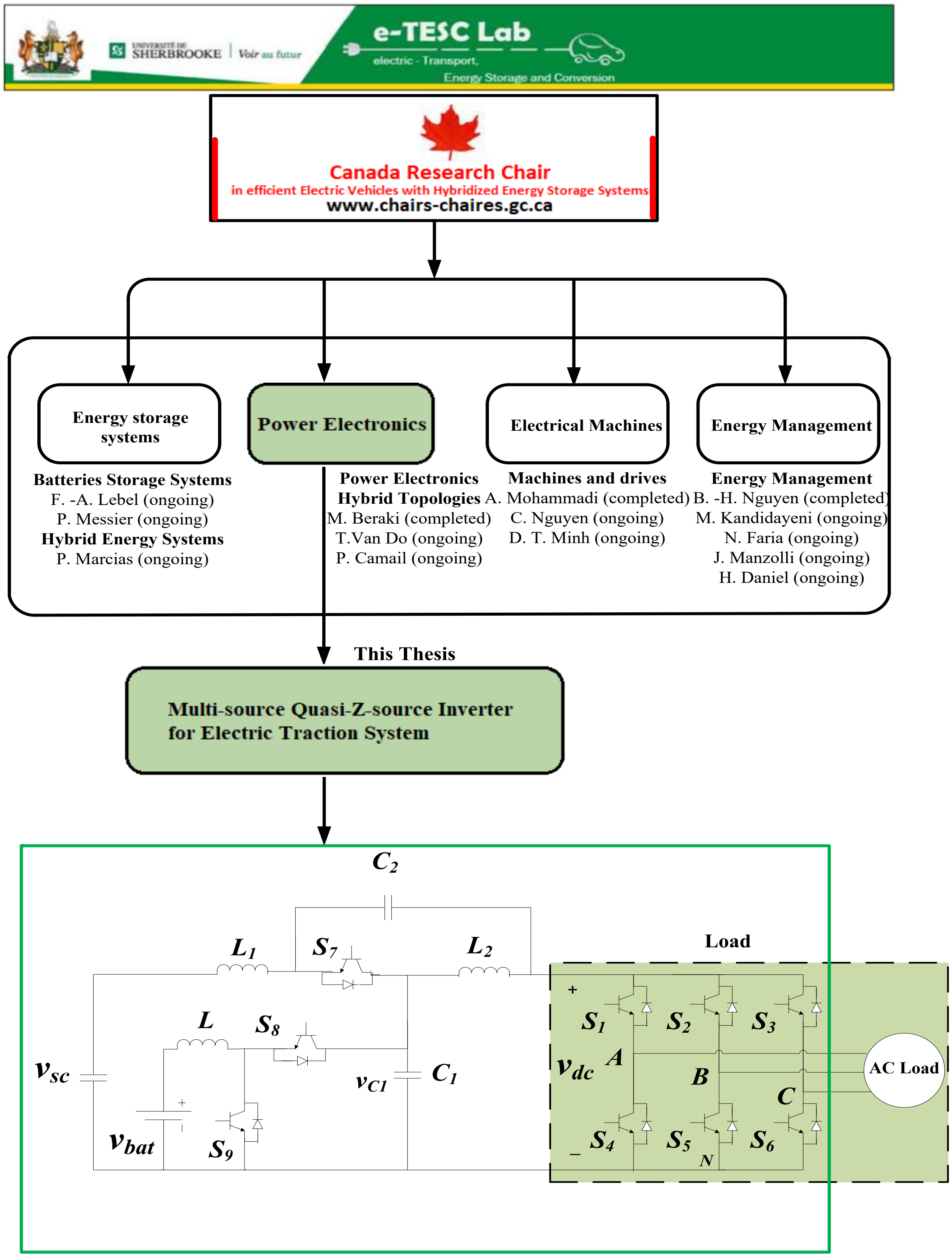

Figure 1.2: Position of the thesis within Canada Research Chair program in e-TESC lab.

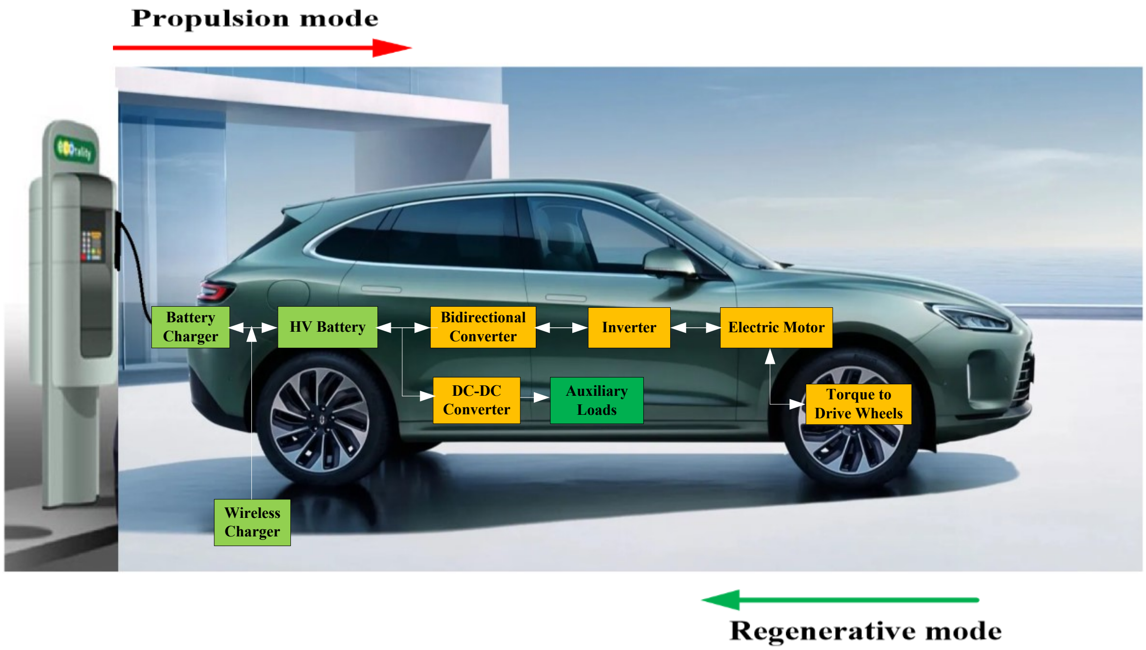

Figure 1.3: Electric traction systems.

As such, this thesis aims to design, to control the power converter to enhance the performance of multi-source EV.

In order to improve the environmental performance of EVs, many countries and organisations have produced their driving cycle. Then, there are certification driving cycles such as NEDC, FTP75, JC08 driving cycles which is used respectively in Europe, in United States and in Japan. A driving cycle commonly represents a set of vehicle speed points versus time. It is used to assess fuel consumption and pollutant emissions of a vehicle in a normalized way. In the PhD research project, Artemis drive cycles and NEDC drive cycles have been used in the simulations to validate the different impedance source inverter and motor models.

1.2.2 Multi-source quasi-Z-source inverter

As mentioned in section 1.1, the ZSI is a new topology appeared in the scientific literature through the work of Professor Fang Zheng Peng in the article of conference published in 2003 [8]. This topology is characterized by the existence of impedance network formed by the inductors and capacitors between the source of input and the inverter stage. ZSI has a unique characteristic of buck-boost capability which permits it to have wide range of voltage. The ZSI has the particularity of being able to use inverter switches to raise the DC bus voltage. The converter equipped with an impedance network of LC type arranged in "X", allows the simultaneous closure of up and down switches of the same inverter arm to perform its function of raising the DC bus voltage v_{dc}. The concept of Z-source can be used for all power conversions. The Figure 1.4 shows the topology of bidirectional ZSI feeding SPMSM.

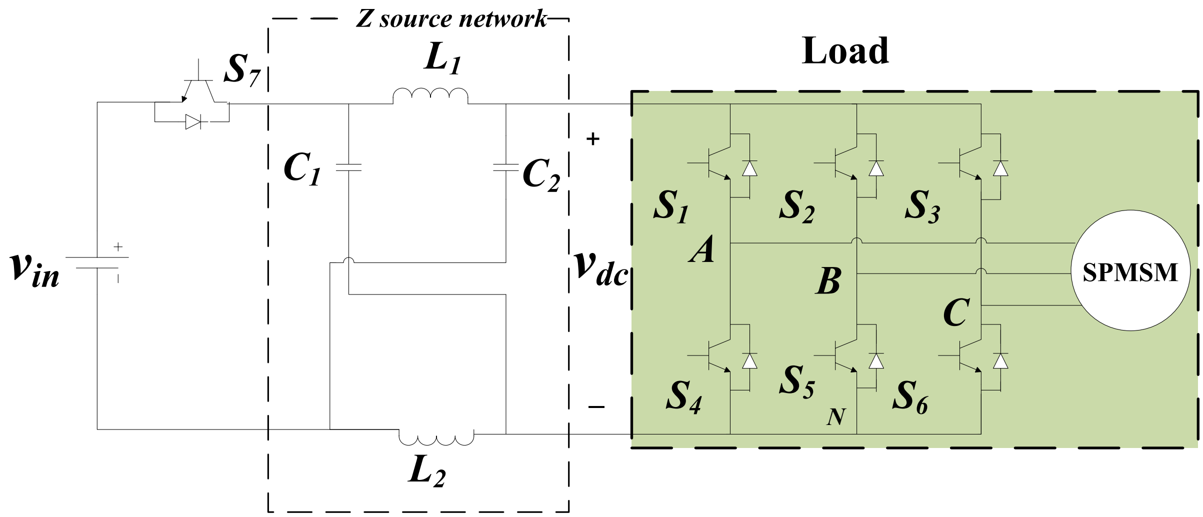

Figure 1.4: Bidirectional Z-source inverter.

ZSI have different configurations. By rearranging the components in the Z-source network, a new topology named multi-source quasi-Z-source inverter (QZSI) can be obtained. Quasi-Z-source is the first modification of the Z-source network that overcomes the drawbacks of the Z-source network. The Z-source network in a ZSI can produce a discontinuous input source current, which can lead to increased stress on the system components. Additionally, the Z-source network may not be able to completely suppress the inrush current, which can result in increased stress on the switches and other components. Furthermore, the high voltage capacitors required for the Z-source network can increase the cost and volume of the system. These factors should be considered when deciding whether to use a ZSI or another type of inverter architecture. Multi-source QZSI is a promising architecture as it presents the advantage of having a continuous input current, two inputs source voltage and retain all the merits of the ZSI, which makes it a good candidate for multi-source EV applications. EVs designed with the multi-source QZSI can provide better performances thanks to the ability to boost voltage, and to smoothly handle bidirectional power flows during motoring and braking operations. The configuration of multi-source QZSI connected with a SPMSM is shown in Figure 1.5. Various control strategies can be used for impedance source network. In the literature, many small-signal analysis and mathematical models have been presented for the study of the dynamic behavior of the system. It is possible to implement different closed loop control strategies with different complexities using these models depending on applications [9]. Traditional PWM schemes can be used to control impedance source inverter switches and their theoretical input-output relationship still holds. The most common switching control strategies which can be used for impedance source network are the simple boost method [10], maximum boost method [11], maximum constant boost method [12] and space vector method [13]. Some of these control strategies can be compared in terms of the voltage gain [14].

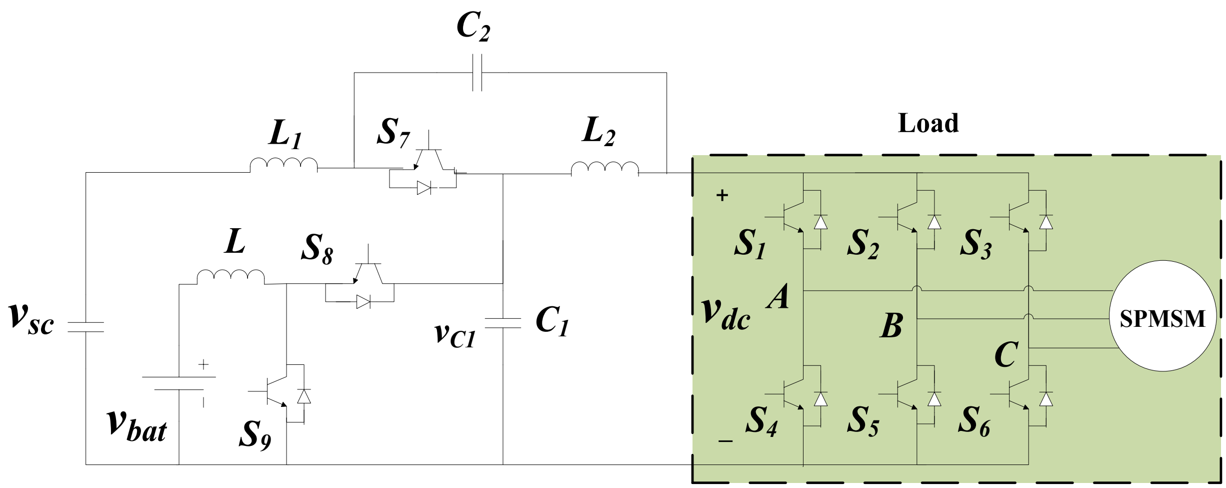

Figure 1.5: The multi-source bidirectional QZSI.

In the literature, several modified PWM control techniques for impedance source inverters have been also proposed. The objective of these techniques is to achieve simple implementation, wide range of modulation, less commutation per switching cycle and low device stress.

This thesis is focused on the multi-source QZSI application for multiple sources electric vehicle traction system, control and management of the system shown in Figure 1.6. The complete configuration of this proposed hybrid energy storage system (HESS) is based on the quasi-Z-source network consisting of capacitors C_1, C_2, inductors L_1, L_2 and the DC-DC converter. This DC-DC converter comprises inductor L, switches S_8, S_9 where C_1 represents its output capacitor. The DC-DC converter is used to control the absorbing and the releasing of the battery power. The supercapacitor and the battery are the power sources in this HESS. The switch S_7 and S_8 contribute to a bidirectional power flow between energy storage devices and motor. From the SPMSM side, the feedback signals are the rotor speed and the three-phase stator currents i_{abc}. The 3-phase stator currents of the SPMSM are measured and converted into i_d and i_q currents. The actual rotating speed is compared with the reference speed and the FOPI controller allows to obtain the reference current i_{qref}. The flux-weakening (FW) method is applied to provide correct operation with the maximum available torque at any speed within current and voltage limits V_{max}. This method is achieved by considering the maximal allowable motor phase voltage and phase current. The FW strategy permits to obtain negative current reference i_{dref}. While from the multi-source QZSI side, the inductor current i_{L1} and the capacitor voltage v_{c1} represents the main measurements. The DC link measured voltage compared with the reference voltage, and the voltage controller allows to obtain the inductor reference current i_{L1ref}.

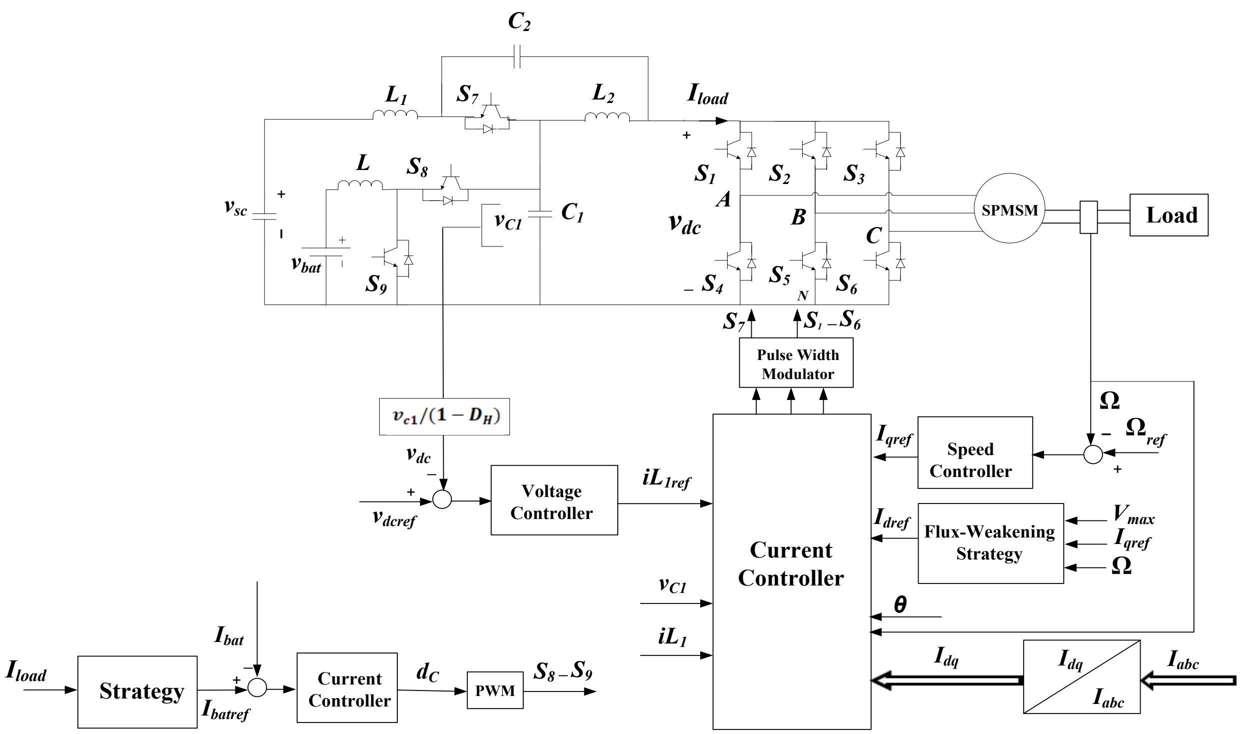

Figure 1.6: Schematic Diagram of the Study System.

The optimal switching state is selected and applied to the QZSI and the SPMSM. Voltage and current controller are used to regulate the DC-link voltage and the inductor current of the DC-DC converter. The switch S_7 of QZSI operates to allow a bidirectional power flow. It is controlled using pulse width modulation technique (PWM) technique to have signal that is complementary with the shoot-through signal of the inverter. In the proposed HESS control, management strategy is used for determining the battery reference current I_{batref} .

1.3 Scope and Objectives

The principal objective of this thesis consists of enhancing the overall performance of multi-source electric vehicle traction system by using multi-source QZSI to interface its power source to the drivetrain of the multi-source EV. It includes the selection of impedance source inverter, the technique of control and the management approaches for EV application. Impedance source inverter is a power electronic circuit which convert DC input voltage to a symmetrical AC output voltage of desired magnitude and frequency using a unique impedance network to couple the main circuit of the converter to the power source. In order to determine the suitable impedance source inverter for EV, comparison of bidirectional QZSI and bidirectional conventional two-stage-inverter for electric traction system has been studied. This study enables to prove and choose QZSI as an attractive alternative power converter for EV applications. It is a buck-boost inverter with unique feature that traditional voltage-source and current-source inverters cannot provide. It can be applied in applications where the input voltage changes widely. The cost of QZSI is reduced and efficiency is increased. Other comparative study between different power train topologies regarding batteries aging index factors for an off-road EV permits to select the QZSI as a good candidate for multi-source EV system. Furthermore, the QZSI performance depends on the selection of the parameters of quasi-Z-source network elements. To determine the appropriate values of these parameters, the critical values of the inductances and the capacitances are used to design the QZSI. The technique of control used QZSI can globally enhance the performance of the EV by optimizing the electric power consumption and extending its driving range. To this end, in this thesis, the optimization of FOPI controller and the finite control set model predictive controller (FCS-MPC) for bidirectional QZSI have been applied for the EV with management approaches. Management approaches consist of methods to control the power flows through the HESS to improve the efficient use of battery energy for longer distance coverage. An ant colony optimization algorithm combined with a constrained Nelder-Mead method (ACO-NM) is used for the optimization of the controller parameters. FOPI controller designed with the ACO-NM algorithm provides more suitable aging performance indexes values for the battery of the EV. FCS-MPC is an optimal control technique and provides easy handling of constrains and fast dynamic performance.

In order to do that, the key sub-objectives of this thesis are illustrated below:

- To examine and select the suitable impedance source inverter for multi-source electric traction system.
- To prove QZSI is an alternative power converter taking into consideration the lifetime of the battery used for multi-source EV.
- To provide an optimization method to enhance the performance of the controllers used for QZSI in EV.
- To study QZSI management approaches for an efficient energy use of the battery for multi-source EV.
- To perform real-time simulation to validate the effectiveness of the proposed hybrid energy storage system control strategy.

1.4 Originality and Contributions

The QZSI represents an emerging topology of impedance source converter with interesting properties such as buck-boost characteristics and single stage conversion. It is suitable for improving the performance, efficiency, and power density of power converters for multi-source EV applications. The application of the performant impedance source converter for EV with optimized controller and its management approaches for multi-source constitute the originality of this thesis. The main contributions are represented in six published papers generated by this thesis as follows:

1. <u>Comparison of Bidirectional Quasi-Z-Source and Bidirectional Conventional Two-Stage-Inverter for Electric Traction System</u> (IEEE VPPC 2018)

   The comparative study in this paper has served to prove QZSI as an attractive alternative power converter for EV applications.
2. <u>Comparison of Different Power Train Topologies for an Off-Road Electric Vehicle</u> (IEEE VPPC 2019).

   This paper details and proves QZSI topology as an alternative inverter taking into consideration the lifetime of the battery used for multi-source off-road EV traction purpose.
3. <u>Comprehensive Review on Main Topologies of Impedance Source Inverter Used in Electric Vehicle Applications</u> (WEVJ MDPI 2020)

   This paper has permitted to select the QZSI topology for multi-source EVs application.

4. Optimization of Fractional Order PI Controller for Bidirectional Quasi-Z-Source Inverter Used for Electric Traction System (IET ESET WILEY 2020)

   This paper provides optimization method used to enhance the performance of FOPI control for bidirectional QZSI in an electric traction system.
5. Multi-source Bidirectional Quasi-Z-source Inverter using Fractional Order PI Controller for Electric Traction System (IEEE VPPC 2021).

   In this paper, QZSI management approaches and application for multi-source EV has been investigated using FOPI controller.
6. Dual-source Bidirectional Quasi-Z-source Inverter Development for Off-Road Electric Vehicle (WEVJ MDPI 2022)

   This paper performs real-time simulation to validate the QZSI for multi-source off-road EV with management approaches using FOPI controller and finite control set model predictive controller.

1.5 Outline of the thesis

This thesis presents the multi-source bidirectional QZSI with its study, control, and management approach for electric vehicle traction system application. It is organized into eight chapters.

Chapter 1 provides a general introduction, overview of the study system, the objectives, originality, and main contributions of the thesis.

Chapter 2 provides the comprehensive review on main topologies of impedance source inverter used in EV Applications. The concise review of the main existing topologies of impedance source inverters allows to select the QZSI topology among the various impedance source inverters as the promising architecture which can be used in EVs, with better performance and better reliability. The use of this new topology will open the door to several axis of development with appreciable impacts on EVs.

Chapter 3 presents the comparison of bidirectional quasi-Z-source and bidirectional conventional two-stage-inverter for electric traction system. This comparison contributes to prove and choose the QZSI selected in chapter 2 as an attractive alternative power converter for EV application. This topology superiority compared to the conventional two stage inverter has been shown.

The fourth chapter provides the comparison of different powertrain topologies for an off-road EV. This comparative study between different power train topologies regarding batteries aging index factors for an off-road EV application has permitted to retain the QZSI topology selected in previous chapter as a good candidate for multi-source EV system.

Chapter 5 presents an optimization of fractional order PI controller for bidirectional QZSI used for electric traction system. After the selection of the QZSI in the previous chapter, optimization method is used in this chapter to enhance the performance of FOPI control for bidirectional QZSI in an electric traction system. QZSI needs suitable control techniques for its performance enhancement. This optimized method contributes to obtain more suitable aging performance index values for the battery.

Chapter 6 provides a multi-source bidirectional quasi-Z-source inverter using fractional order PI controller for electric traction system. FOPI controller designed in chapter 5 for bidirectional QZSI has been applied for the multi-source EV with management approaches. The control configuration using FOPI controller for bidirectional QZSI helps to improve the multi-source EV system performance, allowing an efficient energy use of the battery for a longer distance coverage, and thus extending EV driving range.

Chapter 7 presents dual-source bidirectional quasi-Z-source inverter (Bq-ZSI) development for off-road electric vehicles. A hybrid energy storage system (HESS) topology control scheme using the FCS-MPC and the FOPI has been investigated to achieve the dynamic response that is required for energy storage devices. It is then implemented for the multi-source EV with management approaches. Opal-RT-based real-time simulation has been performed to validate the performance and the effectiveness of the proposed HESS control strategy. The control enhancement of the dual-source Bq-ZSI allows to improve efficacy and dynamic performance for multi-source EV.

Finally, the conclusions, future work, and research to be conducted are summarized in the last chapter. The main conclusions of this thesis have been presented and research works which can be explored in the future and to enhance the proposed HESS performance have been offered. The scientific contributions of this thesis have been also highlighted.

Chapter 2 Comprehensive Review on Main Topologies of Impedance Source Inverter Used in EV Applications

Original Title: Comprehensive Review on Main Topologies of Impedance Source Inverter Used in EV Applications

Authors and affiliation :

- **Daouda Mande**: Ph.D. student, e-TESC Laboratory, Department of Electrical & Computer Engineering, University of Sherbrooke
- **João P. Trovão**: Professor, e-TESC Laboratory, Department of Electrical & Computer Engineering, University of Sherbrooke
- **Minh C. Ta**: Professor, e-TESC Laboratory, Department of Electrical & Computer Engineering, University of Sherbrooke

Date of Acceptance: **21 April 2020**

State of acceptance: Published

Reference: World Electric Vehicle Journal, DOI:10.3390/wevj11020037

Summary

<u>Content</u>: Power electronics play an increasingly important role for electric transportation, renewable energy conversion and many other industrial applications. They have the ability to help achieving high efficiency and performance in power systems. This article reviews the state of art of impedance source inverter main topologies and points out their applications for multi-source EVs. A concise review of main existing topologies is presented. The basic structural differences, advantages and limitations of each topology has been illustrated. Many impedances source inverter has been compared in order to choose a best, efficient and convenient inverter topology for multi-source EV.

<u>Results</u>: From this state of art review of impedance source inverters, the QZSI topology presents one of the promising architectures which can be used in multi-source EVs, with better performance and reliability.

<u>Contribution to this thesis</u>: This article provides the state of art of impedance source inverter main topologies and points out their applications for multi-source EVs. It enables to select the QZSI topology for multi-source EVs application. The utilization of this new topology will open the door to several development axes with great impact to EVs.

Abstract

Power electronics play a fundamental role for electric transportation, renewable energy conversion and many other industrial applications. They have the ability to help achieving high efficiency and performance in power systems. But traditional inverters such as voltage source and current source inverters present some limitations. Consequently, many research efforts have been focused on developing new power electronics converters suitable for many applications. Compared with the conventional two-stage inverter, Z-source Inverter (ZSI) is a single stage converter with lower design cost and high efficiency. It is a power electronics circuit of which the function is to convert DC input voltage to a symmetrical AC output voltage of desired magnitude and frequency. Recently, ZSIs have been widely used as replacement of conventional two-stage inverters in the distributed generation systems. Several modifications have been carried out on ZSI to improve its performance and efficiency. This paper reviews the state of art of impedance source inverter main topologies and points out their applications for multi-source electric vehicles. A concise review of the main existing topologies will be presented. The basic structural differences, advantages and limitations of each topology will be illustrated. From this state of art review of impedance source inverters, the embedded quasi-Z-source inverter presents one of the promising architectures which can be used in multi-source electric vehicles, with better performance and reliability. The utilization of this new topology will open the door to several development axes with great impact to EVs.

Keywords: Impedance source inverter; Z-source inverter; quasi-Z-source; embedded Z-source inverter; embedded quasi-Z-source inverter; trans-Z-source inverter; Γ-Z-source inverter; LCCT Z-source inverter; electric vehicle.

2.1 Introduction

The strong energy demand in our society results from increased consumption and population growth [15]. This energy demand leads to a scarcity of fossil fuels and ecological problems. The automotive sector is at the heart of these concerns, and it invokes the research and development of technologies associated to electric vehicles (EVs). In EVs, inverters represent very important elements, which convert DC voltage into AC voltage to feed the electric motors. The traditional inverters are divided in two categories: voltage source and current source inverters. It is known that voltage source inverters suffer from shoot-through problems, and limited output voltage gains while current source converters have open-circuit problems and limited output current gains [16]. With the objective of solving these problems, a Z-Source inverter (ZSI) was first proposed by Peng, by coupling an LC impedance network with the DC source to form a novel source [17]. This topology, commonly called Z-source, is a sort of impedance source [18]. Impedance source inverters have been considered as a good candidate for EV applications, especially because of the ability of increasing the inverter output range (between 0 and ∞). The ZSI can improve the stability and safety of a motor drive system under complex conditions [19]. It overcomes voltage sags without any additional circuits, minimizes the motor ratings to deliver required power, enhances the power factor, reduces harmonic current [19].

Moreover, it is possible to have different configurations of Z-source inverters with addition of non-linear elements such as diodes or switches into the impedance network to improve the performance of the circuit. The concept of Z-source can be used for all power conversions. After the apparition of ZSI, various impedance source inverters have been proposed for different specified applications. Current-fed quasi-Z-source inverter with high efficiency has been developed using reverse-blocking IGBT for hybrid EV application [20]. It has been also used for photovoltaic (PV) cell [21]. In PV generation plants with the conversion of the AC voltage into DC voltage, ZSIs are the best choice. It is possible to boost the required voltage and decrease the overall size of converter systems. ZSI along with LC output filter is used to reduce the voltage harmonics of an uninterruptible power supply (UPS) system caused by non-linear and unbalanced load. In an ordinary UPS, transformers or DC-DC converters are utilized to step up the voltage [22]. ZSIs have been also used for grid applications in distributed generation systems (DGS). Normally, DGSs do not give all their maximum output due to the inaccessibility of sources. That makes the inverters remaining idle and producing harmonics in output voltage [23]. To overcome this problem, DG framework in light of ZSI is proposed [24]. Offshore wind farms are usually distant from demand centers. ZSIs used for wind farms enable them to obtain high DC link which further advances the quality of transmission [25]. The main impedance source inverter topologies based on the typical Z-source inverters such as quasi-Z-source inverters, embedded-Z-source inverters, trans-Z-source inverters have been widely applied in wind energy systems [26], motor drives [27], vehicle systems [28] and solar energy systems [29]. Other alternative impedance source inverters have been proposed such as embedded quasi-Z-source inverters, Y-source inverters [30], Γ-Z-source inverters [31] and LCCT-Z-source inverters [32].

Many control strategies have been used for impedance source network. In the literature, a lot of small-signal analyses and mathematical models are presented for the study of the dynamic behavior of the system. Using these models, it is possible to implement different closed loop control strategies with different complexities depending on applications [9]. Traditional PWM schemes can be used to control impedance source inverter switches and their theoretical input-output relationship still holds. The most common switching control strategies are the simple boost method [10], maximum boost method [11], maximum constant boost method [12] and space vector method [13]. Some of these control strategies can be compared in terms of the voltage gain [14]. Several modified PWM control techniques for impedance source inverters have been also proposed in the literature. The objective of these techniques is to obtain simple implementation, wide range of modulation, less commutation per switching cycle and low device stress.

This paper provides a comprehensive start of the art review of impedance source inverter main topologies and multi-source EV applications. Section 2.1 introduces the impedance source inverters. In Section 2.2, the main impedance source inverter topologies are presented. Section 2.3 presents the ZSIs for EV applications, from single to multi-source feeding systems, including a specific example, and future trends. Conclusion is drawn in Section 2.4.

2.2 Impedance Source Inverters

2.2.1 Z-source Inverter

As mentioned in introduction, the ZSI is a topology that appeared in the scientific literature through the work of F. Z. Peng in the article published in 2003 [17]. This topology is characterized by the existence of impedance network formed by the inductors and capacitors between the source of input and the inverter stage. The ZSI has the particular ability to use inverter switches to raise the DC bus voltage. The converter equipped with an impedance network of LC type arranged in "X", allows the simultaneous closure of up and down switches of the same inverter arm to perform its function of raising the voltage, v_{dc}. Figure 2.1 shows the topology of bidirectional ZSI feeding AC load. ZSI has a unique characteristic of buck-boost capability which permits it to have wide voltage range. Then, ZSI offers novel power conversion concept. Simultaneous triggering of both switches from the same leg of ZSI does not cause any failure because the inductor of current fed ZSI can sustain high current. However, ZSI is not suitable for very low input DC voltages [33]. It cannot suppress the inrush current and also produces discontinuous input source current [34]. There are also different grounds for source and inverter circuits [35]. High-voltage capacitors are required which leads to increase the cost and volume of the system [34]. In recent years, many Z-source single-phase inverters have been proposed [26 - 32].

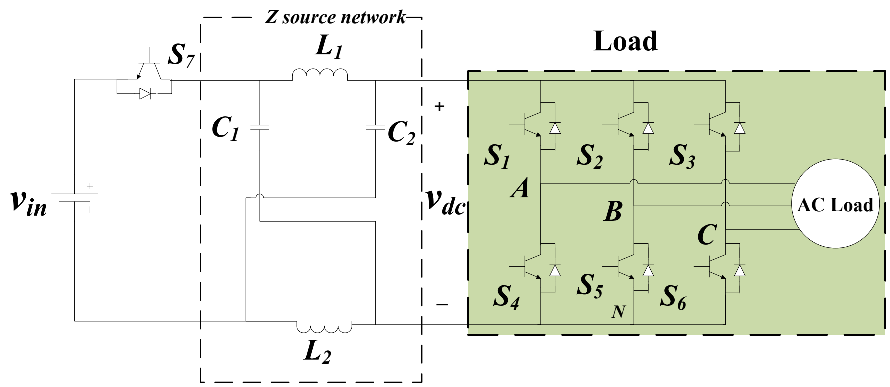

Figure 2.1: Bidirectional Z-source inverter main topology.

2.2.2 Quasi-Z-source Inverter

By rearranging the components in the Z-source network, a new topology called quasi-Z-source inverter (QZSI) has been proposed by Anderson and Peng in 2008 [36]. It is inspired by the typical ZSI and it is mainly applied in motor systems, new energy systems, and micro-grid systems. Quasi-Z-source is the first modification of the Z-source network which overcomes the drawbacks of Z-source network. Quasi-source inverter has a lot of advantages such as reducing the switching stress of the switches and the passive component ratings which enhance the efficiency and reliability of the inverter. According to the operational modes in voltage-type or current-type and continuous or discontinuous current, quasi-Z-source inverters can be classified into four categories. We can have the voltage-fed quasi-Z-source inverters with continuous input current, voltage-fed quasi-Z-source inverters with discontinuous input current, current-fed quasi-Z-source inverters with continuous input current, and current-fed quasi-Z-source inverters with discontinuous input current [35]. Different kinds of QZSI feeding AC load are shown in Figure 2.2. The QZSI topology shown in Figure 2.2 (a) presents the advantage of having a continuous input current and retains all the merits of the ZSI, which makes it a good candidate for EV applications, renewable energy generation and many other power conversion applications [37].

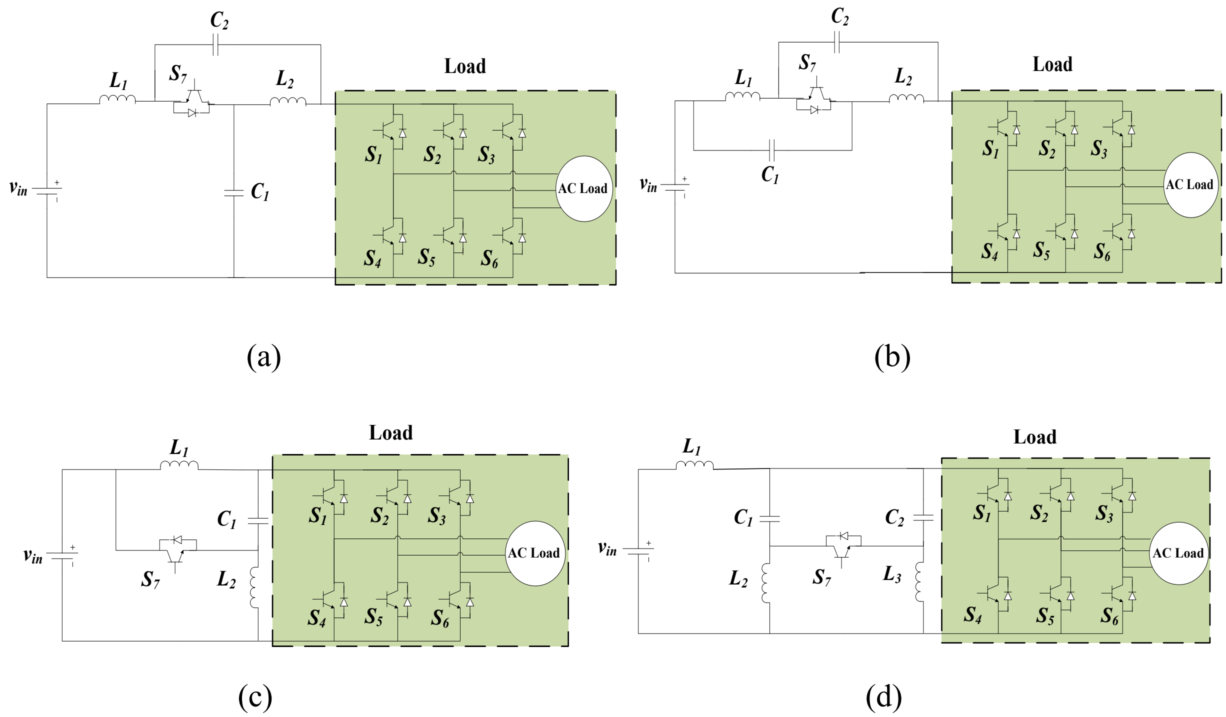

Figure 2.2: Bidirectional quasi-Z-source inverter topologies: Voltage-fed one with continuous current (a) Voltage-fed one with discontinuous current (b) Current-fed one with continuous current (c) Current-fed one with discontinuous current (d).

2.2.3. Embedded Z-Source Inverter

The embedded Z-source inverter was proposed to achieve smaller volume and higher robustness [38]. This impedance source inverter uses the concept of embedding the input DC sources within the LC impedance network. For the situation where implicit source filtering is critical, the embedded Z-source inverter represents one of the important alternatives. The embedded-Z-source inverter produces continuous input current. It also maintains the features of typical Z-source inverters and enables to produce smaller ripples of input voltage and current. It is able to draw smooth current from source without adding another component. The main inconvenient of the embedded Z-source inverter constitutes the stress distribution among the components provided by its asymmetrical structure.

Figure 2.3 shows the typical topology of a two-level-embedded ZSI. Its multi-source feature is suitable for PV power generation [38] and battery storage systems.

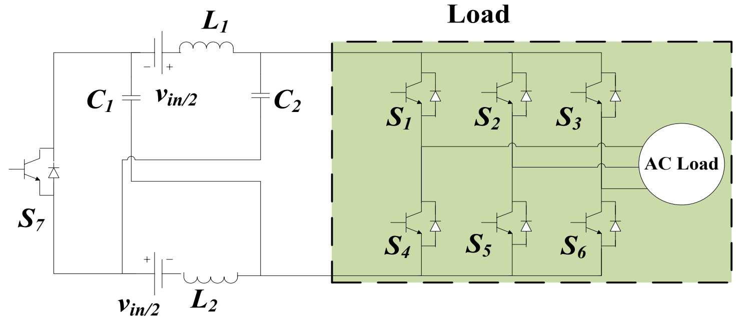

Figure 2.3: Bidirectional embedded Z-source inverter topology.

2.2.4 Embedded Quasi-Z-Source Inverter

The embedded quasi-Z-source inverter (EQZSI) maintains the features of typical quasi-Z-source inverter and also enables to produce smaller ripples of input voltage and continuous current [39, 40]. It is able to draw smooth current from source without adding other components. Figure 2.4 shows typical topology of an EQZSI. In this configuration, an additional DC source is embedded in the DC link of the classical QZSI. The concept of embedding the DC source permits to inherit the advantages of both QZSI and embedded topologies. The EQZSI topology enables operating well with one or two sources without altering the voltage gain of QZSI topology. Its operating principle can be described in two states such as the non-shoot-through state and the shoot-through one like quasi-Z-source network. It can be suitable for battery storage systems and multi-source power conversion systems. Other similar embedded topologies with one or two DC sources also exist.

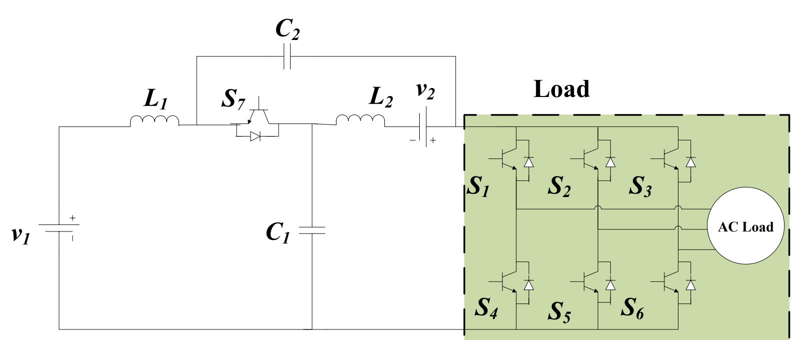

Figure 2.4: Bidirectional embedded quasi-Z-source inverter topology.

2.2.5 Trans-Z-Source Inverter

In theory, Z-source, quasi-Z-source, embedded Z-source and embedded quasi-Z-source all have unlimited voltage gain. But in practice, a high voltage gain can be imposed a high voltage stress on the switches. To overcome the aforementioned problem, Trans-Z-source (two voltage-fed and two current-fed) inverters were proposed to have higher voltage gains and to keep voltage stress low with Z-source network reduced to one transformer (or one coupled inductor) and one capacitor [41]. Trans-Z-source inverters not only maintain the main features of traditional Z-source inverters, but also exhibit some unique advantages by increasing voltage gains and reducing voltage stress. It is also able to operate at very low input voltage. Trans-Z-source network has the operation and working principle similar to Z-source network and also eliminates the shoot-through barriers. However, transformers and coupled inductors which are used in its design increase volume and cost. Figure 2.5 shows the typical topology of Trans-Z-source inverter. This topology is very suitable for renewable energy generation [42].

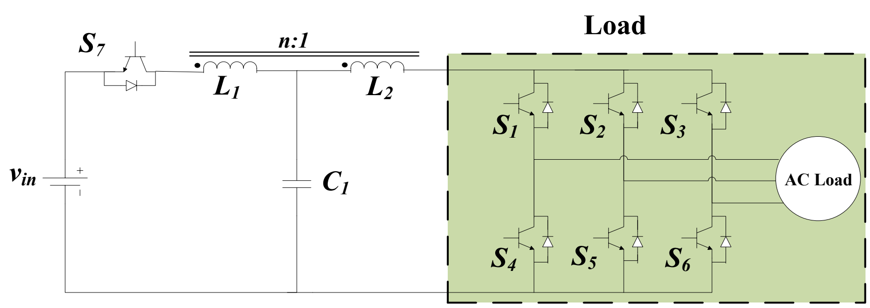

Figure 2.5: Bidirectional Trans-Z-source inverter topology.

2.2.6 Y-Source Inverter

Y-source inverter is designed based on the Trans-Z-source inverter. The performance of the Y-source network inverter is close to that of the Trans-Z-source inverter. Y-source inverter topology was proposed in [30] using coupled inductors with three windings transformer (N1, N2, N3). It has one more degree of freedom such as the three windings and shoot-through duty cycle of switches. This degree of freedom permits to choose the boost voltage comparatively to a classical impedance network design with boost converter. It reduces the total harmonic distortion (THD) of the inverter and realizes a higher voltage gain with small shoot through duty cycle. The higher voltage boost and higher modulation index can be obtained at the same time with Y-source inverter. Y-source impedance network also has the operation and working principle similar to Z-source network. However, its leakage inductances of the coupled inductor due to discontinuous input current can produce the voltage overshoots [43]. With the diverse properties and the specifics future of Y-source network, many researchers and engineers continue to examine and modify the topology for the wide range of power conversion applications. Figure 2.6 shows the Y-source inverter main topology.

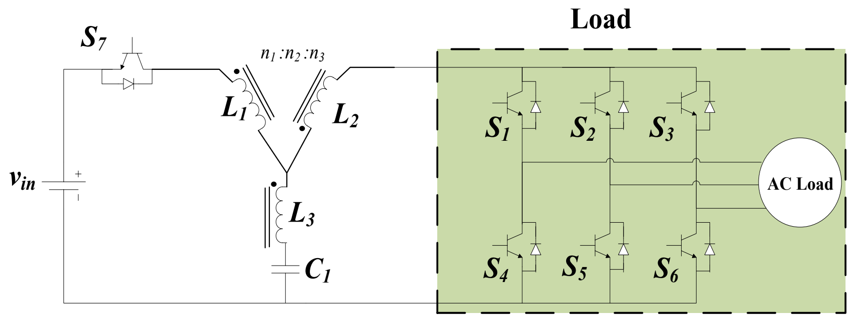

Figure 2.6: Bidirectional Y-source inverter topology.

2.2.7 Γ-Z-source Inverter

Γ-Z-source inverter is also derived from Trans-Z-source inverter [44]. Two Γ-shaped inductors are coupled in Trans-Z-source inverter to form Γ-Z-source inverter which permits to increase the gain and modulation ratio, simultaneously [44]. Γ-Z-source network gain is increased by decreasing the turn ratio. Figure 2.7 shows the Γ-Z-source inverter topology.

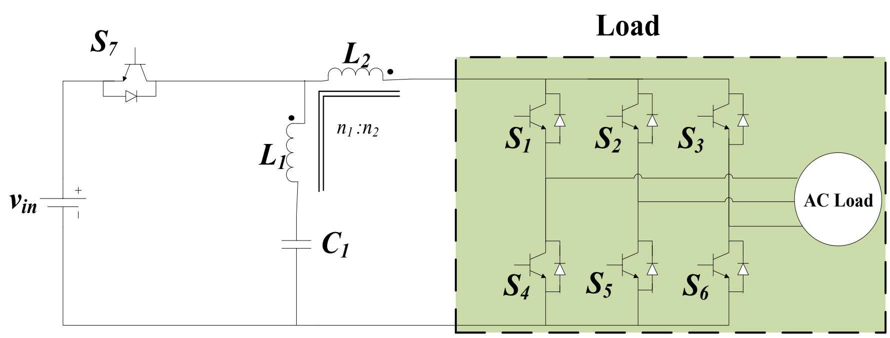

Figure 2.7: Bidirectional Γ-source inverter topology.

Unlike other impedance source inverter whose gains increase with an increased turns ratio such as Trans-Z-source and LCCT Z-source, e.g., Γ -Z-source inverter uses fewer components and a coupled transformer to achieve a high voltage gain by lowering the turn ratio. It represents the impedance source inverter which provides a better spectral performance. The drawback of this topology constitutes the presence of the leakage inductance that can affect the voltage and current stress on semiconductors. This topology is more convenient for renewable energy generation.

2.2.8 LCCT-Z-source Inverter

As shown in Figure 2.8, LCCT-Z-source inverter is extended from the Trans-Z-source. LCCT Z-source network is an inductor-capacitor-capacitor-transformer Z-source network [19]. It can also be represented as an integration of high frequency transformer with quasi-Z-source inverter. This topology produces continuous current even during light load and filters out high-frequency ripples from source current. It is able to achieve higher voltage gain and modulation index [32]. The unique feature of LCCT Z-source network is that its network helps to prevent the transformer core from saturation due to two capacitors which blocks the source current [45] and during the boost operation, only one inductive element is used to store the energy. LCCT-Z-source inverter is appropriate for renewable energy generation and power conversion applications.

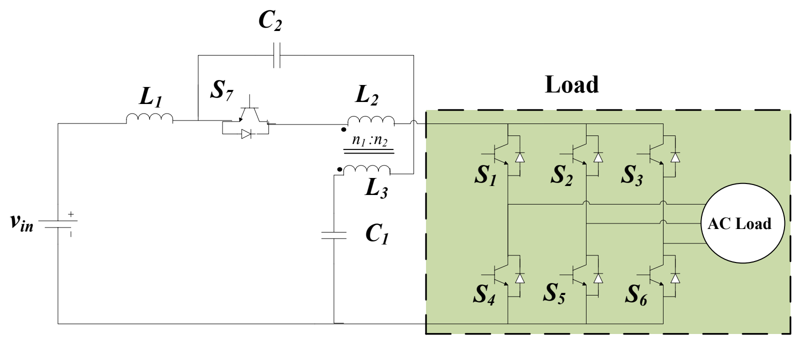

Figure 2.8: Bidirectional LCCT-Z-source inverter topology.

2.2.9 Advantages and disadvantages of the main impedance source network topologies

The main impedance source network topologies exhibit several advantages and disadvantages. Table 2.1 shows the summary of the impedance source network topologies. Table 2.2 shows the main impedance source network topologies advantages and disadvantages. Their applications with the typical used power are also shown in Table 2.3. From the study of these various main impedance source inverters, we can see that the EQZSI is a promising architecture for multi-source EV. It presents the advantage of having a continuous input current and retaining all the merits of both QZSI and embedded topologies.

Table 2.1: Summary of the impedance source network topologies

Impedance Network	Figure number	Boost Factor B	Switching Devices	Number of Capacitors	Number of Inductors	Voltage Stress on the Switching Device
Z-Source	2.1	$\frac{1}{1-2D}$ where, $0 \leq D \leq 0.5$	1	2	2	$\frac{1}{1-2D}v_{in}$
Quasi-Z-Source	2.2 (a)	$\frac{1}{1-2D}$ where, $0 \leq D \leq 0.5$	1	2	2	$\frac{1}{1-2D}v_{in}$
Embedded Z-Source	2.3	$\frac{1}{1-2D}$ where, $0 \leq D \leq 0.5$	1	2	2	$\frac{1}{1-2D}v_{in}$
Embedded Quasi-Z-Source	2.4	$\frac{1}{1-2D}$ where, $0 \leq D \leq 0.5$	1	2	2	$\frac{1}{1-2D}(v_1+v_2)$
Trans Z-Source	2.5	$\frac{1}{1-(n+1)D}$ where, $0 \leq D \leq (n+1)^{-1}$ $n \in \mathbb{N}$	1	1	Integrated two windings	$\frac{n}{1-(n+1)D}v_{in}$
Y-Source	2.6	$\frac{1}{1-KD}$ where, $K \geq 2$ *and* $0 \leq D \leq \frac{1}{K}$	1	1	Integrated three windings	$\frac{K-1}{1-KD}v_{in}$
Γ-Z-source	2.7	$\frac{1}{1-[1+(n-1)^{-1}]D}$ where, $0 \leq D \leq [1+(n-1)^{-1}]^{-1}$ $1 < n < 2$ $n \in \mathbb{N}^*$	1	2	One inductor and one 2 windings coupled inductor	$\frac{1}{(n-1)[1-(1+(n-1)^{-1})D]}v_{in}$
LCCT-Z-source	2.8	$\frac{1}{1-(n+1)D}$ where, $0 \leq D \leq (n+1)^{-1}$ $n \in \mathbb{N}$	1	2	2	$\frac{n}{1-(n+1)D}v_{in}$

Table 2.2: Summary of the impedance source network topologies advantages and disadvantages

Impedance network	Advantages	Disadvantages
Z-Source	- Overcomes the disadvantages of voltage source and current source inverters. - Offer novel power conversion concept. - Both switches from the same leg trigger at the same time don't cause any failure. - Inductor of current fed ZSI sustains high current. - Benefits to motor drives and renewable energy generation applications.	- Discontinuous input current. - Not suitable for very low input DC voltages [33]. - Cannot suppress the inrush current. - Different grounds for source and inverter circuits [34]. - High voltage capacitors which are required increase the cost and volume of the system. - The shoot through duty ratio always be less than 0.5.
Quasi-Z-Source	- Continuous input current. - Reduces passive component ratings. - Provides lower current stress on inductors compared to ZSI. - Shares common ground with input DC supply [26]. - Benefits to motor drives and renewable energy generation applications.	- The shoot through duty ratio always be less than 0.5. - Not suitable for very low input DC voltage.
Embedded Z-Source	- Draws smooth current from source without additional component. - Produce smaller ripples of input voltage and current. - Suitable for battery storage systems and PV power generation.	- Different stress distribution among components, provided by its asymmetrical structure. - Supplied current is no longer maintained. - The shoot through duty ratio always be less than 0.5.
Embedded Quasi-Z-Source	- Continuous input current. - Draws smooth current from source without additional component. - Appropriate for battery storage systems and multi-source power conversion systems.	-The shoot through duty ratio always be less than 0.5. - Not suitable for very low input DC voltages.
Trans-Z-Source	- Increases voltage gain more than the case of Z-Source and quasi-Z-Source network. - Reduces component stress. - Able to operate on very low input voltage. - Suitable for renewable energy generation.	- High gain is obtained with high winding turns ratio. - Discontinuous input current. - Transformers and coupled inductors increase volume and cost.
Y-Source	- Very high gain can be obtained with small shoot through duty cycle. - Higher voltage boost and higher modulation index can be obtained at the same time. - Reduced THD of the inverter. - Suitable for power conversion applications.	- Discontinuous input current. - Electromagnetic interference noise affects its reliability.
Γ-Z-source	- High gain can be achieved by lowering turn ratio. - Better spectral performance. - Continuous input current. - Convenient for renewable energy generation.	- Leakage inductance affects on the voltage and current stress over semiconductors.
LCCT-Z-source	- Have continuous current during even light load. - Filter out high-frequency ripples from source current. - Appropriate for renewable energy generation and power conversion applications.	- Have high winding turns ratio. - Electromagnetic interference noise affects its reliability.

Table 2.3: Summary of the impedance source inverter applications with typical used power

Impedance Network Topology	Switching Frequency	Typical Used Power	Applications
Z-Source	10 kHz	15 kW (maximum output power)	Electric vehicles [46]
		125 kW (maximum output power)	Photovoltaic and Grid systems [47]
	12 kHz	4.5 kW (rated power)	Wind Turbines [48]
Quasi-Z-Source	100 kHz	10.6 kW (maximum output power)	Electric vehicles [49]
	20 kHz	300 W (rated power)	Hybrid electric vehicles [50]
	10 kHz	2.6 kW (rated power)	Photovoltaic and Grid systems [51]
Embedded Z-Source	7 kHz	6 kW (maximum output power)	Photovoltaic and Grid systems [52]
Embedded Quasi-Z-Source	10 kHz	375 W (maximum output power)	Photovoltaic [40]
Trans-Z-Source	20 kHz	6 kW (rated power)	Photovoltaic, fuel cell and Grid system [53]
Y-Source	20 kHz	2 kW (maximum output power)	Electric vehicle [54]
	10 kHz	18.25 kW (maximum output power)	Photovoltaic [55]
Γ-Z-source	10 kHz	3 kW (maximum output power)	Photovoltaic and Grid systems [56]
LCCT-Z-source	20 kHz	4.5 kW (rated power)	Permanent magnet synchronous generators [32]

2.3 Z-source inverters for EV applications

2.3.1. Z-source inverters for single-source EV applications

The efficient use of the available resources is one of the greatest technological concerns. With the ZSI, improvements in DC-DC systems are going on in the field of EVs. The ZSI can regulate the voltages and currents of the energy sources and enables bidirectional flow of power in traction applications. In the propulsion mode, the voltage from the energy storage systems is provided by the ZSI in form of three phase voltage to drive the motor to produce the required torque and reach the desired speed of the vehicle. During the regenerative mode, the electric motor acts as a generator. The regenerated energy flows backwards to recharge the energy sources. The inverter operates as a rectifier and the ZSI works as buck inverter to recharge the energy sources. The schematic of diagram of EV system components using impedance source inverter is shown in Figure 2.9.

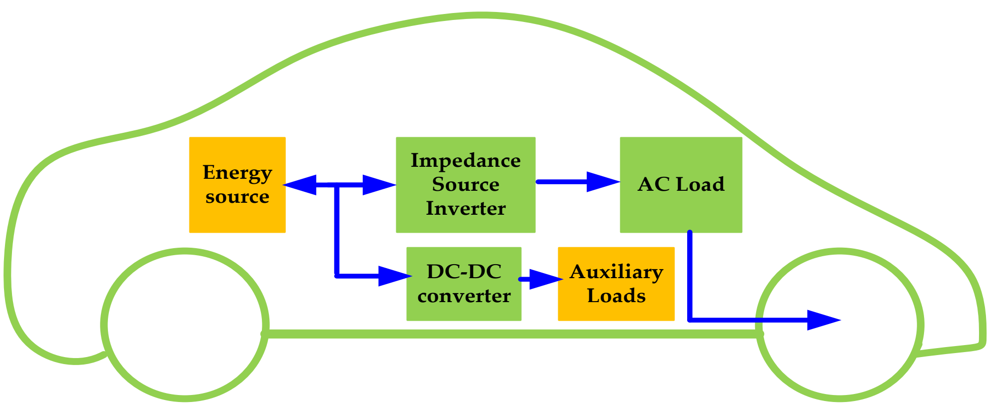

Figure 2.9: Schematic diagram of EV system components.

Since 2003, ZSI has been widely used in industrial applications and in other variety of applications. ZSI has been applied to motor drives to overcome the restrictions of voltage source inverter [27]. Bidirectional QZSI which is the first modified topology of bidirectional ZSI has been also compared with bidirectional conventional two-stage inverter for electric traction system [8]. The results demonstrate that the transient and the steady state performances are comparable for both topologies under the same operating conditions. However, the bidirectional QZSI shows lower inductor current ripples than bidirectional conventional two-stage inverter. The results also prove that the bidirectional QZSI shows higher efficiency than the conventional solution. Bidirectional ZSI which can operate in boost mode, buck mode as a normal voltage source inverter, or a charger mode and applied to double-ended inverter drive system is also proposed in [57]. To investigate the performance of locomotive drives, the ZSI has been used as a replacement of voltage source inverter [58].

Because of many advantages of ZSI, it is suitably applied for fuel cell. A fuel cell configuration using a Z-source network has been represented in [59]. Three different inverters such as traditional voltage source inverter, conventional two-stage inverter, and ZSI applied to fuel cell vehicle has been compared [60]. The result shows that the ZSI has higher efficiency, less switching devices and more passive components requirement than the others type of inverters.

2.3.2. Z-source inverter for multi-source EV applications

EV performance can be influenced by a lot of factors such as size, purpose of use, environment, driving style. For EV, these factors may lead to a deep and quick discharge rate of the battery. EV powered by a combination of multiple sources can contribute to keep the battery in good health [61]. That also enables to help the battery to a slow discharge even when the EV use a heavy load [62]. Hybrid energy storage system (HESS) combining 2 or more energy sources (batteries, ultracapacitor, fuel cell) have been shown to be a suitable solution, which permits to meet need for the load power requirement according to the characteristics of the sources [63]. The conventional two-stage inverters are normally employed in these HESS.

In order to exploit the advantages of ZSIs, ultracapacitor-battery HESS for EVs based on asymmetric bidirectional Z-source topology has been studied [64]. The results demonstrate that the HESS with ZSI can be integrated into the traction system to obtain better performance and lower cost than that with conventional two-stage inverters. Furthermore, the ZSI can also be applied to hybrid electric vehicles using fuel cell and battery as input sources with slight modification in its topology [65].

Nonetheless, this configuration has some disadvantages with the obligation to use high voltage battery and the fact that the DC link voltage is twice the battery voltage during regenerative braking when the fuel cell stack is disconnected from the ZSI input terminals. This disconnection may damage the switches of the inverter.

There are many impedance source inverters which can be used for multi-source EV such embedded Z-source inverter, embedded quasi-Z-source inverter and other topologies obtained with slight modification to include a battery or DC source [65]. Multi-source EVs where power flows during starting and braking operations can be designed with bidirectional EQZSI. The EQZSI is a promising architecture for multi-source electric vehicle as it presents the advantage of having a continuous input current and retaining all the merits of both QZSI and embedded topology [66].

2.3.2.1. Bidirectional EQZSI for multi-source EV applications

2.3.2.1.1 Electric vehicle specifications and modeling

The reference electric vehicle is the e-TESC 4W platform as presented in [66] with its main parameters. In our study, surface permanent magnet synchronous machine (SPMSM) is used as a traction electric motor and its state space representation can be described as presented in [8].

2.3.2.1.2. Modeling of Bidirectional Embedded Quasi-Z Source Inverter

The bidirectional EQZSI as presented in section 2.4 can buck and boost the input voltage in a single stage with two control variables such as the shoot-through duty ratio and the modulation index. Assuming T is one switching cycle, T_0 is the interval of the shoot-through state; T_1 is the interval of non-shoot-through state; their relationship is $T_0 + T_1 = T$, and the shoot-through duty ratio $D = \frac{T_0}{T}$. The dynamic equations can be described as shown in [66]. During the steady state, the capacitor voltages and inductor currents can be deduced as follows:

$$\begin{cases} v_{c_1} = \dfrac{1-D}{1-2D} v_1 + \dfrac{D}{1-2D} v_2 \\ v_{c_2} = \dfrac{D}{1-2D} v_1 + \dfrac{1-D}{1-2D} v_2 \end{cases} \tag{2.1}$$

$$i_{L_1} = i_{L_2} = \frac{1-D}{1-2D} i_{load} \tag{2.2}$$

The DC link peak voltage $\hat{v}_{dc}$ can be derived from the sum of two capacitor voltages, v_{c_1} and v_{c_2}, by:

$$\hat{v}_{dc} = v_{c_1} + v_{c_2} = \frac{1}{1-2D}(v_1 + v_2) = B(v_1 + v_2) \tag{2.3}$$

where $B \geq 1$ is the boost factor resulting from the shoot through the period. With regards to the AC side of the EQZSI, the peak phase voltage can be written as

$$\hat{v}_o = m_e \frac{\hat{v}_{dc}}{2} = \frac{m_e}{1-2D} . \frac{(v_1 + v_2)}{2} = G_e \frac{(v_1 + v_2)}{2} \tag{2.4}$$

where m_e and G_e are the inverter modulation index and total voltage gain of the EQZSI, respectively.

2.3.2.1.3 PI-Based Controllers Design

To achieve the speed control and disturbance rejection for the EV, cascade PI controllers has been designed. The motor (SPMSM) with PI control technique is adopted. The speed control scheme for EQZSI is shown in Figure 2.10.

2.3.2.2. Simulation results and discussion

A simulation was carried out, to validate the model of EQZSI and shows its performance for multi-source EV. The bidirectional EQZSI performance depends on the selection of the parameters of embedded quasi-Z-source network elements. There are equations which can be used to determine the appropriate values of these parameters [67]. The critical values of the inductances and the capacitances are used to design the EQZSI parameters by the following equations:

$$L_1 = L_2 = \frac{Dv_{c1}}{f_s \Delta i_{L1}} \tag{2.5}$$

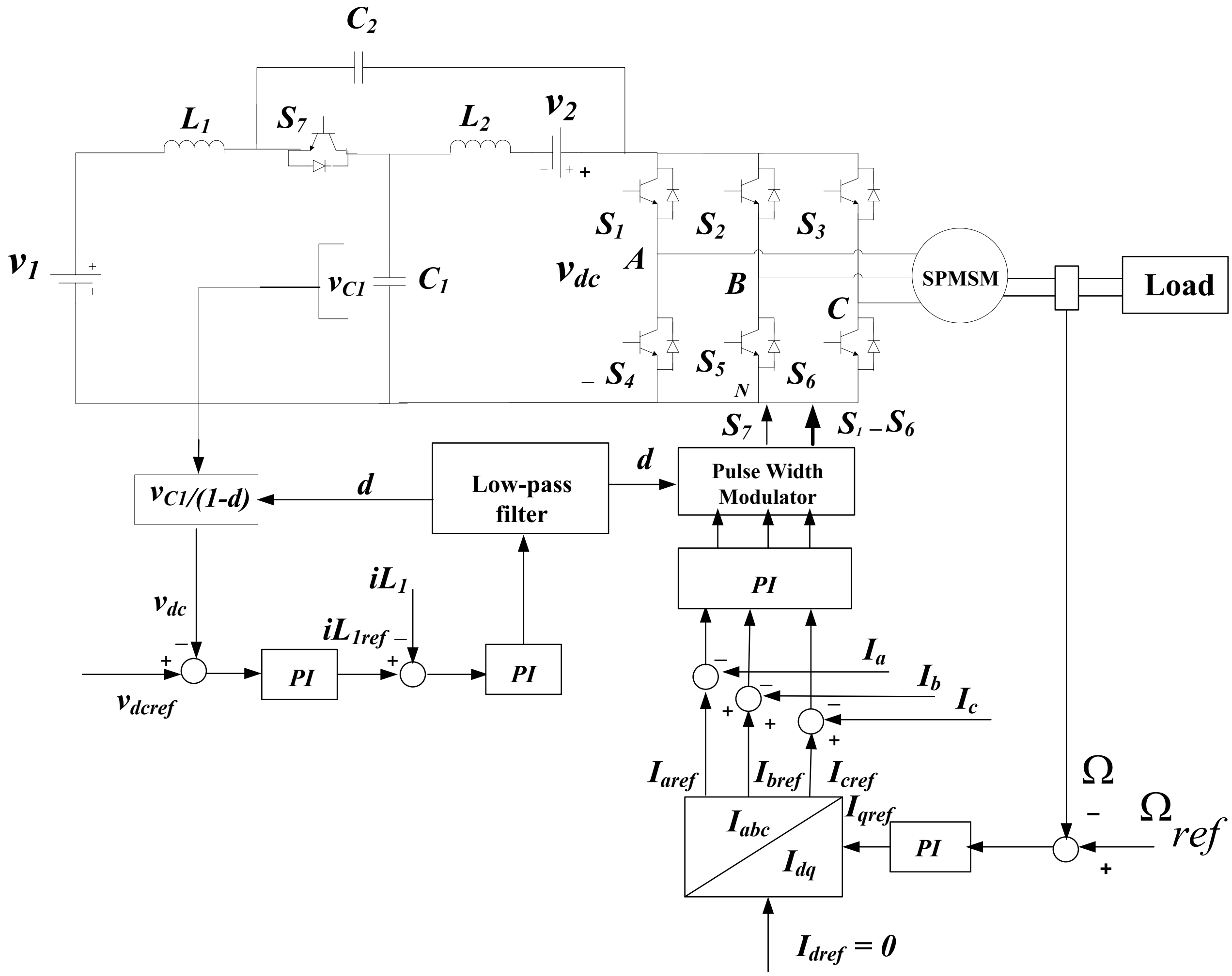

Figure 2.10: Speed control scheme based on PI controllers for EQZSI.

$$C_1 = C_2 = \frac{D i_{L1}}{f_s \Delta v_{c1}} \tag{2.6}$$

where D is the shoot-through duty ratio, f_s is the switching frequency, v_{c1} is the average capacitor voltage, Δi_{L1} is the value of inductor current ripple at peak power to certain value, i_{L1} is the average current of the inductor and Δv_{c1} represents the value of capacitor voltage ripple at peak power.

The simulation parameters are $L_1 = L_2 = 230$ µH; $C_1 = C_2 = 2.2$ mF. PWM carrier frequency for three-phase inverter is 10 kHz. The control scheme is shown in section 3.2.1. Maximum constant boost control method as shown in [66] has been used to generate the gate signals of the EQZSI switches.

The electric vehicle motor used in the simulation is a SPMSM with three phases as defined in section 2.3.2.1.1. The parameters of the motor are $L_d = L_q = 1$ mH; $r_s = 0.08$ Ω; $p = 2$; $J = 1$ kg.m^2; $\psi_f = 0.1$

Wb. The rated power is 15 kW. The Figures 2.11 and 2.12, show the speed and torque waveforms respectively. The Figures 2.13 and 2.14 represent the v_{dc} voltage and i_{L1} current, and also their references, respectively.

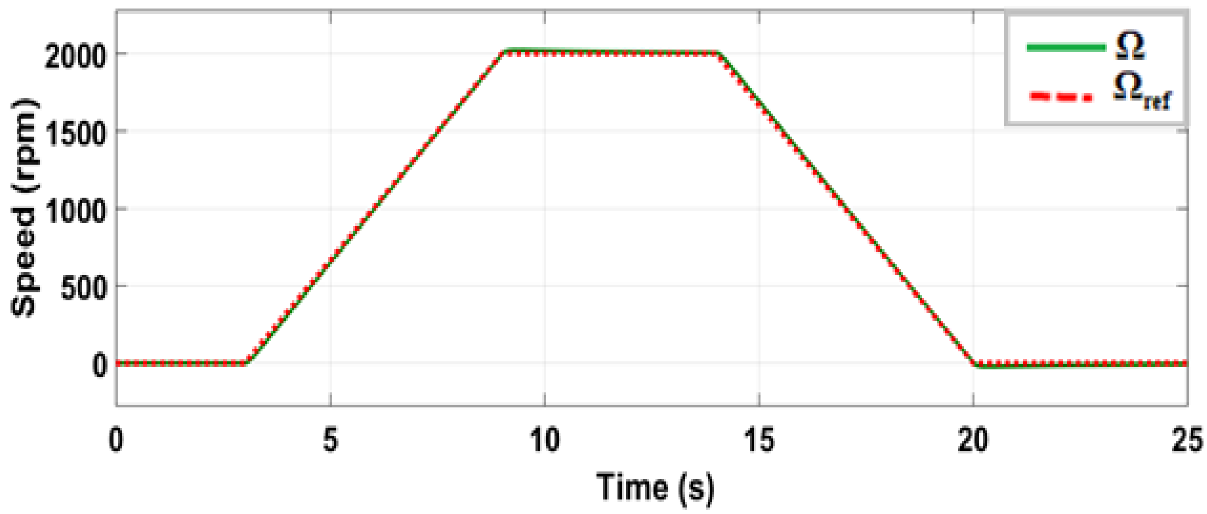

Figure 2.11: Motor speed and reference with EQZSI.

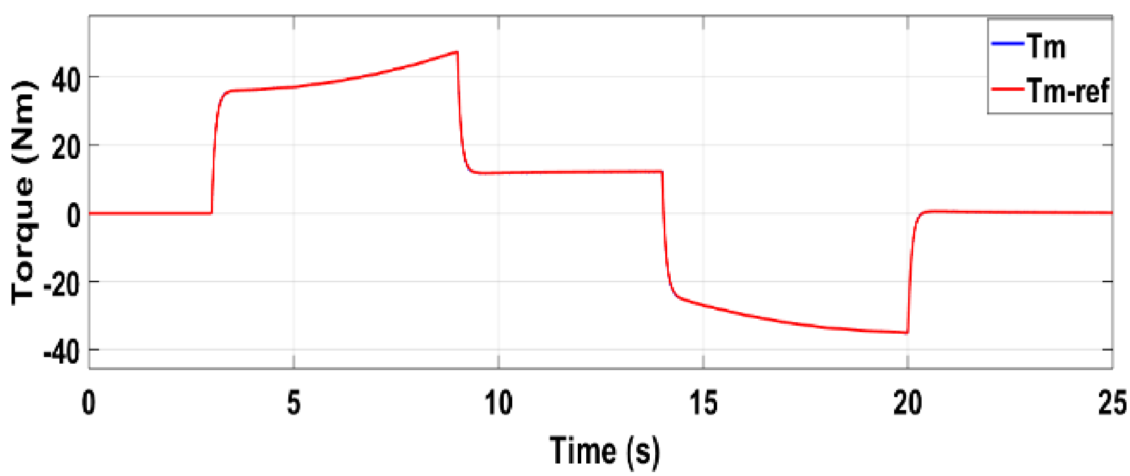

Figure 2.12: Motor torque and reference with EQZSI.

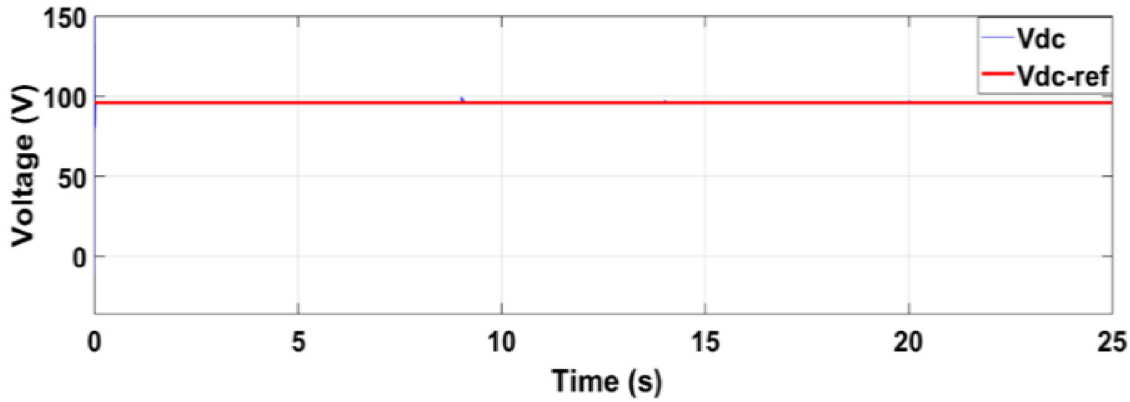

Figure 2.13: The v_{dc} voltage and reference with EQZSI.

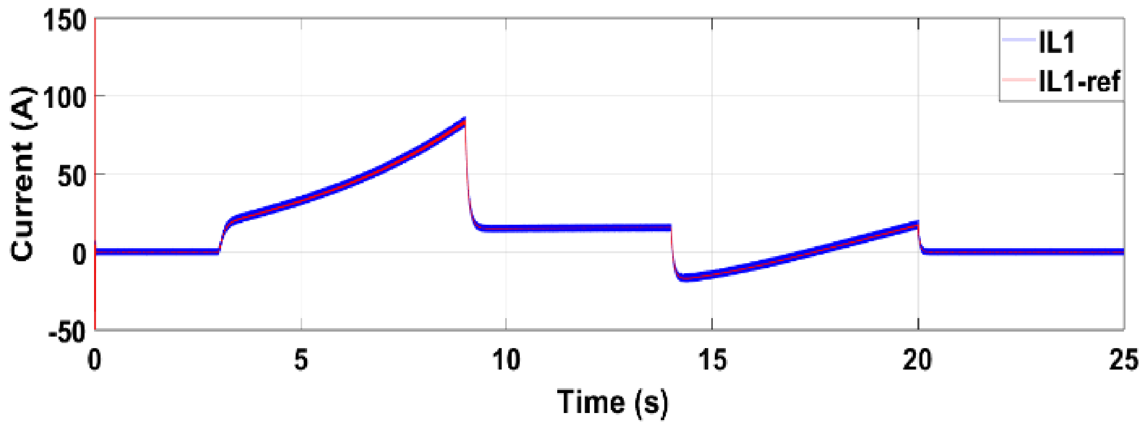

Figure 2.14: The i_{L1} current and reference with EQZSI.

The results point out the ability of the inverter to respond quickly to the load and the input voltage. These results verify the bidirectional EQZSI as an alternative inverter for multi-source EVs. The disparity of voltage levels and currents between the sources (fuel cell, batteries, ultracapacitors) and the loads of the EVs (traction motor, auxiliaries) requires the use of power converters. This kind of power converter architecture provides an interesting new resource for on-board energy management in multi-source EVs. The bidirectional EQZSI can enhance the performance of the EV by optimizing the electric power consumption and extending its driving range.

2.3.3. Future trends

The concept of impedance source inverter has clearly opened a new area of research in the field of power electronics. The study in section 2.1 only provides a summary on topologies of impedance source inverters. It also shows the modifications whose it is possible to have with ZSI. Any topology possesses its own unique features and adapted applications. New impedance source inverters topologies may continue to appear to meet needs and improve performance in different applications. EVs, motor drives and renewable energy generation will be perspective applications for impedance source inverter, because it has a unique voltage buck–boost ability with minimum number of components and potential reduced cost. The control strategy is very important to ensure reliable and efficient operation of the impedance source inverter. The impedance source inverter system performance will be improved with novel control method. The use of the control method such as model predictive control (MPC) can contribute to enhance impedance source inverter system performance. The cost function of MPC is fundamental to the system performance and different constraints can be added to improve the complete functioning of the system. The performance of impedance source inverter will also be enhanced with the new power electronics devices such as the SiC and GaN because they have high switching frequency, high temperature capacity and expected low cost. That can contribute to achieve smaller size for passive components of impedance source inverter, to reduce its cost, to increase its efficiency. The design of new impedance source inverters has attracted more and more attentions from scientists and engineers. Impedance source inverter is still progressing in terms of topologies and applications.

2.4 Conclusion

A comprehensive start of the art review of impedance source inverter main topologies is presented. The impedance source inverter for EV application and for other applications has been outlined. Several topologies of ZSI are investigated. Many impedances source inverter has been compared in order to choose a best, efficient and convenient inverter topology for multi-source EV. In the literature, a lot of approaches have been proposed and their benefits and drawbacks have been identified. The advantages and disadvantages of the impedance source inverter main topologies has been presented. The impedance network becomes popular by the fact that it has specific features and attractive power conversion ability. Impedance source inverters overcome many problems of traditional inverters.

Since the apparition of Z-source network, numerous contributions in the literature modifying the basic topology to suit the needs of many applications have been proposed. It has been advanced to quasi-Z-source network, embedded Z-source network, embedded quasi-Z-source network, trans-Z-source network, and many other types of Z-source network topologies. The EQZSI is one of the promising architectures which can be used in EV multi-source with better performance and reliability. The utilization of this new topology will open the door to several development axes with great impact to EVs. Various researchers continue to work towards the modification of impedance source inverter main topologies to increase their performance and applicability.

2.5 Acknowledgment

This work was supported in part by Grant 950-230672 from Canada Research Chairs Program, in part by Grant RGPIN-2017-05924 from the Natural Sciences and Engineering Research Council of Canada, in part by FCT-Portuguese Foundation for Science and Technology project UIDB/00308/2020, and by the European Regional Development Fund through the COMPETE 2020 Program within projects ESGRIDS (POCI-01-0145-FEDER-016434) and MAnAGER (POCI-01-0145-FEDER-028040).

Chapter 3 Comparison of Bidirectional Quasi-Z-Source Inverter and Bidirectional Conventional Two-Stage Inverter for Electric Traction System

Original Title: Comparison of Bidirectional Quasi-Z-Source Inverter and Bidirectional Conventional Two-Stage Inverter for Electric Traction System

Authors and affiliation :

- **Daouda Mande**: Ph.D. student, e-TESC Laboratory, Department of Electrical & Computer Engineering, University of Sherbrooke
- **João P. Trovão**: Professor, e-TESC Laboratory, Department of Electrical & Computer Engineering, University of Sherbrooke
- **Ruben Gonzalez Rubio**: Professor, eXit Laboratory, Department of Electrical & Computer Engineering, University of Sherbrooke
- **Minh C. Ta**: Professor, e-TESC Laboratory, Department of Electrical & Computer Engineering, University of Sherbrooke

Date of Acceptance: **27 August 2018**

State of acceptance: Published

Reference: 2018 IEEE Vehicle Power and Propulsion Conference (VPPC),

DOI: 10.1109/VPPC.2018.8604968

Summary

<u>Content:</u> This article provides a comparative study between the bidirectional conventional two-stage inverter and bidirectional QZSI for EV applications. The comparison is conducted in terms of the voltage gain, current ripple, the transient and the steady state performances, and the inverters efficiency. The modeling and the control design for both inverters are also presented and discussed. Simulation investigations are conducted to verify the inverter.

<u>Results</u>: The simulation and comparative results show that the bidirectional QZSI has best performance than the bidirectional conventional two-stage inverter. The results demonstrate that the transient and the steady state performances of the bidirectional QZSI are comparable with the ones of the bidirectional conventional two-stage inverter under the same operating conditions. However, the bidirectional QZSI has a higher voltage gain than the bidirectional conventional two-stage inverter for some small duty cycle. It shows lower inductor current ripple than the bidirectional conventional two-stage inverter. The results prove that the bidirectional QZSI shows higher efficiency than the conventional solution.

<u>Contribution to this thesis</u>: This comparative study enables to prove QZSI as an attractive alternative power converter for EV applications. It is a buck-boost inverter, feature that traditional voltage source and current source can't provide. It can be applied in applications where the input voltage changes widely. The cost of QZSI is reduced and efficiency is increased. The disparity of voltage levels and currents between the sources and the load of the EV requires the use of efficient power converters. This kind of impedance source inverter is essential for on-board energy management in multi-source vehicles.

Abstract

This paper presents a comparative study between the bidirectional conventional two-stage inverter (Topology A) and the called bidirectional quasi-Z-source inverter (Topology B) for electric vehicle (EV) applications. The comparison is conducted in terms of the voltage gain, current ripple, the transient and the steady state performances, and the inverters efficiency. The modeling and the control design for both inverters are presented and discussed. Simulation investigations are conducted to verify the inverter. It is shown that the Topology B has a higher voltage gain than the Topology A for some small duty cycle. The results demonstrate that the transient and the steady state performances of Topology A are comparable with the ones of Topology B under the same operating conditions. However, the Topology B shows lower inductor current ripple than Topology A. The results prove that the Topology B shows higher efficiency than the conventional solution. With these observations, the Topology B proposes an attractive alternative for EV applications.

Keywords: Quasi-Z-source inverter; DC-DC boost converter; voltage source inverter; sinusoidal pulse width modulation; simple boost control

3.1 Introduction

Nowadays, energy storage and conversion play the important role in the field of distributed generation systems. Many of them uses boost converter. Boost type converters are essentially used for many renewable energy applications and other varieties of applications such as electric, hybrid electric, plug-in-hybrid electric, fuel cell vehicles [68], photovoltaic power systems [69], offshore wind turbines [70], medium-voltage DC and high-voltage DC power systems [71], telecommunication power supply [72], on ship- board power system [73] and in offshore petroleum and gas applications of subsea compressors [74], FC based power supply [75] etc. These converters often have lower input voltage than the required load.

In bidirectional conventional two-stage inverter (Topology A), the output voltage produced is always greater in magnitude than the input voltage [76]. The demanded voltage gain normally requires higher duty cycle (sometimes close to unity), which leads to high conduction losses, higher voltage and current stresses on the switching devices. The voltage gain which can be achieved using any DC-DC converter topology is limited by the parasitic elements [77]. The two-stage system increases not only the complexity of circuitry and control but also the cost and the space requirement [78]. Recently the Z-source inverter (ZSI) has been used as replacement of two-stage converter in the distributed generation systems [23, 79]. Z-source inverter (ZSI) is a power electronic circuit whose function is to convert DC input voltage to a symmetrical AC output voltage of desired magnitude and frequency. It employs a unique impedance network to couple the main circuit of the converter to the power source and it utilizes the shoot-through state to boost the input voltage, which improves the inverter reliability and enlarges its application fields. It is widely used in industrial applications such as variable speed AC motor drives, induction heating, standby power supplies, and uninterruptible power supplies and in other variety of applications [23, 80]. ZSI can also be used for power factor improvement. The input to the inverter may be from a battery, fuel cell, solar cell, or other DC source. Since 2003 when this recently conversion concept appeared [23], it proved able to solve many conversion problems mentioned in this article.

As opposed to the Topology A, a Z-source network is used as a boost converter in the ZSI, without introducing additional power electronic stage operating as a one stage buck-boost inverter. Its superiority compared to traditional solutions has been shown [81]. The main advantages are: the new concept using ZSI can be applied to the entire spectrum of power conversion; the ZSI is a buck-boost inverter, feature that traditional voltage source and current source can't provide; it can be applied in applications where the input voltage changes widely; all traditional pulse width modulation (PWM) schemes can be used to control the ZSI and their theoretical input-output relationship still hold; cost is reduced and efficiency is increased. These most switching control strategies are simple boost method [23], maximum boost method [34], constant boost method [82] and space vector method [83]. It has the increasing operating of the voltage occurs via the allocation of shoot-through intervals in inverter that was not allowed in voltage source inverter. According to the above converter characteristics, this type of converter has been used in a variety of applications. Therefore, it has attracted more attention than the other converters over the last decade and has already been tried with many applications.

However, the input current of ZSI is not continuous. The design of electric vehicle (EV) represented for example by electric traction systems shown in Figure 3.1 with ZSI will shorten the lifetime of its battery pack and degrades its performance. By rearranging the components in the Z-source network, a new topology called quasi-Z-source inverter (QZSI) is proposed. Electric vehicles which are charged by the batteries and the power flow during starting and braking operations can be designed by bidirectional QZSI (Topology B) to have best performance. The QZSI [84] is a promising architecture as it presents the advantage of having a continuous input current and retain all the merits of the ZSI, which makes it a good candidate for EV applications [43] and recognized to be used in many power conversion applications [85, 86].

This paper, on the other hand, makes a comparison between Topology A and Topology B which can be more useful for energy management multi-source in electric vehicle. It is organized in several sections. Section 3.2 introduces the EV under study and the model of its surface synchronous machine (SPMSM). In Section 3.3, the Topology A configuration and the modeling validation are presented. Section 3.4 presents the Topology B with its modeling validation. The controllers design is described in Section 3.5. In Section 3.6, the Topology A and the Topology B are implemented using the Simscape Power Systems library of MATLAB / Simulink for the EV motor with the same source voltage. The simulated result and comparison of the two architectures is then presented. Conclusion is mentioned in Section 3.7.

3.2 Electric vehicle under study

Electric vehicle is characterised by an electric energy conversion chain upstream of the drive train [7] consisting of an electricity storage system (battery, fuel cell, etc.) and an electric motor with its controller. The schematic of electric traction systems is shown in Figure 3.1.

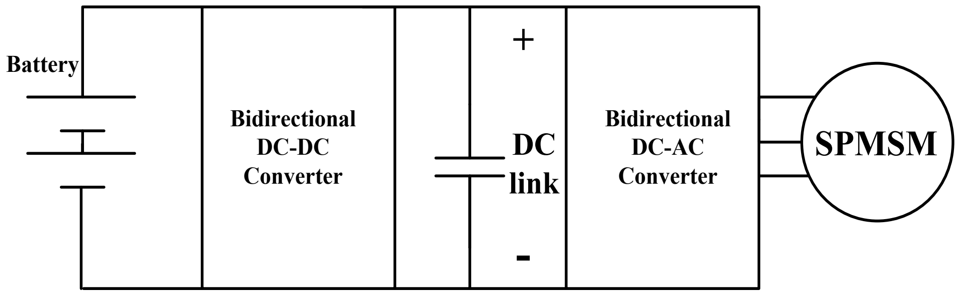

Figure 3.1: Electric traction systems.

During the motor mode where the power is transferred from the source battery to the load (motor), the DC-DC converter corresponds to the boost chopper. AC motor power is supplied via a voltage source inverter. Electric vehicle motion depends on the torque applied to overcome the motor resistant torque. In our study SPMSM is used as an electric motor. It is a synchronous motor with two phases. Its state space representation can be described as follows:

$$\begin{cases} L_d \dfrac{di_d}{dt} = -r_s\, i_d + v_d + p\Omega L_d i_q \\ L_q \dfrac{di_q}{dt} = -r_s\, i_q + v_q - p\Omega\left(L_d i_d + \psi_f\right) \\ J\dfrac{d\Omega}{dt} = p\psi_f i_q - \Gamma_{ch} - f\Omega \end{cases} \tag{3.1}$$

where i_d and i_q are winding currents on the phases d and q, respectively [A], v_d and v_q are phase voltage on the phases d and q, respectively [V], r_s is phase resistance [Ω] and L is phase inductance [H] and assumed to be constant, p is the number of pole pair, f is coefficient of viscous friction [kg.m^2/s], J and ψ_f are rotor inertia [kg.m^2] and magnet flux linkage [Wb], respectively, Ω is a rotor angular velocity [rpm].

Simulations were carried out for one part of Artemis driving cycles to validate the model of the motor and to compare between the Topology A and Topology B about reference tracking performance. A driving

cycle commonly represents a set of vehicle speed points versus time. It is used to assess fuel consumption and pollutants emissions of a vehicle in a normalized way. The simulation parameters are same used for Topology A and B modeling validation. The following figures show the simulation result of Topology A and Topology B fed SPMSM using PI based sinusoidal PWM and simple boost control techniques studied in section 3.3, 3.4 and 3.5. Figures 3.2, 3.3, 3.4 and 3.5 show the speed and torque waveforms respectively.

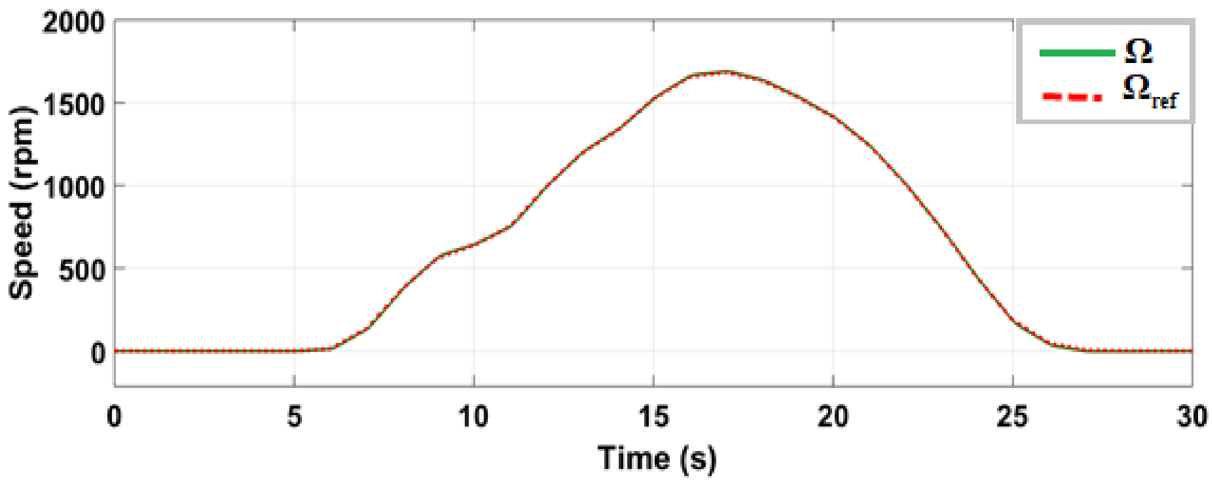

Figure 3.2: Motor speed and reference with Topology A.

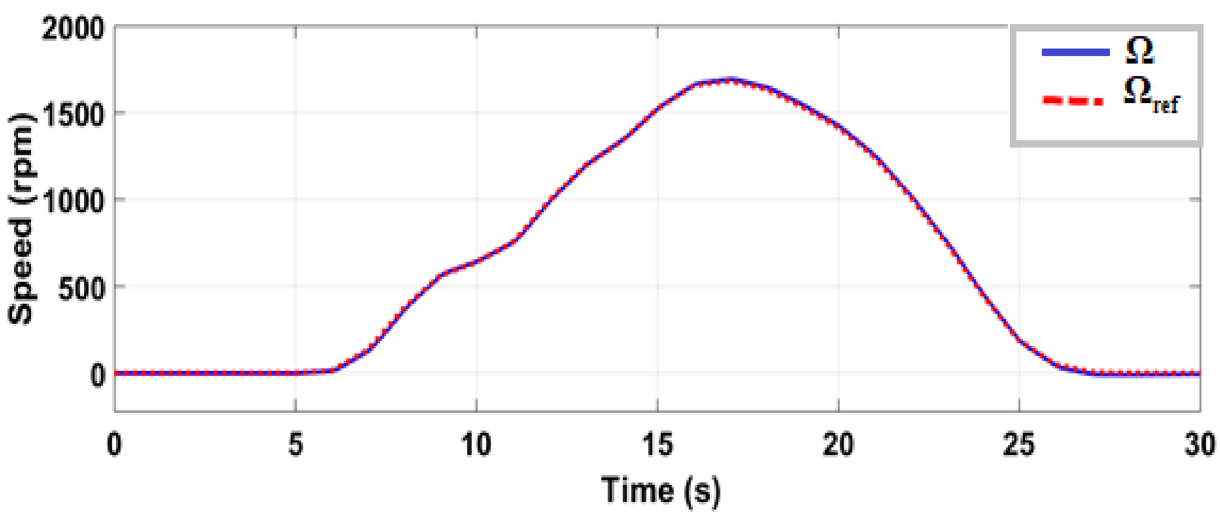

Figure 3.3: Motor speed and reference with Topology B.

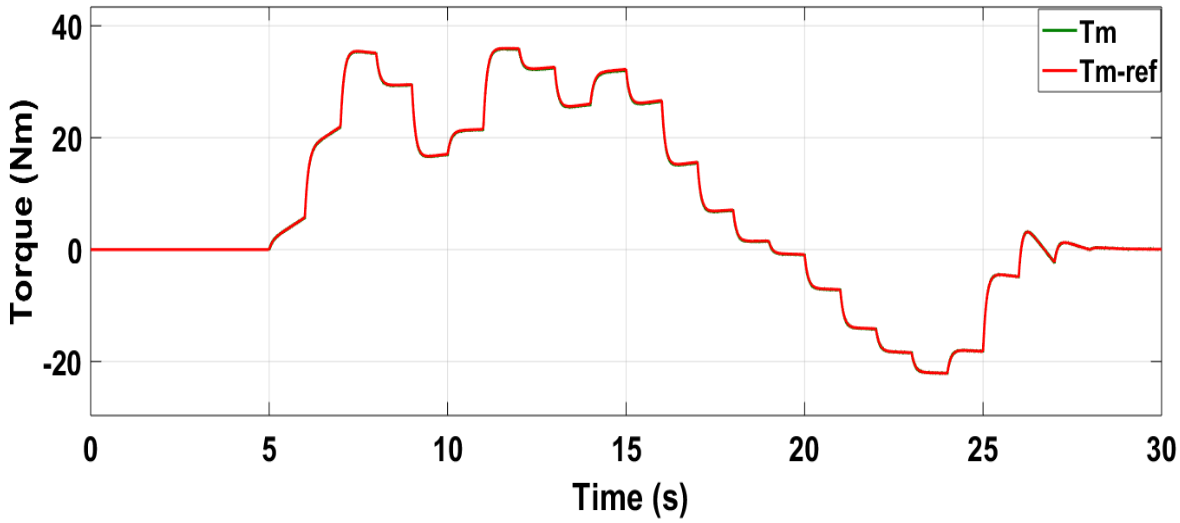

Figure 3.4: Motor torque and reference with Topology A.

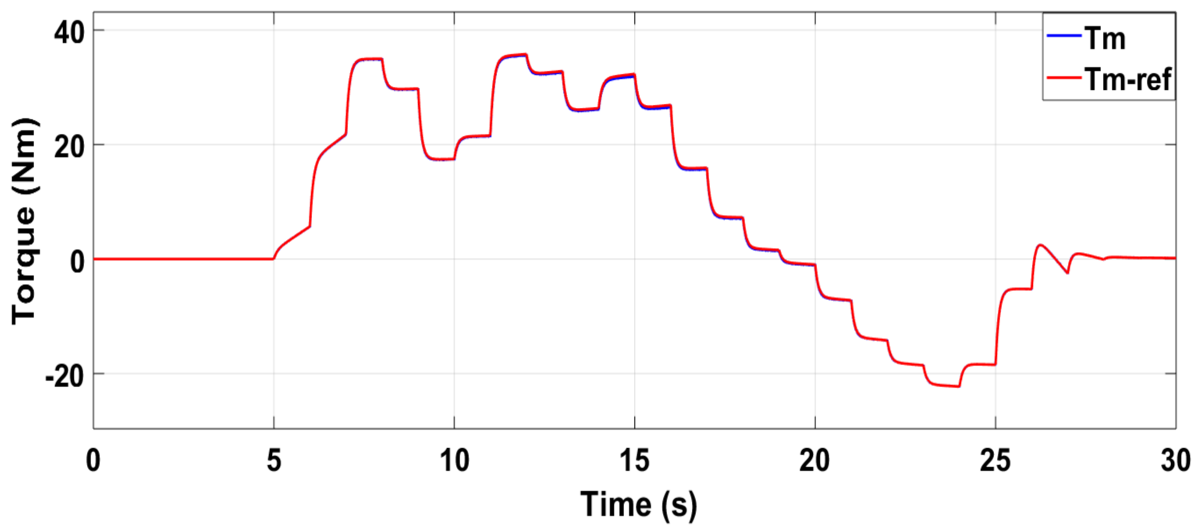

Figure 3.5: Motor torque and reference with Topology B.

3.3 Bidirectional conventional two-stage inverter

The conventional two-stage inverter used for the comparison consists of two separated stages: DC-DC boost converter and voltage source inverter. The configuration of the bidirectional conventional two-stage inverter (Topology A) connected with a SPMSM is shown in Figure 3.14.

3.3.1 Modeling of Bidirectional DC-DC Boost Converter

The bidirectional DC-DC boost converter shown in Figure 3.14 has two operation states: ON and OFF state when the switch *S* is closed and open, respectively. The three-phase inverter is represented by a constant current source i_{load}.

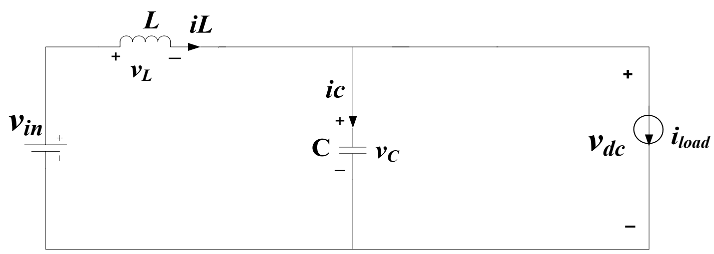

(a) OFF state

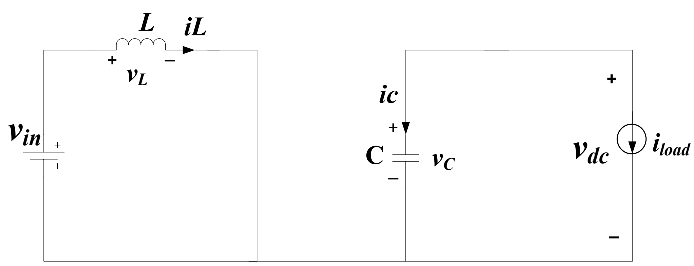

(b) ON state

Figure 3.6: Operation states of the Topology A.

During ON state (see Figure 3.6(b)), the input voltage charges the inductor and the capacitor voltage feeds the load. Thus, the following equation can be obtained:

$$\begin{cases} L\dfrac{di_L}{dt} = v_{in} \\ C\dfrac{dv_c}{dt} = -i_{load} \end{cases} \tag{3.2}$$

In OFF state (see Figure 3.6(a)), the input voltage and the inductor voltage charge the capacitor and supply energy to the load. The equation describing this condition is:

$$\begin{cases} L\dfrac{di_L}{dt} = v_{in} - v_c \\ C\dfrac{dv_c}{dt} = i_L - i_{load} \end{cases} \tag{3.3}$$

3.3.2 Steady State Analysis

In the steady-state operation, the average voltage of the inductor is zero over one complete switching period *T*. Accordingly, the DC-link voltage v_{dc} can be deduced as follows:

$$v_{dc} = \frac{v_{in}}{1-D} \tag{3.4}$$

The peak AC output voltage can also be calculated by

$$\hat{v}_o = m_c \frac{v_{dc}}{2} = \frac{m_c}{1-D} . \frac{v_{in}}{2} = G_c \frac{v_{in}}{2} \tag{3.5}$$

where m_c and G_c are the inverter modulation index and total voltage gain of the Topology A inverter, respectively.

3.3.3 Sinusoidal Pulse Width Modulation Method

The sinusoidal pulse width modulation method (SPWM) technique is based on the comparison of a carrier signal and a pure sinusoidal modulation signal. The intersections between the sinusoidal waveform and the carrier waveform give the opening and closing times of the switches. The SPWM for inverter has been the main choice in power electronic for decades, because of its circuit simplicity and rugged control scheme. Sinusoidal pulse width modulation switching technique is commonly used in industrial applications [87]. The Figure 3.7 shows the wave forms of SPWM technique.

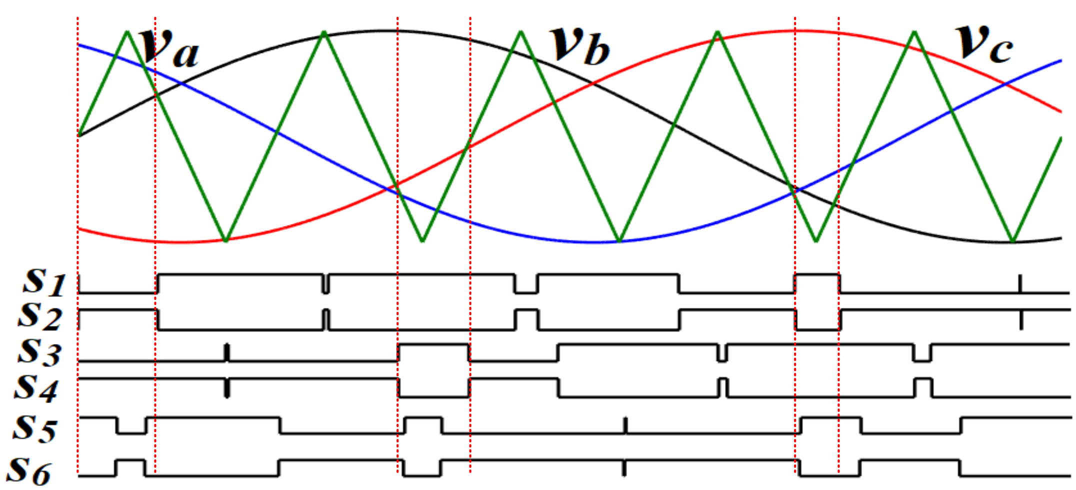

Figure 3.7: The wave-forms of SPWM technique.

3.3.4 Model Validation

A simulation was carried out to validate the model of Topology A. The simulation parameters are as follows:

For Topology A, L = 0.2 mH; C = 4.5 mF.

For the motor, $L_d = L_q$ = 1 mH; r_s = 0.08 Ω; p = 2; J = 1 kg.m^2; ψ_f= 0.1 Wb. The rated power is 15kW and the motor model is shown in section 3.2. PWM carrier frequency for bidirectional DC–DC converter is 50 kHz and PWM carrier frequency for three-phase inverter is 10 kHz. The control scheme is shown in section 3.5.

The following Figure 3.8 and 3.9 represents respectively the v_{dc} voltage and i_L current with their reference.

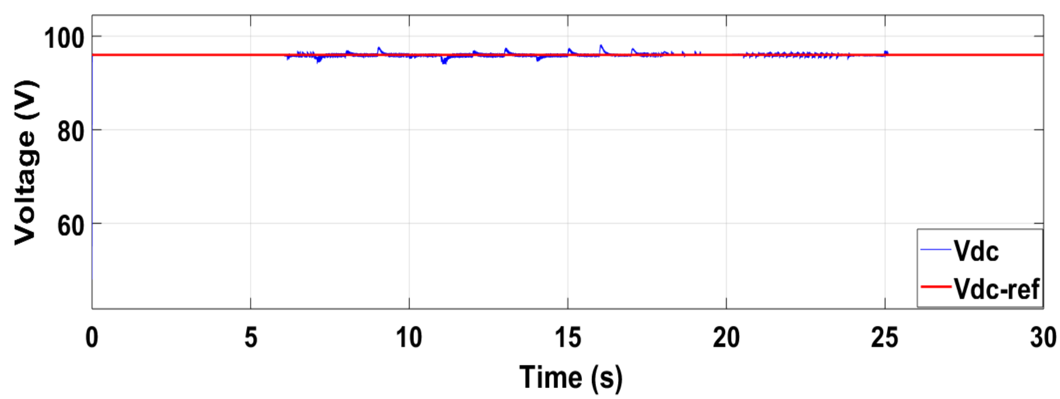

Figure 3.8: The v_{dc} voltage and its reference.

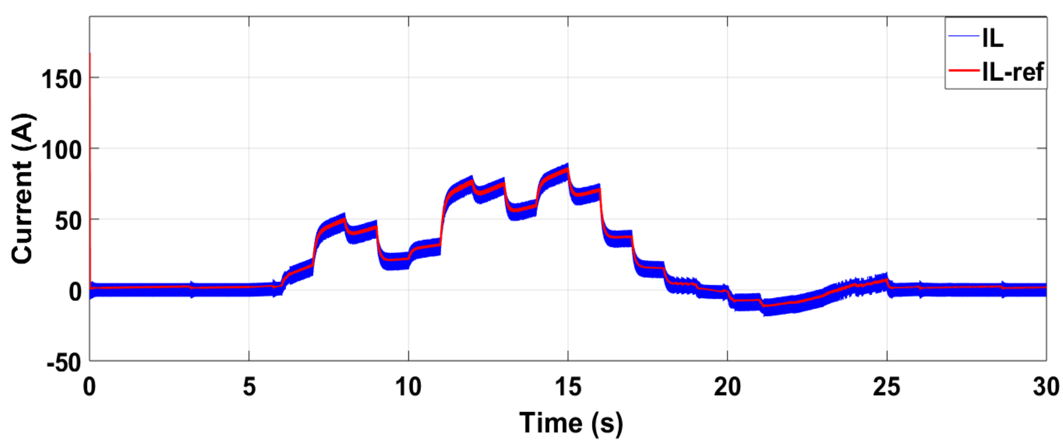

Figure 3.9: The i_L current and its reference.

3.4 Bidirectional Quasi -Z-Source Inverter

The configuration of the Topology B connected with a SPMSM is shown in Figure 3.15. It can buck and boost the input voltage in a single stage with two control variables such as the shoot-through duty ratio and the modulation index [23]. The equivalent circuits are shown in Figure 3.10 a and b, when the proposed circuit operates in two states: non-shoot-through state and the shoot-through state, respectively. All the voltages and the currents are defined in Figure 3.10.

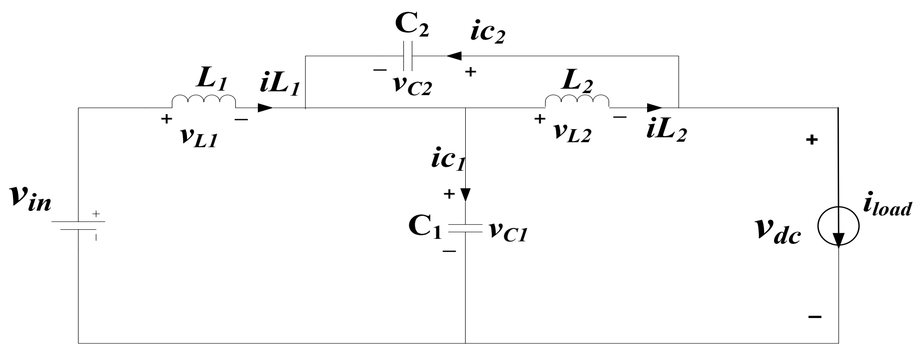

(a) Non-shoot-through state

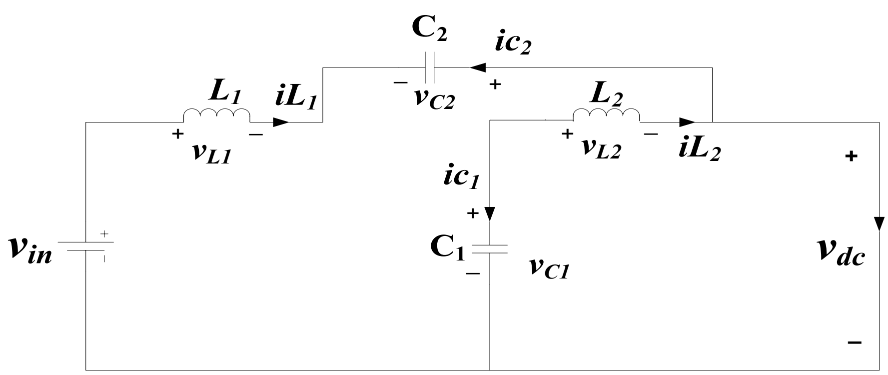

(b) Shoot-through state

Figure 3.10: The operation states of Topology B.

3.4.1 Modeling of Bidirectional Quasi-Z-Source Inverter

Assuming T is one switching cycle, T_0 is the interval of the shoot-through state; T_1 is the interval of non-shoot-through state; their relationship is $T_0 + T_1 = T$, and the shoot-through duty ratio $D = \frac{T_0}{T}$.

In Figure 3.10(a), the inverter operates at the non-shoot-through state T_1. The dynamic equations are:

$$\begin{cases} L_1 \dfrac{di_{L_1}}{dt} = v_{in} - v_{c_1} \\ L_2 \dfrac{di_{L_2}}{dt} = -v_{c_2} \\ C_1 \dfrac{dv_{c_1}}{dt} = i_{L_1} - i_{load} \\ C_2 \dfrac{dv_{c_2}}{dt} = i_{L_2} - i_{load} \end{cases} \tag{3.6}$$

In Figure 3.10(b), the inverter operates at the shoot-through state T_0. The dynamic equations are:

$$\begin{cases} L_1 \dfrac{di_{L_1}}{dt} = v_{in} + v_{c_2} \\ L_2 \dfrac{di_{L_2}}{dt} = v_{c_1} \\ C_1 \dfrac{dv_{c_1}}{dt} = -i_{L_2} \\ C_2 \dfrac{dv_{c_2}}{dt} = -i_{L_1} \end{cases} \tag{3.7}$$

3.4.1 Steady state Analysis

In steady state, the average voltages of the inductors over one switching cycle T are zero and the average currents of the capacitors over one switching cycle T are zero. Consequently, the capacitor voltages and inductor currents are deduced as follows:

$$\begin{cases} v_{c_1} = \dfrac{1-D}{1-2D} v_{in} \\ v_{c_2} = \dfrac{D}{1-2D} v_{in} \end{cases} \tag{3.8}$$

$$i_{L_1} = i_{L_2} = \frac{1-D}{1-2D} i_{load} \tag{3.9}$$

The DC-link peak voltage $\hat{v}_{dc}$can be derived from the sum of two capacitor voltages, $v_{c_1}$and v_{c_2}, by:

$$\hat{v}_{dc} = v_{c_1} + v_{c_2} = \frac{1}{1-2D} v_{in} = B v_{in} \tag{3.10}$$

where $B \geq 1$ is the boost factor resulting from the shoot through period. With regards to the Ac-side of the Topology B, the peak phase voltage can be written as

$$\hat{v}_o = m_c \frac{v_{dc}}{2} = \frac{m_c}{1-2D} \cdot \frac{v_{in}}{2} = G_c \frac{v_{in}}{2} \tag{3.11}$$

where m_c and G_c are the inverter modulation index and total voltage gain of the Topology B, respectively.

3.4.2 Simple Boost Control Method

In Simple Boost Control (SBC) method, gate pulses are generated by comparing three sinusoidal reference signals and two constant voltage envelopes with the triangular carrier wave. When the magnitude of the triangular carrier wave becomes higher than or equal to the upper envelope or lower than or equal to the lower envelope, shoot through pulses are produced. The Figure 3.11 shows the SBC technique.

This technique is used because it proposes constant shoot through duty cycle that results in lower inductor ripple which requires lower inductance values.

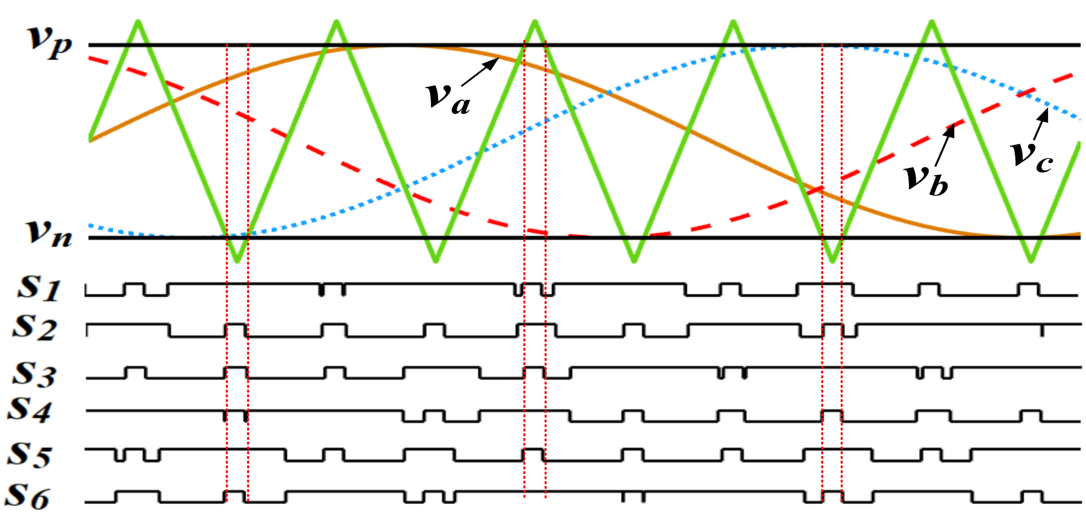

Figure 3.11: The wave-forms of SBC technique.

3.4.3 Model Validation

A simulation was carried out to validate the model of Topology B. The simulation parameters are $L_1 = L_2 = 230$ μH; $C_1 = C_2 = 2.2$ mF and other parameters are the same used for Topology A model validation. The control scheme is shown in section V. The following Figure 3.12 and 3.13 represent respectively the v_{dc} voltage and i_{L1} current and their references.

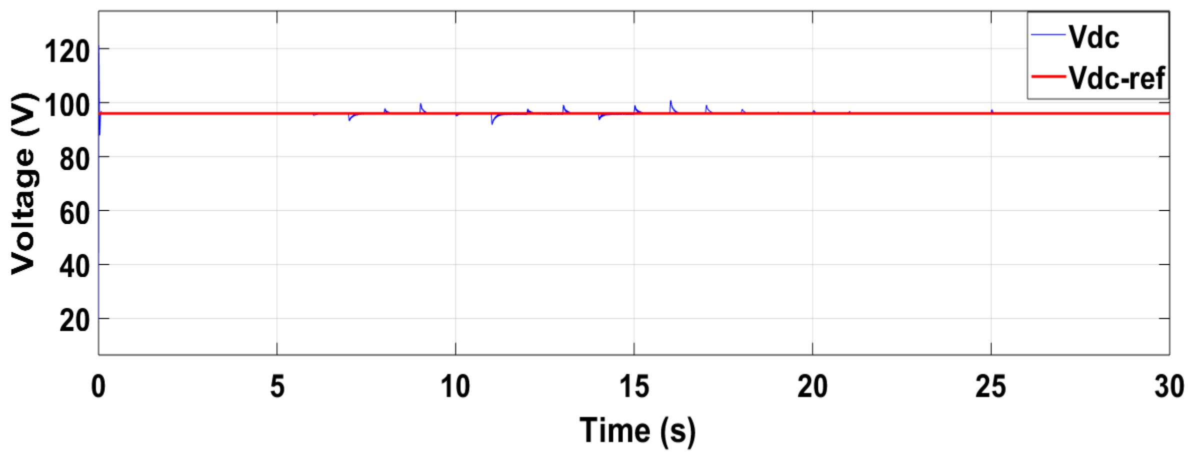

Figure 3.12: The v_{dc} voltage and its reference.

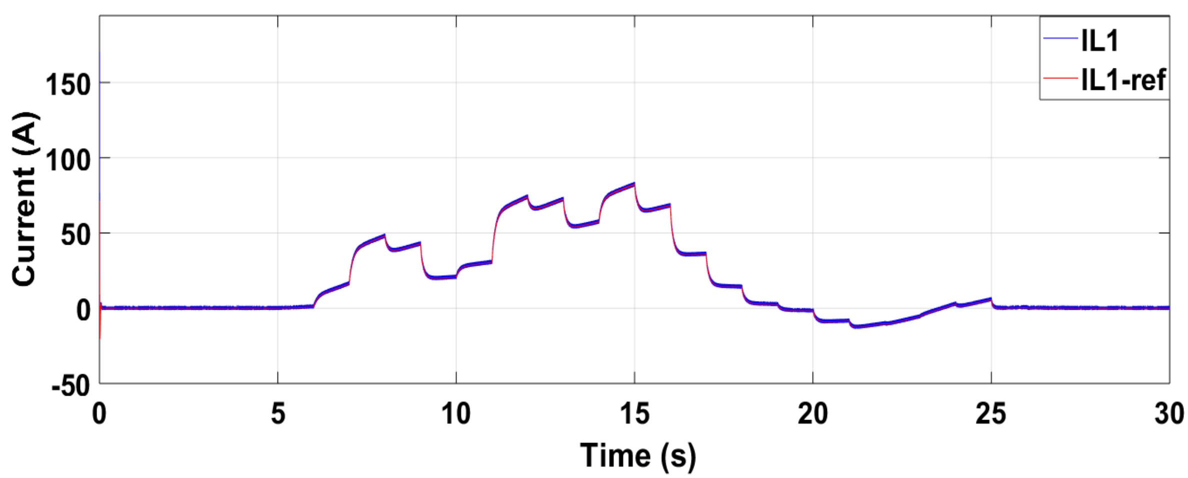

Figure 3.13: The i_{L1} current and its reference.

3.5 PI-Based Controllers Design

Cascade PI controllers can be designed to achieve speed control and disturbance rejection. Figures 3.14 and 3.15 show the speed control scheme of the Topology A and Topology B.

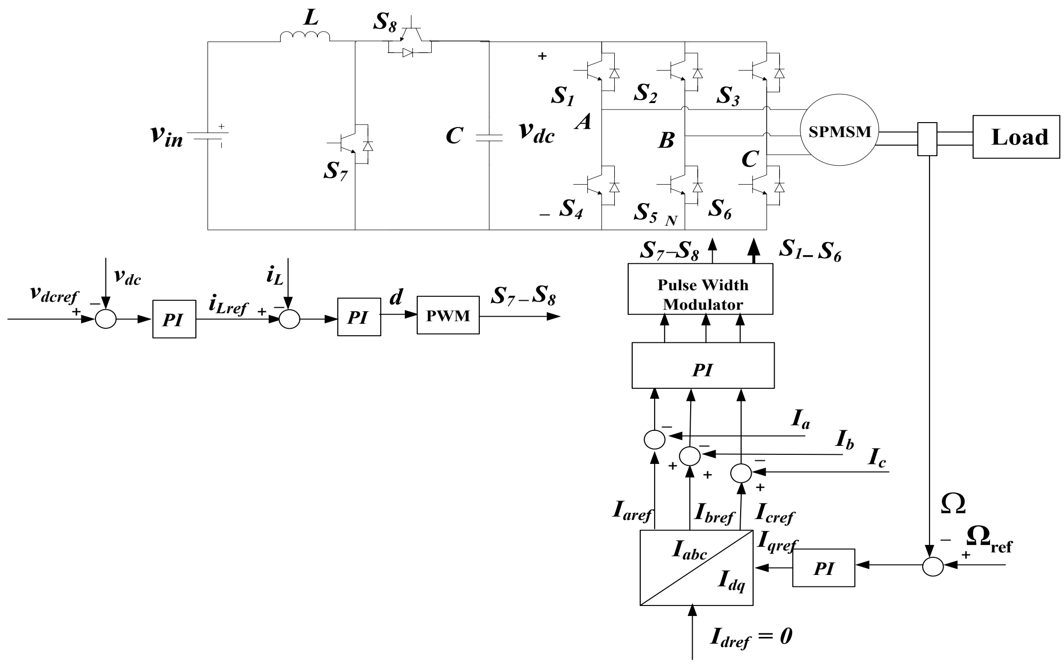

Figure 3.14: Speed control scheme using PI controllers for the Topology A.

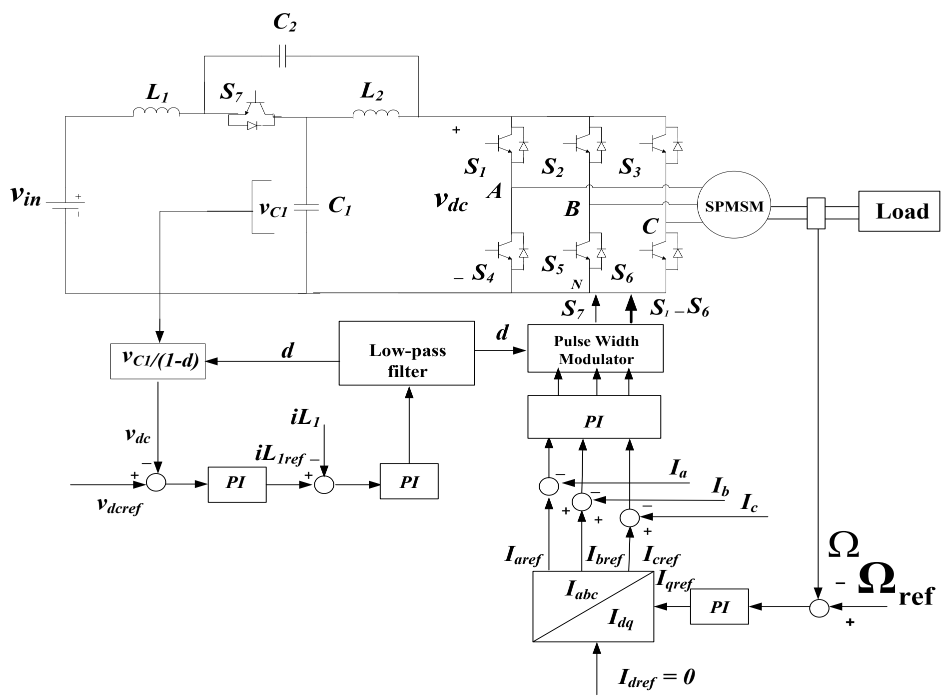

Figure 3.15: Speed control scheme using PI controllers for the Topology B.

3.6 Simulation and Comparative Results

Simulations have been performed for the comparison between the Topology A and Topology B with the same parameters used in Sections 3.3 and 3.4.

Figure 3.16 shows the measured efficiencies for the Topology A and Topology B. The inverter efficiency, which permits the comparison of effectiveness, is defined as the ratio of the output power in the fundamental component to the input power. The efficiencies of the inverters are computed with different output load by

$$\eta = \frac{P_{out}}{P_{in}} \tag{3.12}$$

where the fundamental output power P_{out}, and input power P_{in} are obtained using the MATLAB/Simulink. The comparison results can be concluded that the Topology B shows higher efficiency than the two-stage inverter for the whole operating power range.

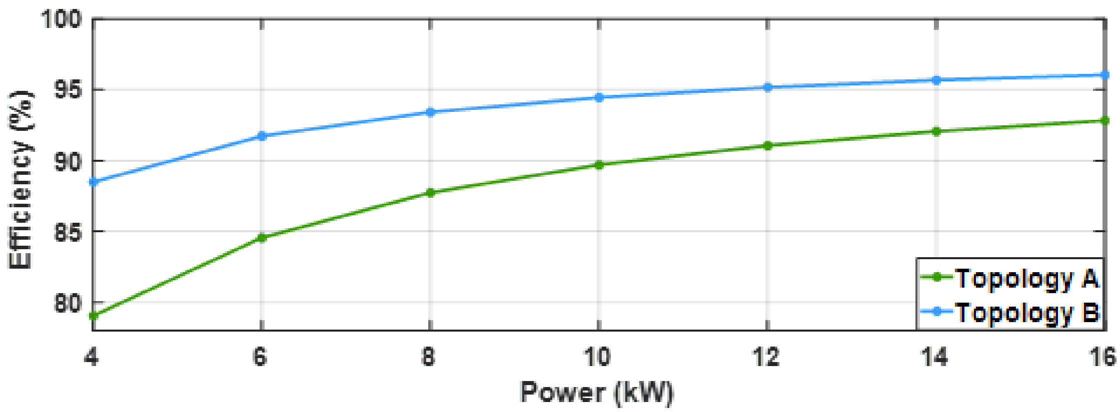

Figure 3.16: Measured efficiencies of the Topology A and Topology B.

During ON state and shoot-through state, the Topology A and the Topology B inductor current increases and their current ripple factor can be expressed as

$$\gamma_A = \gamma_B = \frac{\Delta I}{I} = \frac{V_L \Delta T}{I_L L} \tag{3.13}$$

where ΔT is ON state time for Topology A and represents the shoot-through time for Topology B, ΔI is the current variation, V_L is the voltage across the inductor, I_L is the average inductor current and L the inductance. The calculation of the ripple current factor using this equation gives γ_A= 14 % and γ_B= 4%.

The following section shows the comparison of the voltage gain between Topology A and Topology B. The voltage gain of Topology A is less than that of Topology B as illustrated in Figure 3.17.

Therefore, the Topology B limits excessive voltage stress across the inverter switches than Topology A.

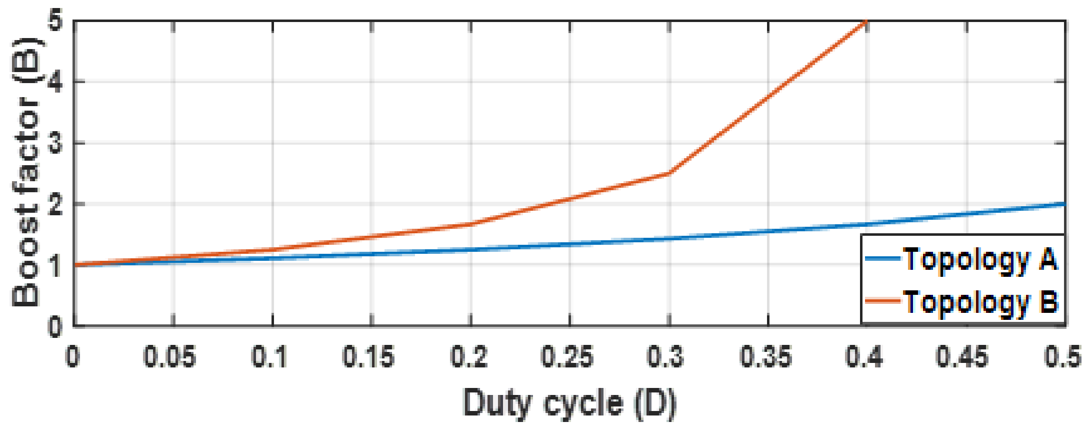

Figure 3.17: Comparison of Topology A and Topology B boost factor.

The following section Table 3.1 also gives the comparison of Topology A and Topology B.

Table 3.1: Comparison results

Inverter Type	Topology A	Topology B
Input voltage (V)	48	48
Inverter voltage Vdc (RMS)	96	96
Maximum Load current	118	117
Total number of switches used	8	7
Conversion stage	2	1
Current ripple of inductor	14 %	4 %

This Table 3.1 illustrates that the Topology B is more convenient for utilizing in EV system compared to Topology A as it utilizes less controller circuit and has best performance.

3.7 Conclusion

The simulation and comparative results show that the Topology B has best performance than Topology A. The results point out the ability of the inverters to respond quickly to the load and the input voltage, where the transient and steady state response are comparable for both inverters. These results verify the Topology B as an alternative inverter for electric vehicle. The disparity of voltage levels and currents between the sources (fuel cell, batteries, supercapacitors) and the loads of the electric vehicle (traction motor, auxiliaries) requires the use of power converters. This kind of architecture is therefore essential for on-board energy management in multi-source vehicles. Hence the future work is to use Topology B for energy management in multisource electric vehicle.

3.8 Acknowledgment

This work was supported by the Canada Research Chairs Program, the Natural Sciences and Engineering Research Council of Canada, and the 14e Commission de Coopération Québec-Vietnam. This work was also partially supported by projects UID/MULTI/00308/2013 and by the European Regional Development Fund through the COMPETE 2020 Program and FCT – Portuguese Foundation for Science and Technology within project MANAGER (POCI-01-0145- FEDER-028040).

Chapter 4 Comparison of Different Power Train Topologies for an Off-Road Electric Vehicle

Original Title: Comparison of Different Power Train Topologies for an Off-Road Electric Vehicle.

Authors and affiliation :

- **Daouda Mande**: Ph.D. student, e-TESC Laboratory, Department of Electrical & Computer Engineering, University of Sherbrooke
- **João P. Trovão**: Professor, e-TESC Laboratory, Department of Electrical & Computer Engineering, University of Sherbrooke
- **Ruben Gonzalez Rubio**: Professor, eXit Laboratory, Department of Electrical & Computer Engineering, University of Sherbrooke
- **Minh C. Ta**: Professor, e-TESC Laboratory, Department of Electrical & Computer Engineering, University of Sherbrooke

Date of Acceptance: **14 October 2019**

State of acceptance: Published

Reference: 2019 IEEE Vehicle Power and Propulsion Conference (VPPC),

DOI: 10.1109/VPPC46532.2019.8952175

Summary

Content: This article provides a comparative study between different power train topologies regarding aging index factors for an off-road EV. The studied power train topologies are battery pack supplying directly the motor-drive, two-stage inverter motor-drive and embedded QZSI motor-drive. The comparison is conducted in terms of the transient and steady state performances and the battery aging performance indexes for an EV considering the same on-board energy capacity. The modelling and the control design for both topologies are also presented and discussed. Simulation investigations are performed to verify the different topologies.

Results: The simulation and comparative results prove that embedded QZSI has better performance than the other topologies. The results demonstrate that under the same operating conditions, the transient and the steady state performances of different topologies are comparable. However, the embedded QZSI produces better aging performance index in terms of root-mean-square of the current, average values of the battery currents than other topologies. Embedded QZSI and two-stage inverter reduce RMS, average values with a slight superiority for embedded QZSI for standard deviation and variation coefficient. Embedded QZSI can contribute to increase the lifetime of the battery used for multi-source EV traction purpose.

Contribution to this thesis: This chapter details and proves QZSI topology as an alternative inverter taking into consideration the lifetime of the battery used for multi-source off-road EV traction purpose. Chapter 4 contributes to prove that the QZSI is a good candidate topology to be used in multi-source EV system. Rearranged topology of QZSI can be essential for on-board energy management in multi-source off-road EV.

Abstract

This paper deal with a comparative study between different power train topologies regarding batteries aging index factors for an off-road electric vehicle (EV) applications. The studied power train topologies are battery pack supplying directly the motor-drive (original), two-stage inverter motor-drive and embedded quazi-Z-source inverter motor-drive. The comparison is conducted in terms of battery aging performance indexes for an electric vehicle considering the same on-board energy capacity. The modelling and the control design for both topologies are presented and discussed. Simulation investigations are performed to verify the different topologies. It is shown that the embedded quasi-Z-source inverter produces better aging performance index in terms of root-mean-square of the current, average values of the battery currents than other topologies. Embedded quasi-Z-source inverter and two-stage inverter reduce RMS, average values with a slight superiority for embedded quasi-Z-source inverter for standard deviation and variation coefficient. The results demonstrate that under the same operating conditions, the transient and the steady state performances of different topologies are comparable. These results prove that embedded quasi-Z-source inverter is a good candidate topology to be used in multi-source electric vehicle system.

Keywords: Embedded quasi-Z-source inverter; DC-DC boost converter; voltage source inverter; sinusoidal pulse width modulation; maximum constant boost control; aging index factors.

4.1 Introduction

World energy demand is growing strongly under the effect of demographics and economic development. This strong demand leads to a scarcity of fossil fuels and ecological concerns. The automotive sector is at the heart of these issues and is involved in the research and development of technologies related to electric vehicles (EVs). The power converter is one of the key research topics as it represents a major element of the powertrain in electric vehicle (EV). Current research in power electronics in the field of automotive applications including EVs and the hybrid EVs has focused on new DC-DC converters and inverters topologies. DC-DC converters are essentially used for many varieties of applications including EVs [88], hybrid EV, plug-in-hybrid EV, fuel cell vehicles, multi-source EV (battery and supercapacitor), photovoltaic power systems, etc.

The demanded voltage gain of the bidirectional conventional two-stage inverter to boost the input voltage normally needs higher duty cycle. That contributes to high conduction losses, higher voltage and current stresses. The two-stage inverter with its requirement component also increases the cost and affects the miniaturization of the system. To solve these problems of two-stage inverter, a Z-source inverter (ZSI) was firstly proposed by Peng in [89]. ZSI is gotten by coupling an LC impedance network with the DC source to form a new source, named Z-source, that is a kind of impedance source. The concept of Z-source can be applied for all power conversions. ZSI has a buck-boost capability which enables it to have wide variety of voltage range. Many control strategies have been used for Z-source network. In the literature, a lot of small-signal analyses and mathematical models are presented for dynamical behaviour of the Z-source network system studies. These models permit to implement different closed loop control strategies with different complexities for various applications. Regarding the control of ZSI switches, traditional PWM method, the simple boost method, maximum boost method, maximum constant boost method and space vector method are the switching control strategies widely proposed. In the literature, several modified PWM control techniques for ZSI have been also proposed [89].

Otherwise, ZSI have different configurations. With its proprieties and the above remarks, the development of EV power train using ZSI can increase the battery lifetime and its performance. The usage mode of the battery affects profoundly its lifetime [90]. The variations of large and frequent currents highly stress the battery [91]. The influence of different charging current rates and cut-off voltages on the aging mechanism of batteries has been presented in [92]. It proved that the battery degradation speed accelerates greatly when the charging stress exceeds some critical value. The computation of the aging performance indexes of the battery enables to quantify the effect of the current. Then, the control methods of the current delivered by the battery can also seriously affect its performance. In [93], the aging index of the battery is used to evaluate the performance of the model predictive control using the nonuniform sampling time concept and other model predictive control approaches.

By rearranging the components in the Z-source network, a new topology named embedded quasi-Z-source-inverter is proposed. Embedded quasi-Z-source inverter, already proposed in the literature [39], is a promising architecture as it presents the advantage of having a continuous input current, two inputs source voltage and retain all the merits of the ZSI, which makes it a good candidate for multi-source EV applications [40].

This paper presents a comparison between different power train topologies regarding aging index factors which can be more useful for multi-source off-road electric vehicle. Section 4.2 introduces the EV under study and the original power train modelling. In Section 4.3, the two-stage inverter configuration and simulation results are presented. Section 4.4 presents the embedded quasi-Z-source inverter with the results of simulation. In Section 4.5, the comparison of the different architectures in terms of aging performance indexes of the battery is presented. Conclusion is drawn in Section 4.6.

4.2 Vehicle and Powertrain Modelling

4.2.1 Electric Vehicle Specifications

The reference electric vehicle is the e-TESC 4W platform as presented in Figure 4.1. The main parameters are presented in Table 4.1. It is an off-road EV supplied by a battery pack of lithium-iron magnesium phosphate ($LiFeMgPO4$) cells.

Electricity storage system and an electric motor with its controller constitutes the core of EV traction system. EV can be represented by an electric energy conversion chain upstream of the drive train [7]. The inverter, the two-stage inverter and the embedded quasi-Z-source inverter represent different power train topologies which can be used to supply the EV under study. The traditional inverter is used for original power train where battery pack directly supplies the motor-drive. Two-stage inverter is composed by a bidirectional DC-DC converter and a traditional 3-phase inverter as presented in Figure

4.2. Embedded quasi-Z-source inverter is a topology whose function is to convert DC input voltage to AC output voltage with desired magnitude and frequency.

During the propulsion mode, the voltage from the energy storage systems is converted by the two-stage inverter into 3-phase voltage to drive the motor and produce the required torque. During the regenerative braking, the two-stage inverter behaves as a step-down inverter to charge the storage systems. The motion of EV depends on the torque applied to overcome the motor resistant torque.

Figure 4.1: e-TESC 4W platform (adapted from BRP e-Commander vehicle).

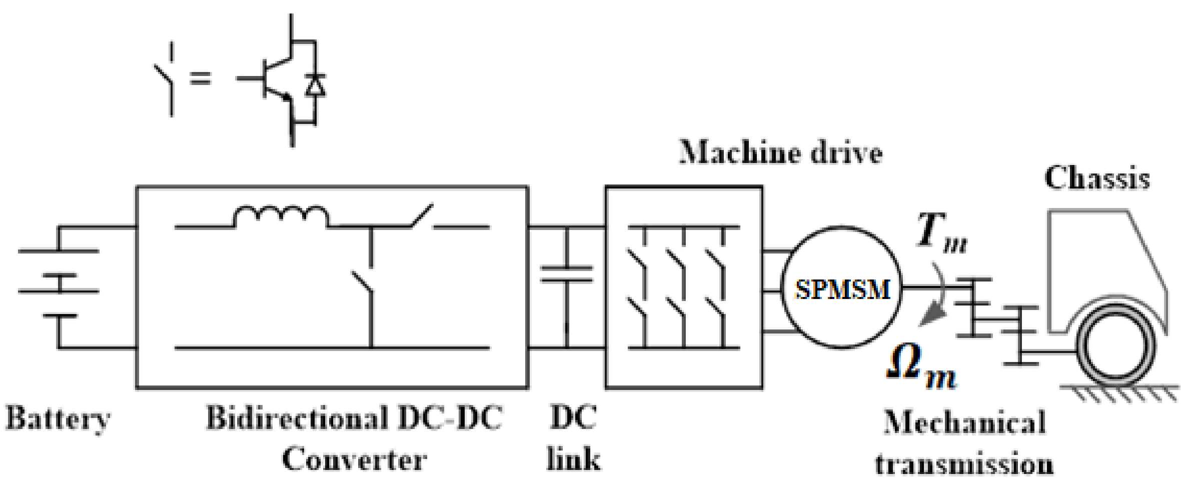

Figure 4.2: Two-stage inverter for electric traction system.

Table 4.1: EV PLATFORM PARAMETERS

Parameters	Variable Name	Values
Vehicle (e-Commander)		
Total mass of the EV	M_{veh}	857 kg
Aerodynamic standard	$c_x A$	1.3 m^2
Rolling coefficient	k_{roll}	0.035
Air density (at 20^{O} C)	ρ	1.223 kg/m^3
Motor to wheel transmission ratio	G_{tr}	20.5
Efficiency of the transmission	η_{tran}	0.87
Wheel radius	R_{wh}	0.3175 m
SPMSM parameters		
Phase inductance	L_d, L_q	1 mH
Phase resistance	r_s	0.08 Ω
Number of pole pair	p	2
Rotor inertia	J	1 kg.m^2
Magnet flux linkage	ψ_f	0.1 Wb
Rated power	P_r	15 kW
Original configuration parameters		
Inductance	L	1 **µH**
Capacitance	C	4.5 mF
Switching frequency	f_s	10 kHz
Two-stage inverter parameters		
Inductance	L	0.2 mH
Capacitance	C	4.5 mF
Switching frequency	f_s	50 kHz
Embedded quasi-Z-source inverter parameters		
Inductance	L_1, L_2	230 µH
Capacitance	C_1, C_2	2.2 mF
Switching frequency	f_s	10 kHz
Batteries (Lithium-ion valence battery cells)		
Cell capacity	$C_{batcell}$	40 Ah
Cell nominal voltage	$v_{batcellnom}$	12.8 V
Cell minimum voltage (at 20% SoC)	$v_{batcellmin}$	10 V
Cell equivalent serial resistance	$r_{batcell}$	15 $m\Omega$
Number of cells in series	$n_{batcellse}$	4
Number of branches in parallel	$n_{batcellpa}$	4

4.2.2 Modelling of Original Configuration Motor Drive

In our study, surface permanent magnet synchronous machine (SPMSM) is used as a traction electric motor. It is a synchronous motor with 3-phases and its state space representation can be described as presented in [8].

4.2.3 Control Technique of the Inverter

The sinusoidal pulse width modulation (SPWM) technique is used to control the inverter. The SPWM technique consists of making the comparison between a carrier signal and a pure sinusoidal modulation signal. The intersections between the sinusoidal waveform (v_a , v_b , and v_c) and the carrier waveform give the opening and closing times of the switches. The SPWM technique is shown in Figure 4.3. For decades, PWM inverter has been the most used in power electronics due to the simplicity of its circuit and rugged control scheme.

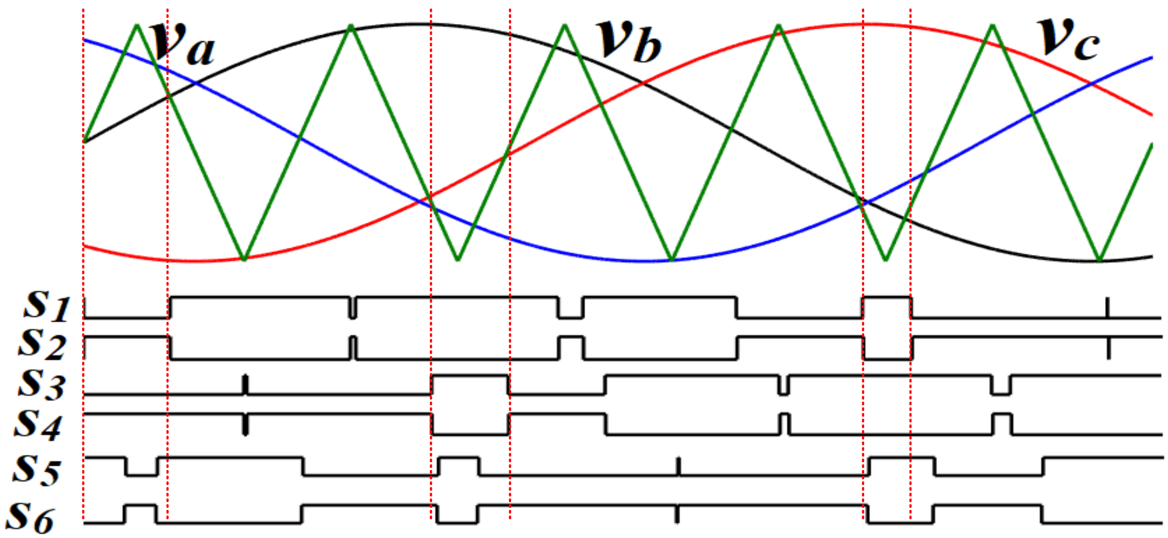

Figure 4.3: The wave-forms of SPWM technique for 3-phase inverter.

4.2.4 PI-based Controllers Design

To accomplish the speed control and disturbance rejection, cascade PI controllers have been designed. SPMSM with PI control technique is adopted based on the model of SPMSM. The 3-phase stator currents of the SPMSM are measured and converted into i_d and i_q currents. The actual rotating speed is compared with the given speed and the PI controller allows to obtain the reference current i_{qref}. i_{dref} is known as field weakening current and has been set to zero for this analysis. Currents i_{dref}, i_{qref} are also converted to the reference current i_{aref}, i_{bref}, i_{cref}. The measured and reference currents are compared, and the PI controller enables to generate the voltages using SPWM technique. The speed control schemes for the two-stage inverter and embedded quasi-Z-source inverter are shown in sections 4.3 and 4.4 respectively.

4.2.5 Simulation Results of Original Configuration

Simulations were performed for the last 90 s of NEDC driving cycles using the original configuration of an inverter supplied by a battery pack of 8s2p (s-series and p-parallel). The simulation results are obtained using SPWM control techniques presented in section 4.2.3 with a switching frequency of 10 kHz. Figure 4.4 and Figure 4.5 show the motor speed and torque waveforms respectively. The battery (4 batteries modules in series (4s)) current and DC bus voltage have been also presented in Figure 4.6.

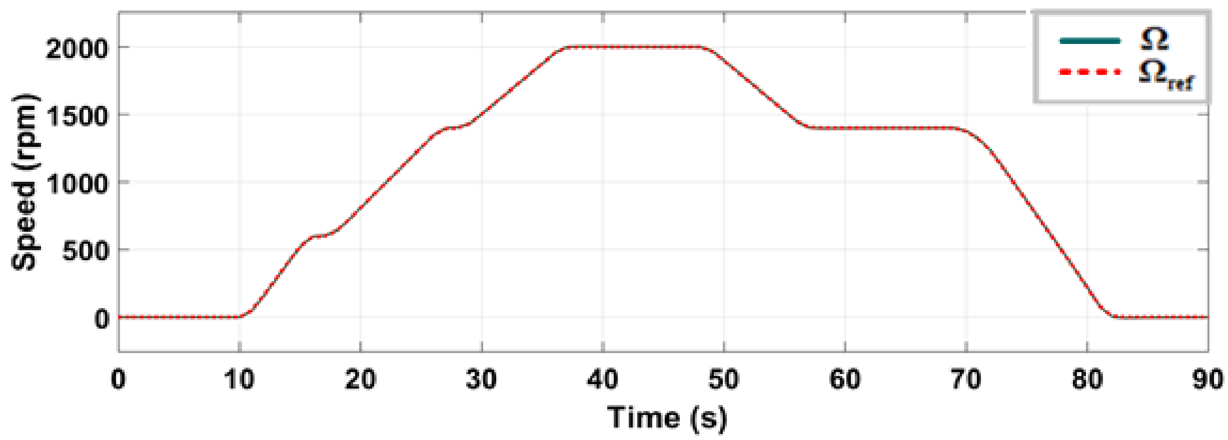

Figure 4.4: Motor speed and reference.

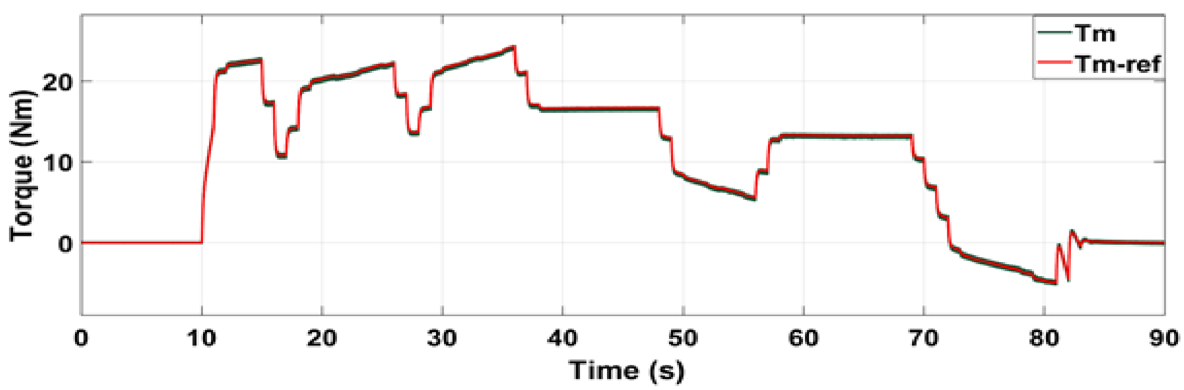

Figure 4.5: Motor torque and reference.

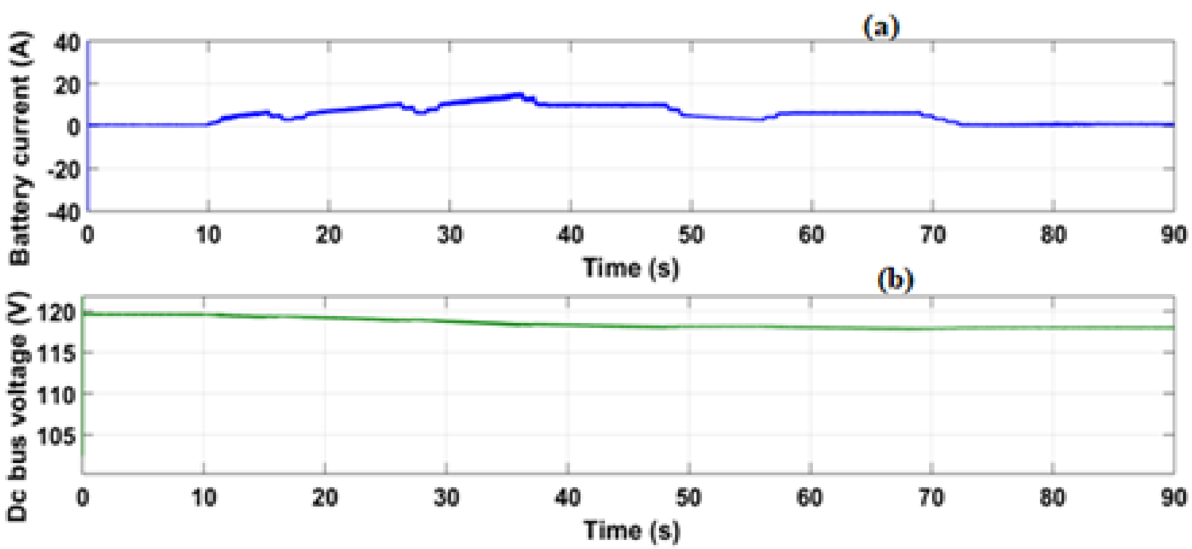

Figure 4.6: (a) Battery (4 batteries modules in series (4s)) current; (b) DC bus voltage.

4.3 Two-stage Inverter Topology

Figure 4.7 shows the configuration of two-stage inverter used for the comparison connected with a SPMSM where the input voltage is stepped up to 96 V. In this figure, one voltage source branch is equal to 4 batteries modules in series (4s). The battery configuration here is 4s4p. The bidirectional DC-DC boost converter shown in Figure 4.7 operates in two states: ON and OFF states when the switch S_7 is closed or opened, respectively [8].

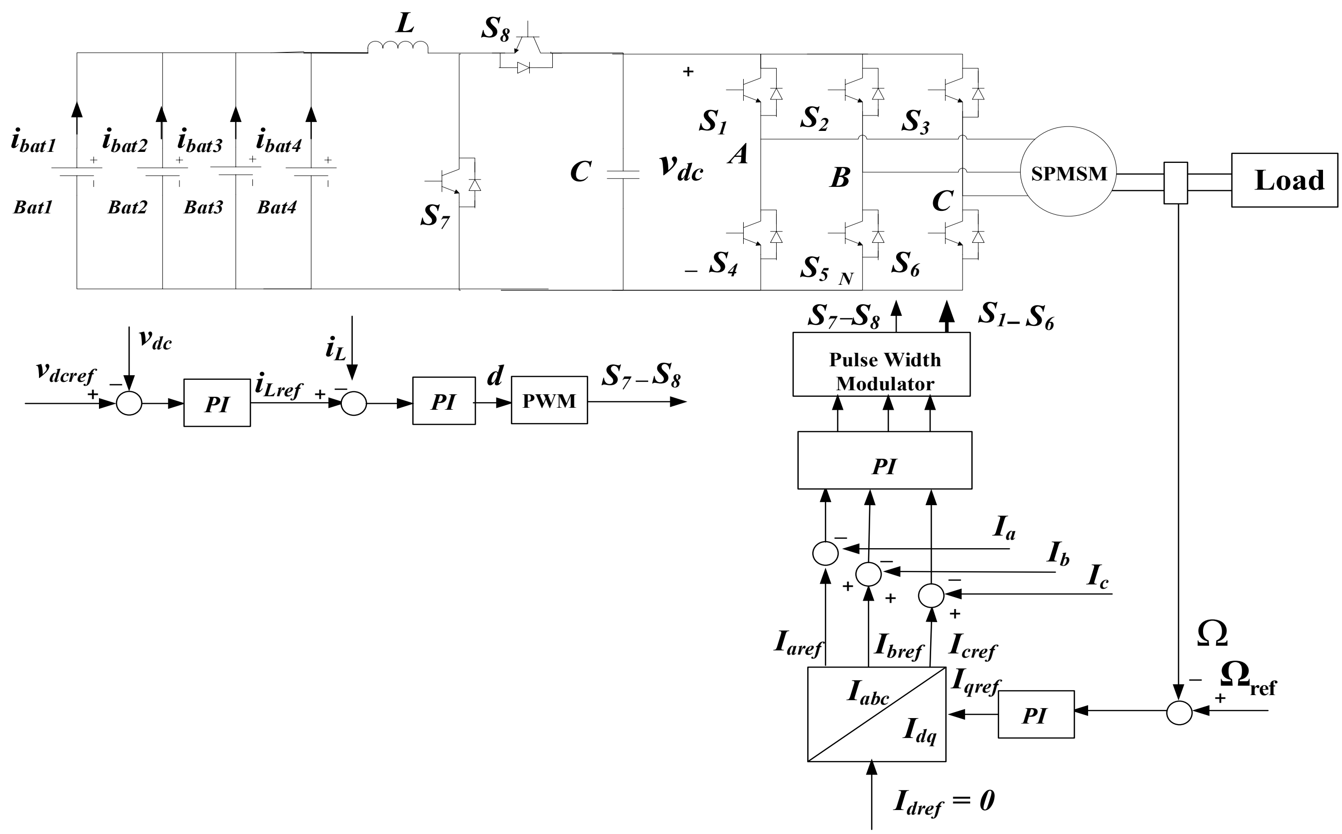

Figure 4.7: Speed control scheme with two-stage inverter.

4.3.1 Modelling of the Bidirectional DC-DC Boost Converter

During ON state, the input voltage charges the inductor, and the capacitor voltage feeds the load. During OFF state, the input voltage and the inductor voltage charge the capacitor and supply energy to the load. These conditions can be described by the equations given in [8]. During the steady state, the DC-link voltage v_{dc} can be determined as follows:

$$v_{dc} = \frac{v_{in}}{1-D} \tag{4.1}$$

The peak AC output voltage can also be calculated by

$$\hat{v}_o = m_c \frac{v_{dc}}{2} = \frac{m_c}{1-D} . \frac{v_{in}}{2} = G_c \frac{v_{in}}{2} \tag{4.2}$$

where m_c and G_c are the inverter modulation index and total voltage gain of the two-stage inverter, respectively.

4.3.2 Simulation Results of Two-Stage Inverter

A simulation was realized to validate the model of two-stage inverter. SPWM technique is used to control the two-stage inverter. Figures 4.8 and 4.9 show the speed and torque waveforms respectively. The v_{dc} voltage and i_L current with their references have been presented in Figures 4.10 and 4.11, respectively. The current i_{bat1} and the voltage v_{bat1} have been also shown in Figure 4.12.

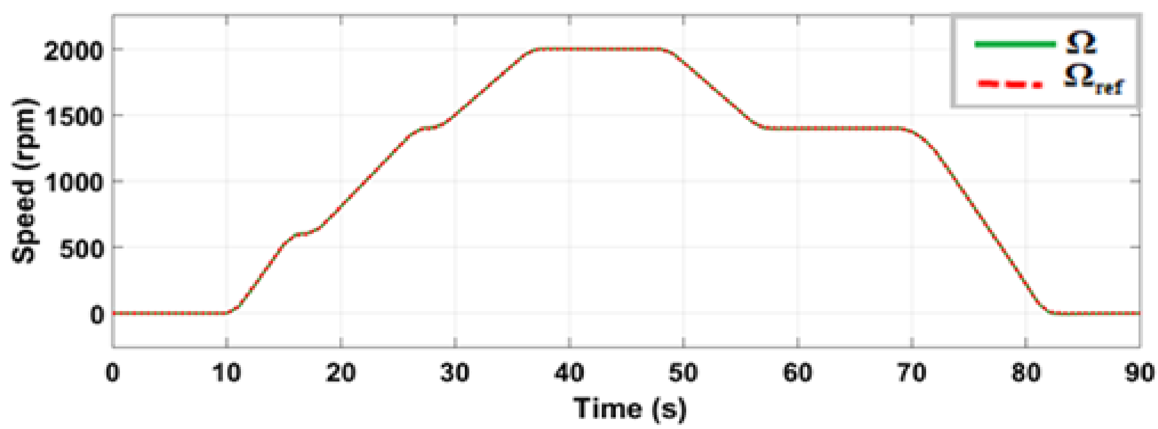

Figure 4.8: Motor speed and reference with two-stage inverter.

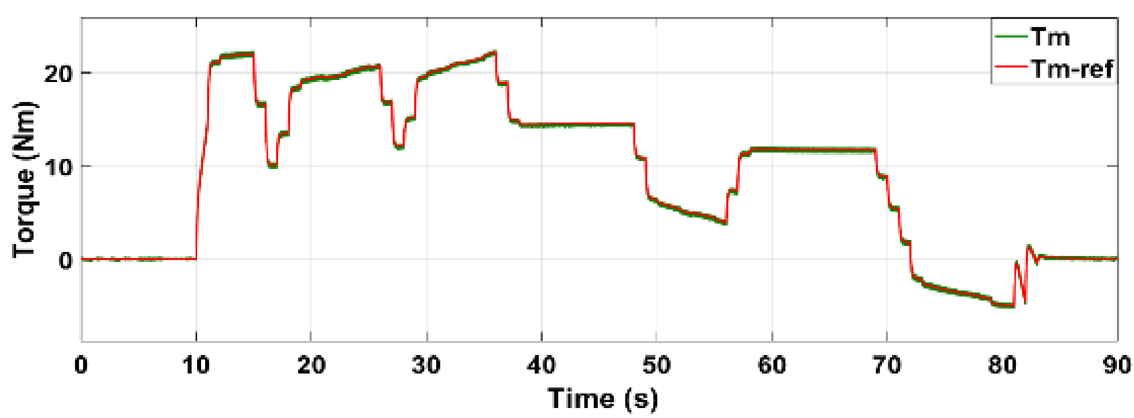

Figure 4.9: Motor torque and reference with two-stage inverter.

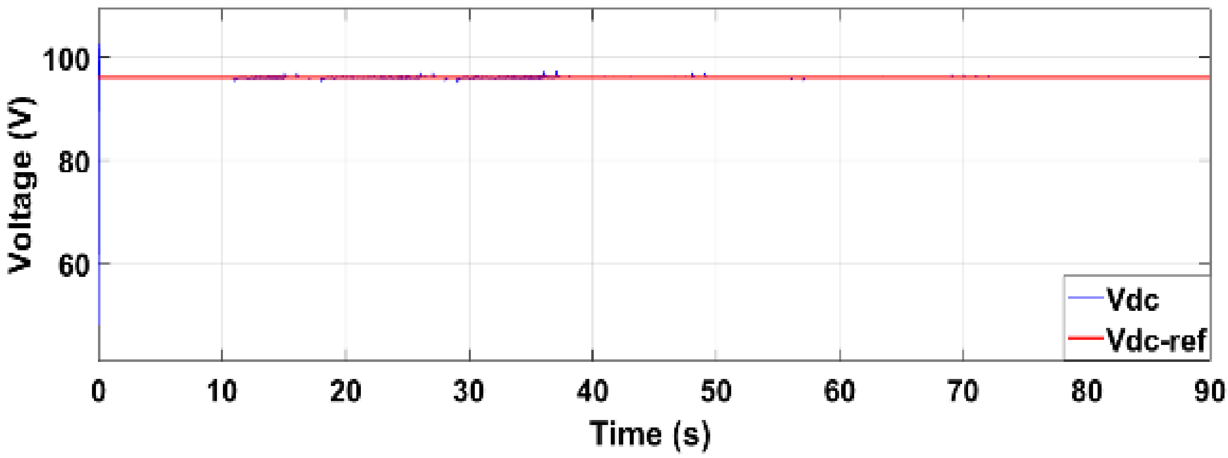

Figure 4.10: The v_{dc} voltage and its reference.

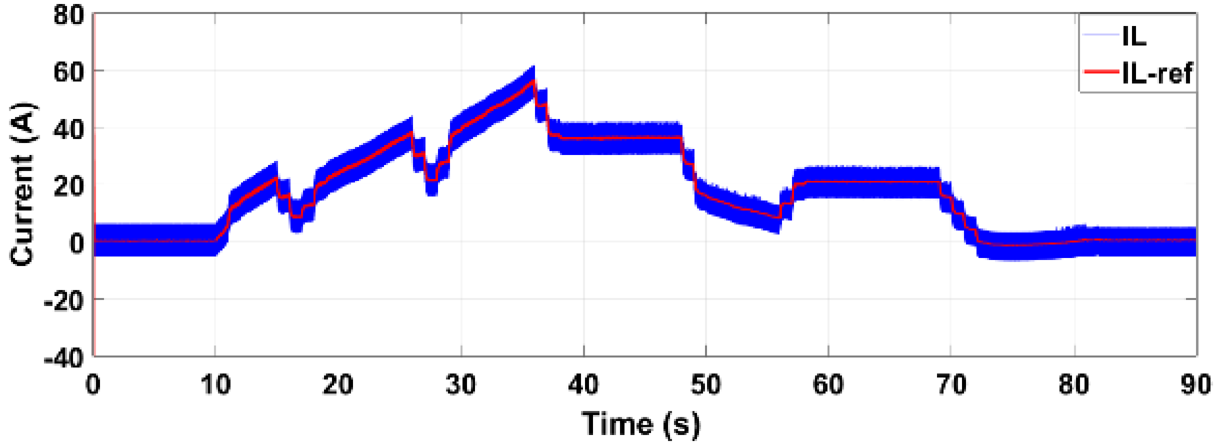

Figure 4.11: The i_L current and its reference.

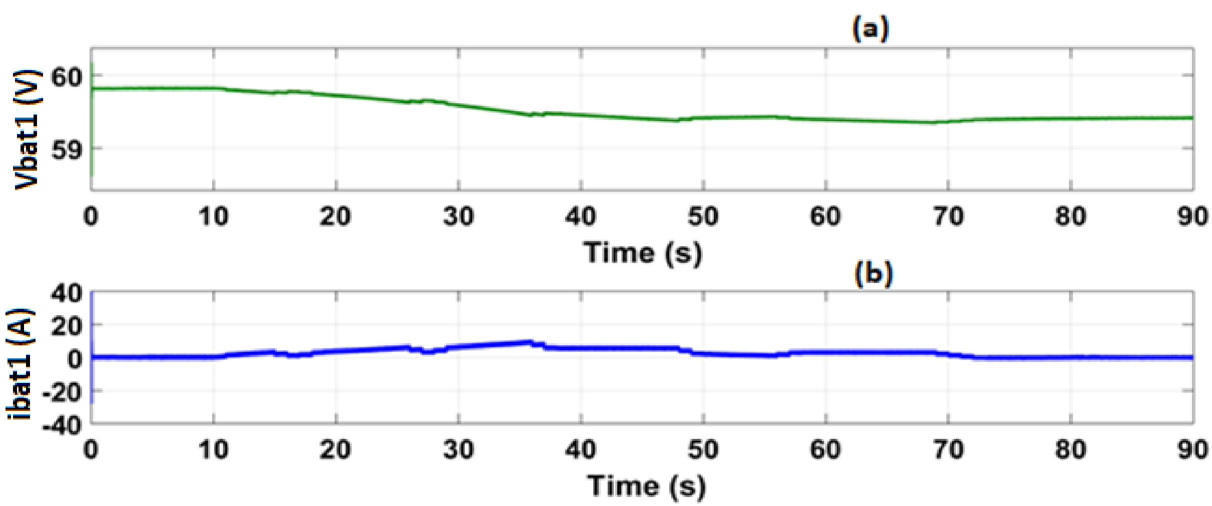

Figure 4.12: (a) Voltage v_{bat1}; (b) Current i_{bat1}.

4.4 Embedded Quasi-Z-Source Inverter Topology

Embedded quasi-Z-source inverter is a power electronic circuit whose function is to convert DC input voltage to AC output voltage with desired magnitude and frequency. Using the two control variables such as the shoot-through duty ratio and the modulation index, it can buck and boost the input voltage in a single stage as presented in [89]. It inherits the advantages of both quasi-Z-source inverter and embedded topology. The configuration of Embedded-quasi-Z source inverter connected with a SPMSM is proposed in Figure 4.13 where one voltage source represents 4 batteries modules in series (4s).

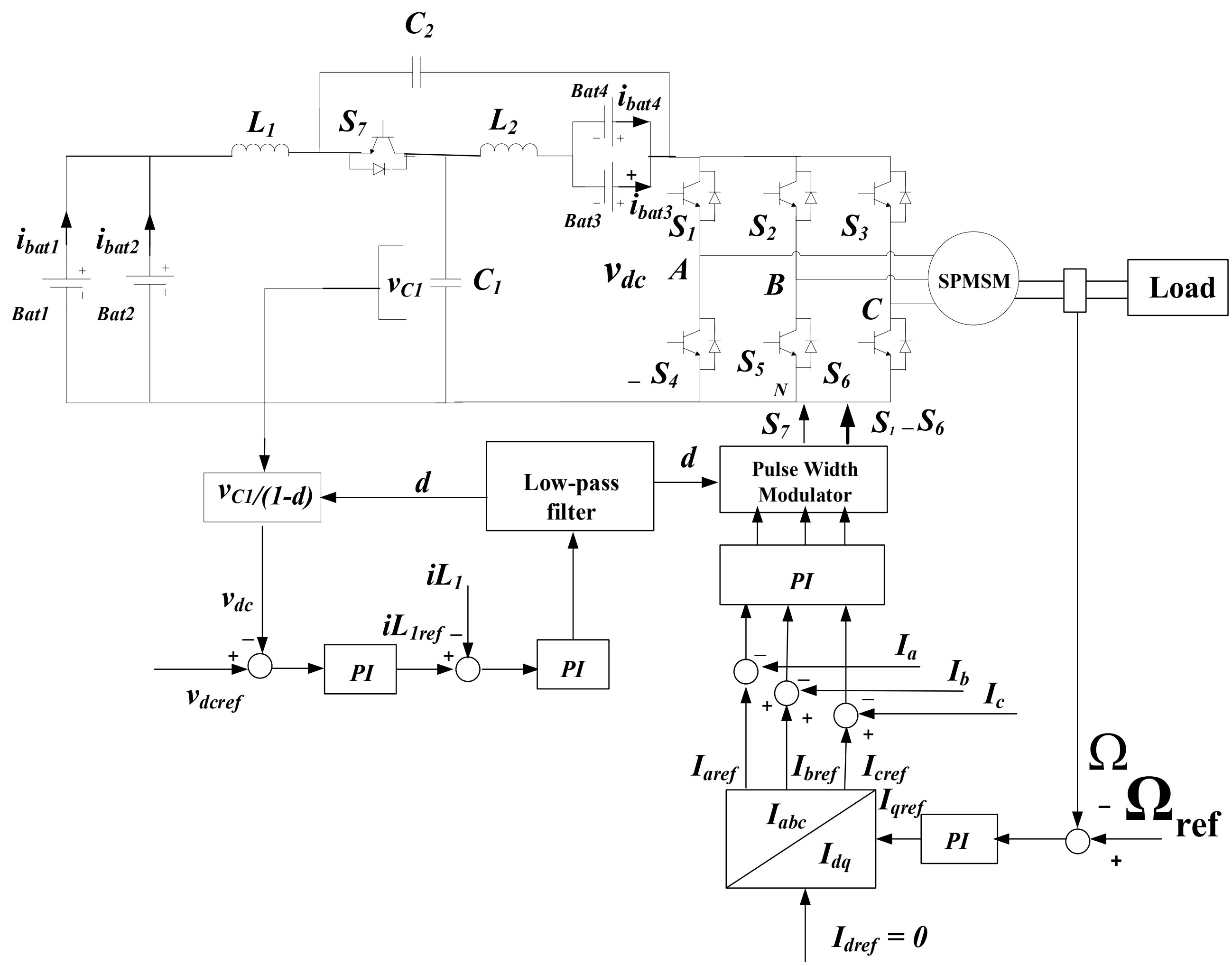

Figure 4.13: Speed control scheme with Embedded quasi-Z-source inverter.

4.4.1 Modelling of Embedded Quasi-Z-source Inverter

Figure 4.14 (a) and (b) present the equivalent circuits of embedded quasi-Z-source inverter operating in two states: non-shoot-through state and the shoot-through state, respectively. In these structural representations, all the voltages and the currents are defined. Let T a one switching cycle, T_0 the interval of the shoot-through state and T_1 the interval of non-shoot-through state; their relationship is $T_0 + T_1 = T$, and the shoot-through duty ratio D is given by $D = \frac{T_0}{T}$.

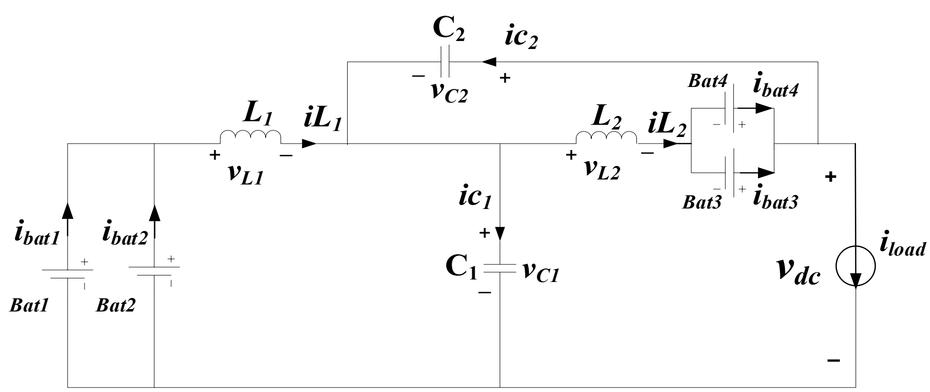

(a) Non-Shoot-through state

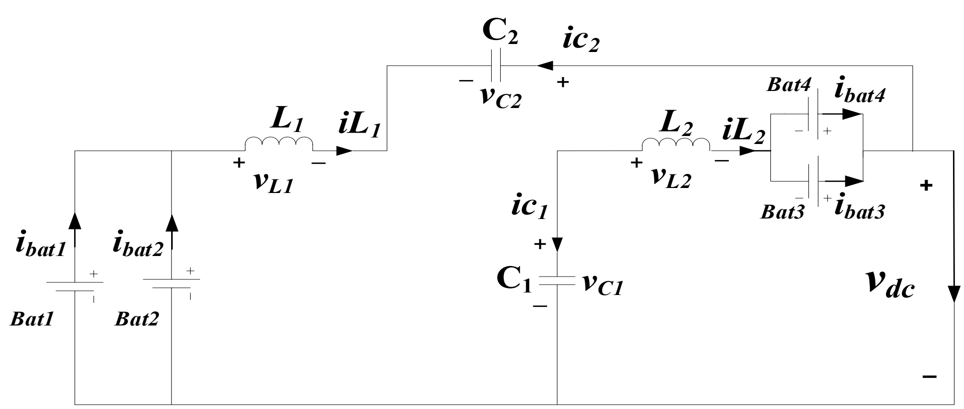

(b) Shoot-through state

Figure 4.14. The operation states of embedded quasi-Z-source inverter.

In Figure 4.14 (a), embedded quasi-Z-source inverter operates at the non-shoot-through state T_1. The dynamic equations are:

$$\begin{cases} L_1 \dfrac{di_{L_1}}{dt} = v_1 - v_{c_1} \\ L_2 \dfrac{di_{L_2}}{dt} = -v_{c_2} + v_2 \\ C_1 \dfrac{dv_{c_1}}{dt} = i_{L_1} - i_{load} \\ C_2 \dfrac{dv_{c_2}}{dt} = i_{L_2} - i_{load} \end{cases} \tag{4.3}$$

where v_1 and v_2 represent the two input voltages, so $v_1 = v_{bat1}$ and $v_2 = v_{bat3}$ in Figure 4.14. In Figure 4.14 (b), embedded quasi-Z-source inverter operates at the shoot-through state T_0. The dynamic equations are:

$$\begin{cases} L_1 \dfrac{di_{L_1}}{dt} = v_1 + v_{c_2} \\ L_2 \dfrac{di_{L_2}}{dt} = v_{c_1} + v_2 \\ C_1 \dfrac{dv_{c_1}}{dt} = -i_{L_2} \\ C_2 \dfrac{dv_{c_2}}{dt} = -i_{L_1} \end{cases} \tag{4.4}$$

In steady state, the average voltages of the inductors and the average currents of the capacitors over one switching cycle *T* are zero. Consequently, the capacitor voltages and inductor currents are deduced as follows:

$$\begin{cases} v_{c_1} = \dfrac{1-D}{1-2D} v_1 + \dfrac{D}{1-2D} v_2 \\ v_{c_2} = \dfrac{D}{1-2D} v_1 + \dfrac{1-D}{1-2D} v_2 \end{cases} \tag{4.5}$$

$$i_{L_1} = i_{L_2} = \frac{1-D}{1-2D} i_{load} \tag{4.6}$$

The DC-link peak voltage $\hat{v}_{dc}$ can be derived from the sum of two capacitor voltages $v_{c_1}$and v_{c_2} by:

$$\hat{v}_{dc} = v_{c_1} + v_{c_2} = \frac{1}{1-2D}(v_1 + v_2) = B(v_1 + v_2) \tag{4.7}$$

where $B \geq 1$ is the boost factor resulting from the shoot through period. With regards to the AC side of embedded quasi-Z-source inverter, the peak phase voltage can be written as

$$\hat{v}_o = m_e \frac{\hat{v}_{dc}}{2} = \frac{m_e}{1-2D} . \frac{(v_1 + v_2)}{2} = G_e \frac{(v_1 + v_2)}{2} \tag{4.8}$$

where m_e and G_e are the embedded quasi-Z-source inverter modulation index and its total voltage gain, respectively.

4.4.2 Maximum Constant Boost Control Method

Maximum constant boost control (MCBC) method consists of comparing three sinusoidal reference signals and two constant voltage envelopes (v_p and v_n) with the triangular carrier wave. Moreover, the third harmonic is injected into the reference. Figure 4.15 describes the MCBC technique. The switch S_7 of embedded quasi-Z-source inverter operates to a bidirectional power flow. It is controlled to have signal that is complementary with the shoot-through signal of the inverter.

This technique is used because it proposes the maximum voltage gain, reduce the volume, the cost of the inverter and the voltage stress across the switches.

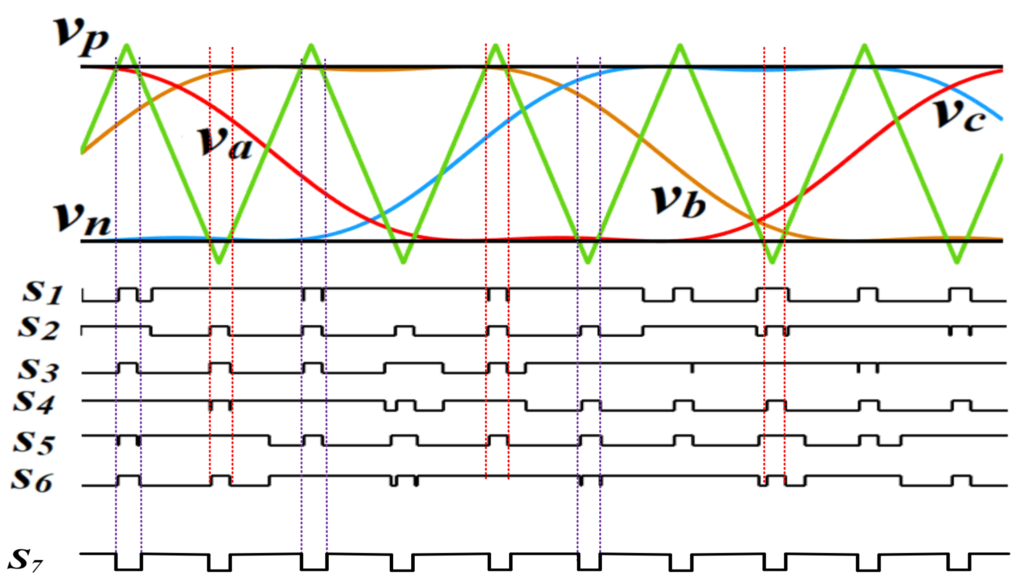

Figure 4. 15: The MCBC technique with switch s_7 drive signal.

4.4.3 Simulation Results of Embedded Quasi-Z-Source Inverter

A simulation was performed to validate the model of embedded quasi-Z-source inverter. Figures 4.16 and 4.17 show the speed and torque waveforms respectively. The v_{dc} peak voltage and i_{L1} current with their references have been presented in Figures 4.18 and 4.19 respectively. Figures 4.20 and Figure 4.21 present the currents i_{bat1}, i_{bat3} and the voltages v_{bat1}, v_{bat3}, respectively.

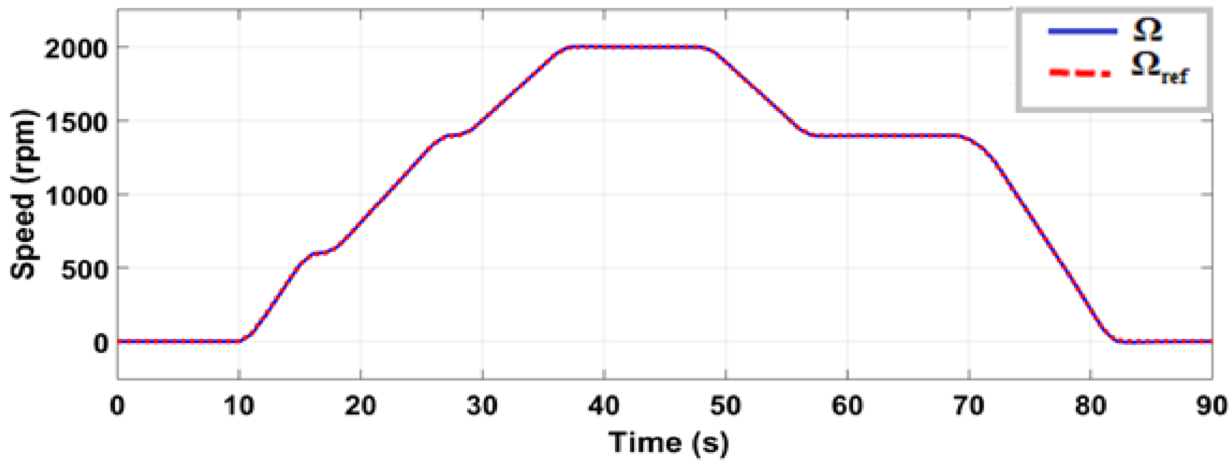

Figure 4.16: Motor speed and reference with embedded quasi-Z-source inverter.

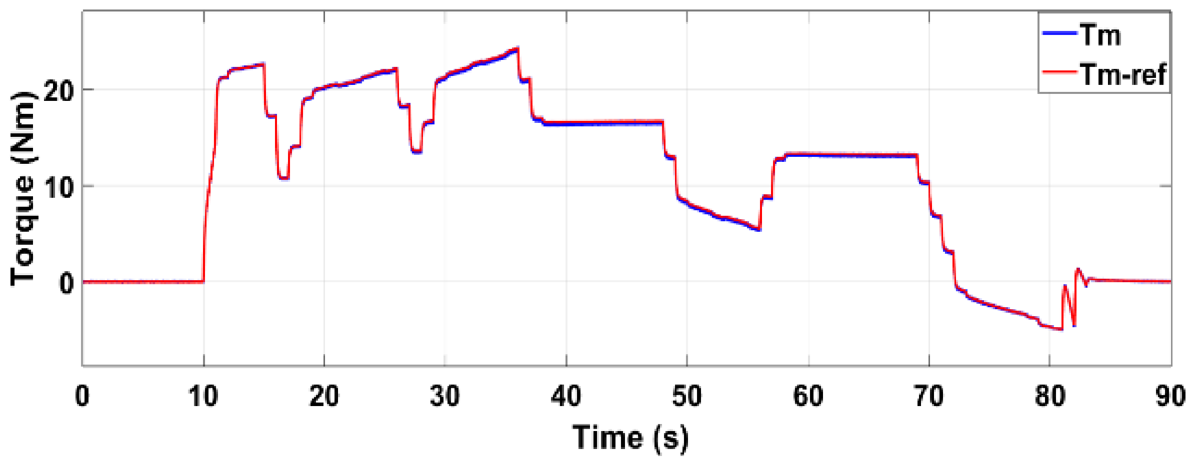

Figure 4.17: Motor torque and reference with embedded quasi-Z-source inverter.

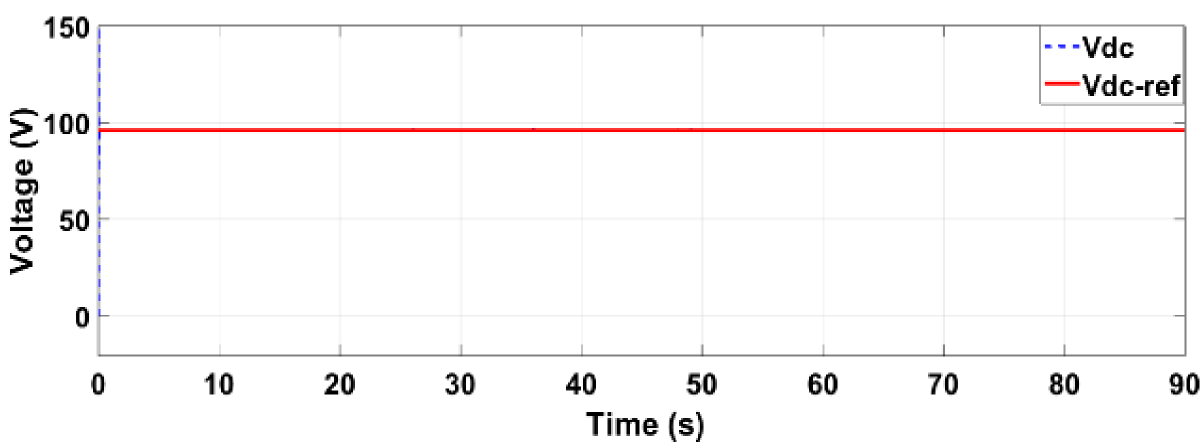

Figure 4.18: The v_{dc} peak voltage and its reference.

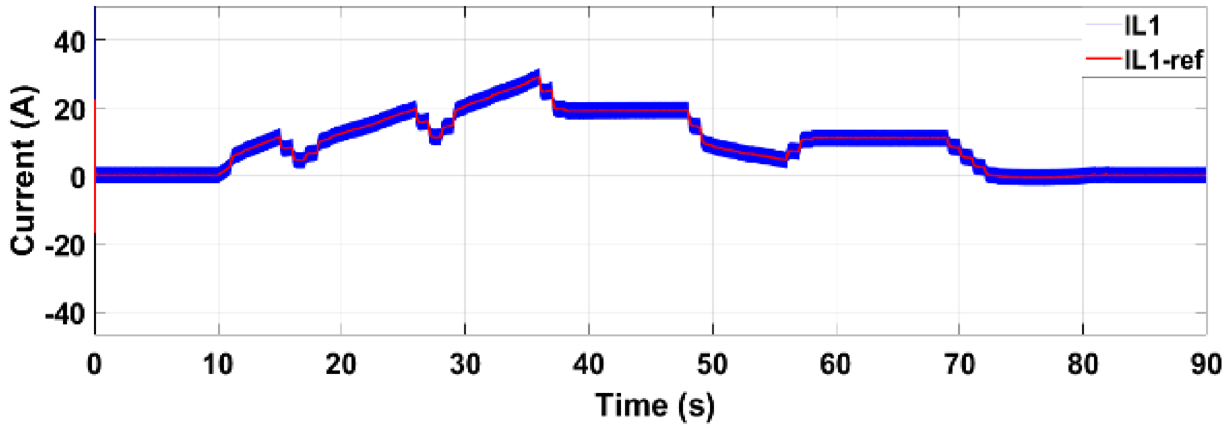

Figure 4.19: The i_{L1} current and its reference.

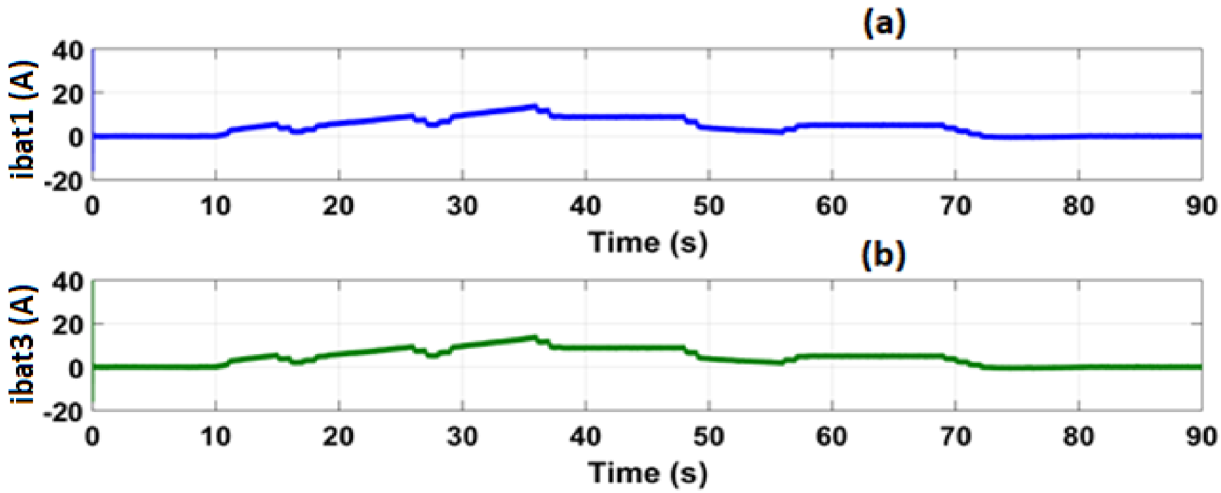

Figure 4.20: (a) Current i_{bat1}; (b) Current i_{bat3}.

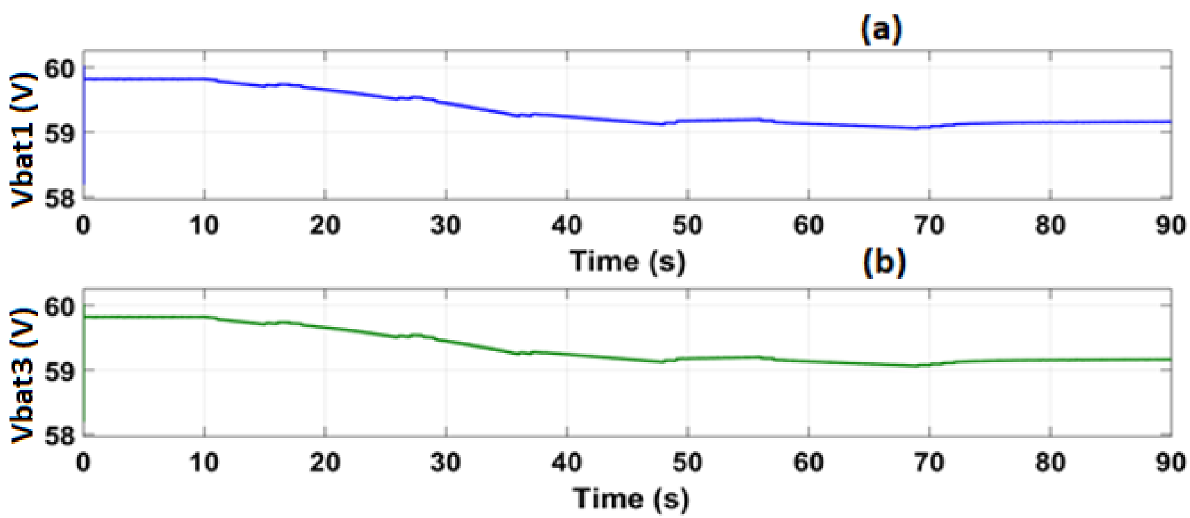

Figure 4.21: (a) Voltage v_{bat1}; (b) Voltage v_{bat3}.

4.5 Batterie Aging Index Comparison

Simulations have been carried out to make a comparison between different topologies. The lifetime of the battery is profoundly affected by their usage mode. The variations of large and frequent currents highly reduced the lifetime of the battery. The root-mean-square (RMS) value, the mean value, μ, the standard deviation, σ, of the battery module current and the coefficient characterizing the instantaneous current peaks, c_v, over the driving profile define the aging performance indexes of the battery. The RMS value of the battery module current specifies the effective current supplied by the battery. It can be given by:

$$RMS = \sqrt{\frac{1}{N}\sum_{i=1}^{N}\left(I_{B,cell}(i)\right)^2} \tag{4.9}$$

The mean value of the module current indicates the long-term stress from losses and respective thermal effect on batteries. It can be written as:

$$\mu = \frac{1}{N}\sum_{i=1}^{N} I_{B,cell}(i) \tag{4.10}$$

The standard deviation defines the strong variation of C-rate of the battery module, and it is determined by:

$$\sigma = \sqrt{\frac{1}{N}\sum_{i=1}^{N}\left(I_{B,cell}(i) - \mu\right)^2} \tag{4.11}$$

The variation coefficient characterizing the instantaneous current peak can be deduced by the following expression:

$$c_v = \frac{\sigma}{\mu} \tag{4.12}$$

Figure 4.22 shows the performance comparison using the aging index of the batteries branches for these topologies considering the same on-board energy. Figure 4.22 illustrates that embedded quasi-Z-source inverter is a bit more convenient to utilize in multi-source EV system compared to other topologies. Embedded quasi-Z-source inverter produces the best aging performance index in terms of the RMS and average values of the current for the battery than other topologies. The use of embedded quasi-Z-source inverter for multi-source EV can better enhance the battery lifetime than the other topologies.

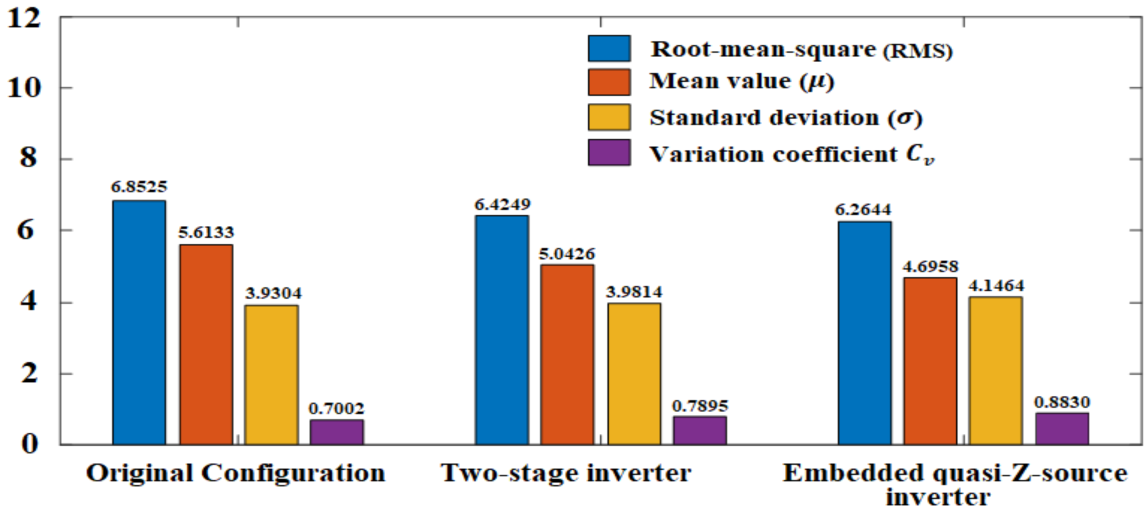

Figure 4.22: Performance comparison using aging index factors.

4.6 Conclusion

This paper has presented a comparative study between different power train topologies regarding aging index factors for an off-road electric vehicle. The simulation and comparative results prove that embedded quasi-Z-source inverter has better performance than the other topologies. The results specify the ability of the topologies to respond quickly to the load and the input voltage, where the transient and steady state response are comparable for both topologies. Embedded quasi-Z-source inverter can contribute to increase the lifetime of the battery used for EV traction purpose. These results verify the embedded quasi-Z-source inverter as an alternative inverter for multi-source EV. This kind of power converter can be very useful for multi-source EV seeing the disparity of voltage levels and currents between the sources (fuel cell, batteries, supercapacitors…) and the loads of the EV (traction motor, auxiliaries). Therefore, embedded quasi-Z-source inverter can be essential for on-board energy management in multi-source off-road EV with flux-weakening control technique of SPMSM. Hence the future work will consist of to use embedded quasi-Z-source inverter for energy management in multi-source off-road EV with flux-weakening control technique of SPMSM.

4.7 Acknowledgment

This work was supported by the Canada Research Chairs Program (grant 950-230672), the Natural Sciences and Engineering Research Council of Canada (grant RDCJP 490763), and the 14e *Commission de Coopération Québec-Vietnam*. This work was also partially supported by European Regional Development Fund through the Operational Program for Competitiveness and Internationalization - COMPETE 2020 Program and by National Funds through the Portuguese funding agency (FCT - *Fundação para a Ciência e a Tecnologia*) within project ESGRIDS (POCI-01-0145-FEDER-016434) and UID/MULTI/00308/2019.

Chapter 5 Optimization of Fractional Order PI Controller for Bidirectional Quasi-Z-Source Inverter Used for Electric Traction System

Original Title: Optimization of Fractional Order PI Controller for Bidirectional Quasi-Z-Source Inverter Used for Electric Traction System

Authors and affiliation :

- **Daouda Mande**: Ph.D. student, e-TESC Laboratory, Department of Electrical & Computer Engineering, University of Sherbrooke
- **João P. Trovão**: Professor, e-TESC Laboratory, Department of Electrical & Computer Engineering, University of Sherbrooke
- **Maude Blondin**: Professor, e-TESC Laboratory, Department of Electrical & Computer Engineering, University of Sherbrooke

Date of Acceptance: **12 October 2020**

State of acceptance: Published

Reference: IET Electrical Systems in Transportation, DOI: 10.1049/iet-est.2019.0113

Summary

Content: This article presents the optimization of fractional order PI (FOPI) controllers for a bidirectional QZSI in an EV off-road application. An ant colony optimization algorithm (ACO-NM) is used for the optimization of the controller parameters. The Ziegler-Nichols (ZN) method with the relay, the pole placement method and the ACO-NM algorithm have optimized the FOPI parameter controller, and the results have been compared. Simulations are performed to verify the efficacy of the proposed controller structure with the bidirectional QZSI for two standardized driving cycles.

Results: FOPI controller designed with ACO-NM algorithm achieves best performance in terms of peak overshoot, settling time and steady-state error. Moreover, FOPI controller designed with this algorithm provides more suitable aging performance index values for the battery. The ACO-NM algorithm permits to reduce the root-mean-square value and the standard deviation by 2 % and 5% of the battery current compared to the ZN tuning method and direct battery supply topology, respectively. The mean value and variation coefficient of the current are also lower. QZSI also contributes to increase the lifetime of the battery used for EV than the voltage source inverter directly supplied by the battery. The results also highlight the ability of the QZSI to give a fast response to the load.

Contribution to this thesis: The previous chapters have permitted to select more efficient and reliable power converter for energy management in multi-source electric vehicle. The multi-source QZSI needs convenient control techniques for its performance enhancement. This chapter provides optimization method used to enhance the performance of FOPI control for bidirectional QZSI in an electric traction system. The tuning method used is perfectly adapted to overcome the non-linearities and uncertainties of QZSI model and FOPI controller structure. The bidirectional QZSI with this type of controller contribute to globally improve the performance of EVs by optimizing the electric power consumption and extending its driving range.

Abstract

This paper presents the optimization of fractional order PI (FOPI) controllers for a bidirectional quasi-Z-source Inverter (QZSI) in an electric vehicle (EV) off-road application. An ant colony optimization algorithm (ACO-NM) is used for the optimization of the controller parameters. This optimization method is applied to enhance the performance of FOPI control for bidirectional QZSI. Ziegler-Nichols (ZN) with relay and the pole placement tuning method are also used for the FOPI controller design for comparison purposes. The modelling and the control design of bidirectional QZSI for an electric traction system are presented and discussed. Simulations are performed to verify the efficacy of the proposed controller structure with the bidirectional QZSI for two standardized driving cycles. The result shows that the FOPI controller designed with the ACO-NM algorithm provides more suitable aging performance index values for the battery. The ACO-NM algorithm permits to reduce the root-mean-square value and the standard deviation by 2 % and 5% of the battery current compared to the ZN tuning method and direct battery supply topology, respectively. The bidirectional QZSI with this type of controller can globally enhance the performance of EVs by optimizing the electric power consumption and extending its driving range.

Keywords: Quasi-Z-source Inverter, Electric Vehicle, Fractional order PI controller, ACO-NM algorithm.

5.1 Introduction

In the last decades, with the increase in oil price and global environmental issues, there is a growing interest in electric vehicles (EVs) research. In EVs, an electric motor, a power electronic converter, and an electronic controller constitute the core of the EV propulsion system. Currently, there are two basic configurations for power electronic converters widely used in EV, such as voltage source inverter directly powered by a battery (original configuration) and conventional two-stage inverter, where a DC-DC converter step-up the voltage supplied by the battery pack. However, voltage source and current source inverters, which constitute the most currently used inverters, present some conceptual limitations, such as output voltage cannot exceed the DC source voltage. To overcome that, the use of DC-DC boost converter is sometimes needed, especially in vehicular applications, to compensate for the natural voltage drop of the batteries [94, 95, 96, 97]. With the conventional bidirectional two-stage, the circuitry and the control of the system become more complex [96, 98]. With the idea to solve these problems, a Z-source inverter (ZSI) was firstly proposed by Siwakoti et al. [8], as it is highlighted in [97, 99]. The concept of Z-source can be used for all power conversions. ZSI has a unique characteristic of buck-boost capability, which permits to have a wide range of voltage variation. A ZSI structure can improve the stability and safety of a motor drive system under complex conditions at lower losses and overcome voltage sags without any additional circuits [98, 100, 101]. It enables the minimization of the motor ratings to deliver the required power, enhances the power factor, and reduces harmonic current [98, 100, 101]. Many control strategies have been used for the Z-source network and have been implemented with its dynamic model. In literature, to study the dynamic operation of the ZSI system, small-signal analyses and mathematical models have been used [27]. These models enable different closed-loop control strategies implementation for the ZSI. The realization of control techniques exploiting several approaches with different complexities has been employed for some applications [9, 99]. To control ZSI switches, traditional PWM schemes can be used. However, the most used switching control schemes are simple boost method [98], maximum boost method [11], maximum constant boost method [12] and space vector method [13]. Also, there are modified PWM control techniques proposed for the control of ZSI switches control [91]. Nevertheless, to enhance EVs performance, a new topology named quasi-Z-source inverter (QZSI) is obtained after rearranging the components in the Z-source network. QZSI represents one of the most promising topologies for power electronics DC-AC converters, making it an excellent candidate for EV applications when low batterie voltage is chosen, primarily due to their ability to increase the voltage inverter output range (very high boost factor). QZSI superiority compared to conventional two-stage inverter has been presented in [8]. Indeed, EVs designed with the bidirectional QZSI can provide better performances due to QZSI abilities to boost voltage with low losses and deal with batteries behaviours, in which the power flows during motoring and braking operations. The QZSI has continuous input current and retains all the merits of the ZSI. The mode of use of batteries affects profoundly its lifetime [90, 101]. Indeed, large, and frequent current variations highly reduced their lifetime [91]. In [92], it has been demonstrated that different charging current rates and cut-off voltages influence the aging mechanism of batteries. It is also shown that the battery degradation speed accelerates when the charging stress exceeds some critical value. Computing aging performance indexes of the battery enables quantifying the effect of the current on the aging phenomena. Then, the control methods of the current and its behaviour can seriously affect the long-term battery performance. In [92], the aging indexes factors of the battery are computed to evaluate the performance of the model predictive control using the nonuniform sampling time concept and other model predictive control approaches. However, it is only with an appropriate tuned control structure that will enable EVs to take advantage of all benefits the QZSI offers and as a by-product enhances the battery lifetime.

Therefore, regarding the control structures, PI (Proportional-Integral) or PID (Proportional-Integral-Derivative) controllers have been very popular in industrial applications for many decades because of their simple structure and appropriate robustness. PI or PID controllers provide good performances such as small overshoot and fast settling time for slow industrial processes. The noise caused by the derivative term effect in the control process often limits the use of PID controllers [102]. For this reason, PI controllers are generally preferred over PID controllers. Indeed, most industrial applications use PI controllers since they provide satisfactory results for most control systems. To improve PID-based controller performances, fractional-order PID-based controllers have been proposed [103, 104]. In [105, 106], it has been proved that fractional-order PID controllers offer better performances than traditional PID controllers. Along the same line, the fractional-order PI (FOPI) controller offers greater flexibility in improving system performance through the presence of an additional tuning parameter [107]. This additional parameter, i.e. the fractional integrator gain, gives the FOPI controllers additional features, such as flexibility on the system stability [107, 108], robustness to plant uncertainties, high-frequency noise rejection as well as reduced sensitivity to load disturbances [109]. As an additional benefit, FOPI controllers can handle both delicate and complicated processes if correctly tuned [110]. As a result, the FOPI has received considerable attention from the academic community for industrial applications [109], but the optimal tuning needs a pre-analysis, and the off-line optimal tuning is under interest.

Regardless of the PID-based controller structure, controllers have parameters to tune. There exist classical methods to tune PID controllers such as the Ziegler-Nichols (ZN) open-loop method, the ZN closed-loop tuning, and Coon-Cohen open-loop. The ZN method is still popular, especially in industrial application because it is an easy approach to obtain suitable performances. Some improvements have been made to the ZN method to obtain better dynamic performances as load disturbance rejection [111]. However, classical methods such as ZN have some limitations, rarely provide optimal results, and offer limited performance when applied to more complex structures. For that reason, soft computing techniques applied to controller tuning have gained in interest [112]. For example, particle swarm optimization (PSO) [113], genetic algorithms (GA) [114], differential evolution algorithm [115], firefly algorithm [116] and iterative reduction-based heuristic algorithms (IRHA) applied to ZSI used in traction motors have been used for controller tuning. Consequently, soft computing techniques are promising tools for tuning the FOPI controller of a QZSI.

Therefore, this paper contributes to the problems of ZSIs used in electric traction system for EVs in the following aspects: We propose a QZSI for an electric traction system for an adapted BRP e-Commander vehicle. We develop a novel control analysis of the QZSI using FOPIs controllers. FOPIs controllers are chosen in our study, due to their flexibility, which allows full usage of the dynamical properties of the QZSI when used for EV powertrain control. We also present a comparison of controller tuning methods; the most popular and used classical tuning methods, which are the ZN method and the pole placement method compared to a soft computing technique. A deep comparison in terms of batteries aging index is also provided to identify the merits of optimized controller parameters can have in the battery degradation process. The soft computing technique chosen is the ACO-NM algorithm because of its high performance on numerous benchmark functions and controller tuning problems compared to well-known algorithms such as PSO and GA [117]. Besides, the ACO-NM possesses a constraint procedure tailored for controller tuning. The aim of this study is to obtain the best electric traction control system to achieve high dynamic performance while considering the battery aging. This paper is organized into sections. Section 5.2 introduces the EV under study as well as the QZSI configuration with its modelling. The FOPI controller design and its effectiveness are discussed in Section 5.3. Section 5.4 describes the tuning methods. Section 5.5 presents the QZSI implemented using the SimScape™ Power Systems library of MATLAB/Simulink® for the EV powertrain. The simulation results are also presented and discussed. Section 5.6 concludes the paper.

5.2 Electric Vehicle and its Components

5.2.1 Electric Vehicle

The high number of automobiles used around the world has created a serious environmental problem. Automobiles using conventional technologies contribute to air pollution, global warming and the diminution of oil resources. EVs, hybrid EVs or hydrogen fuel cell EVs have been proposed to replace conventional technologies. EV is characterized by an electric energy conversion chain upstream of the drive train [7]. The complete EV is constituted of the electric drive and power electronics for propulsion with other subsystems to make the whole system works. The motor represents the part of the EV powertrain. Energy storage source and EV powertrain are implemented with their controllers. The charging and discharging of the energy storage source are controllable. EV powertrain controller using its power electronics converter enables the motor speed and torque control. Figure 5.1 a shows the electric traction system with the use of QZSI to supply the surface permanent magnet synchronous motor (SPMSM).

During the propulsion mode, the voltage from the energy storage system is converted by the QZSI into three-phase voltages to drive the motor to produce the required torque. During the regenerative braking, the QZSI behaves as a step-down inverter to charge the storage system. In this paper, the SPMSM is used as an electric motor. The SPMSM is a synchronous motor with three phases and its state-space representation can be described as in [40]. The reference EV used in this study is the e-TESC 4WD platform, which is presented in Figure 5.1 b. The main parameters of the studied EV are given in Table 5.1.

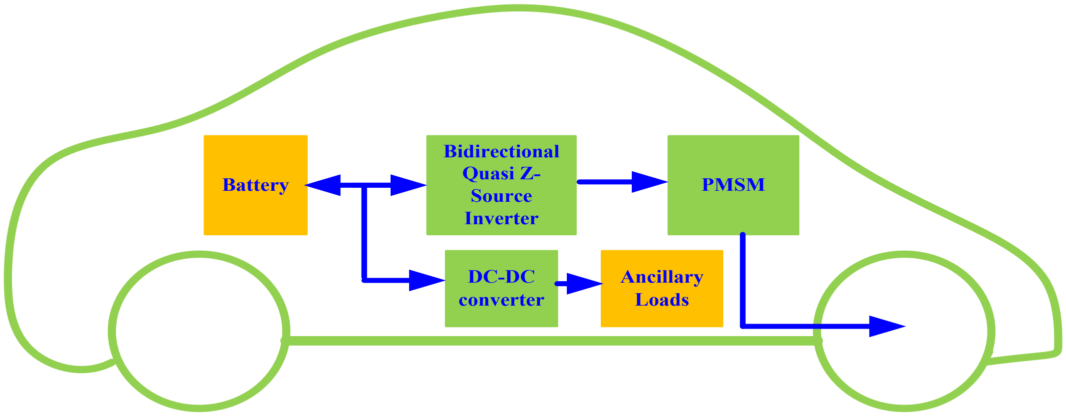

(a)

(b)

Figure 5.1: Electric traction system and off-road vehicle under study.

(a) Electric traction system using bidirectional QZSI.

(b) e-TESC 4W platform (adapted from BRP e-Commander vehicle).

Table 5.1: EV Platform Parameters

Parameters	Variable Name	Values
Vehicle (e-TESC 4W Electric Vehicle)		
Total mass of the EV	M_{veh}	857 kg
Aerodynamic standard	$c_x A$	1.3 m^2
Rolling coefficient	k_{roll}	0.035
Air density (at 20^{O} C)	ρ	1.223 kg/m^3
Motor to wheel transmission ratio	G_{tr}	20.5
Efficiency of the transmission	η_{tran}	0.87
Wheel radius	R_{wh}	0.3175 m
SPMSM parameters		
Phase inductance	L_d, L_q	1 mH
Phase resistance	r_s	0.08 Ω
Number of pole pair	p	2
Global inertia referred to the rotor of the motor	J	1 kg.m^2
Magnet flux linkage	ψ_f	0.1 Wb
Rated power	P_r	15 kW
Original configuration parameters		
Inductance	L	1 µH
Capacitance	C	4.5 mF
Switching frequency	f_s	10 kHz
Quasi-Z-source inverter parameters		
Inductance	L_1, L_2	230 µH
Capacitance	C_1, C_2	2.2 mF
Switching frequency	f_s	10 kHz
Battery		
Rated capacity	C_{bat}	40 Ah
Nominal voltage	v_{batnom}	48 V
Internal resistance	r_{bat}	15 mΩ

5.2.2 Bidirectional Quasi-Z-Source Inverter

The QZSI is a power electronic topology, which can use two control variables such as the shoot-through duty ratio and the modulation index to buck and boost the input voltage in a single stage [118]. The complete configuration of the studied QZSI connected with the SPMSM is shown in Figure 5.2 (a). Figures 5.2 (b) and (c) represent two equivalent circuits of QZSI during non-shoot-through state and the shoot-through state, respectively. In Figure 5.2, the voltages, the currents, and the resistances are also defined. R and r are assumed to be the series resistances of capacitors and the parasitic resistances of inductors, respectively.

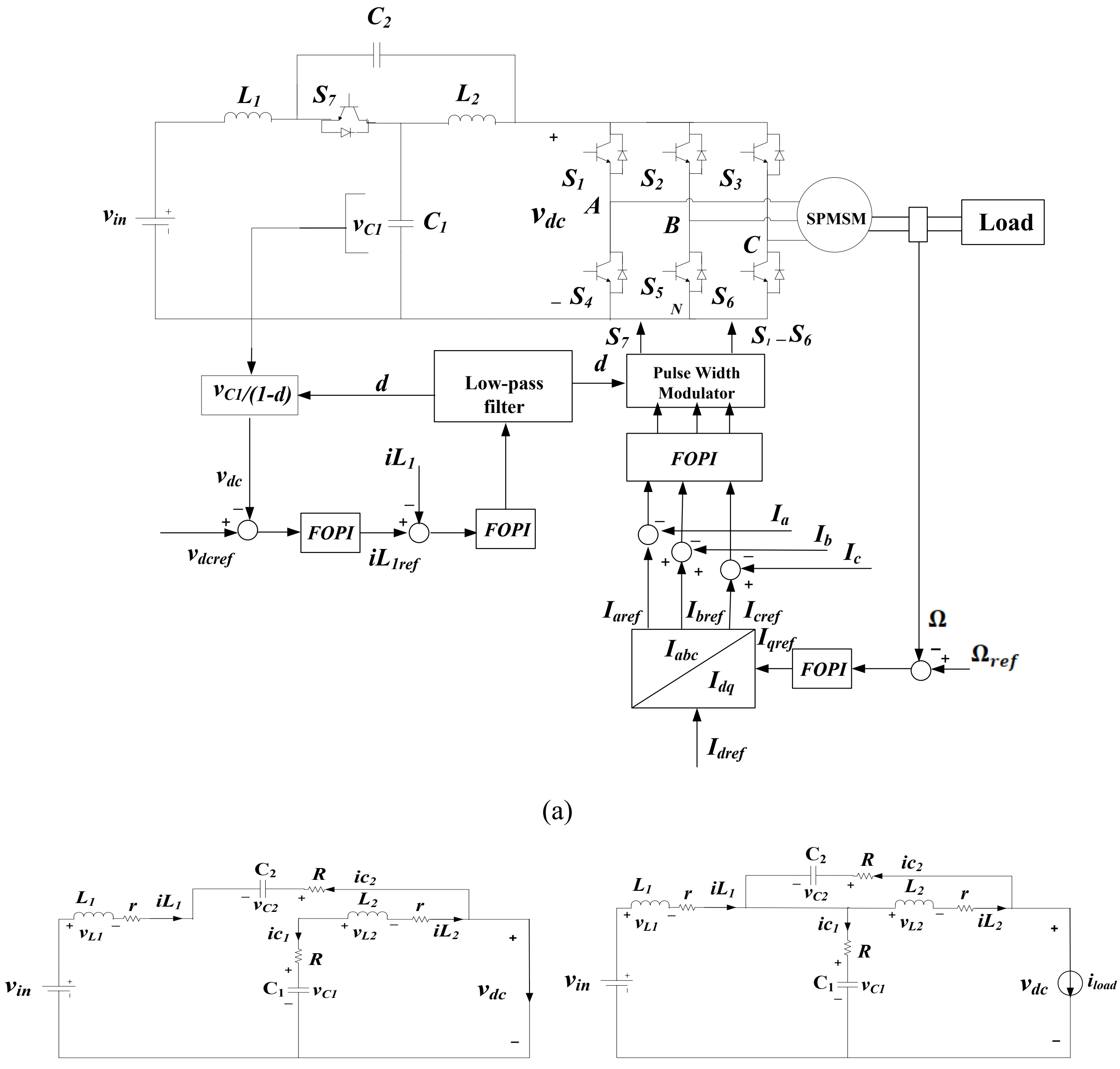

(a)

(b) (c)

Figure 5.2: QZSI control scheme and operation states.

(a) Voltage and current control scheme using FOPI

(b) QZSI Operation: shoot-through state

(c) QZSI Operation: non-shoot-through state

5.2.2.1 Modeling of Bidirectional Quasi-Z-Source Inverter

Modelling QZSI consists of determining its small signal model. The small signal model is used because of its accuracy for infinitesimal disturbances and system behaviour prediction to large non-infinitesimal disturbances. For one switching cycle T, the relationship between the interval of the shoot-through state T_0 and the interval of non-shoot-through state T_1 is $T = T_0 + T_1$. The shoot-through duty ratio is given by:

$$d = \frac{T_0}{T} \tag{5.1}$$

In Figure 5.2 (b), the inverter operates at the shoot-through state T$_1$. Let $x = \begin{bmatrix} i_{L_1} & i_{L_2} & v_{C_1} & v_{C_2} \end{bmatrix}^T \in \mathbb{R}^4$, $u = [i_{load} \quad v_{in}]^T \in \mathbb{R}^2$ and $y = [v_{C_1} \quad i_{L_1}]^T \in \mathbb{R}^2$, the dynamic equations can be expressed as

$$\frac{dx(t)}{dt} = F_1 x(t) + G_1 u(t), \tag{5.2}$$

$$y(t) = Ex(t), \tag{5.3}$$

where,

$$F_1 = \begin{bmatrix} -\frac{r+R}{L_1} & 0 & 0 & \frac{1}{L_1} \\ 0 & -\frac{r+R}{L_2} & \frac{1}{L_2} & 0 \\ 0 & \frac{-1}{C_1} & 0 & 0 \\ \frac{-1}{C_2} & 0 & 0 & 0 \end{bmatrix}, \quad G_1 = \begin{bmatrix} 0 & \frac{1}{L_1} \\ 0 & 0 \\ 0 & 0 \\ 0 & 0 \end{bmatrix}, \qquad E = \begin{bmatrix} 1 & 0 & 0 & 0 \\ 0 & 0 & 1 & 0 \end{bmatrix}.$$

The variables *r, R*, L_1, L_2, C_1 and C_2 represent the resistances, inductances and capacitors of the QZS network, respectively.

In Figure 5.2 (c), the inverter operates at the non-shoot-through state T_0. The dynamic equations in this case are:

$$\frac{dx(t)}{dt} = F_2 x(t) + G_2 u(t), \tag{5.4}$$

$$y(t) = Ex(t), \tag{5.5}$$

where

$$F_2 = \begin{bmatrix} -\frac{r+R}{L_1} & 0 & \frac{-1}{L_1} & 0 \\ 0 & -\frac{r+R}{L_2} & 0 & \frac{-1}{L_2} \\ \frac{1}{C_1} & 0 & 0 & 0 \\ 0 & \frac{1}{C_2} & 0 & 0 \end{bmatrix}, \quad G_2 = \begin{bmatrix} \frac{R}{L_1} & \frac{1}{L_1} \\ \frac{R}{L_2} & 0 \\ \frac{-1}{C_1} & 0 \\ \frac{-1}{C_2} & 0 \end{bmatrix}.$$

5.2.2.2 Average State-Space Model

The average space-state modelling method is considered as the most efficient method for developing small signal model. It provides a complete power converter model with steady-state and dynamic quantities. Using (5.2), (5.3) and (5.4), we obtain the average state-space model as follows:

$$\frac{dx(t)}{dt} = Fx(t) + Gu(t), \tag{5.6}$$

$$y(t) = Ex(t), \tag{5.7}$$

where $F = dF_1 + (1-d)F_2$ and $G = dG_1 + (1-d)G_2$.

Assuming $C = C_1 = C_2$, and $L = L_1 = L_2$, F and G can be expressed as

$$F = \begin{bmatrix} -\frac{r+R}{L} & 0 & \frac{-1+d}{L} & \frac{d}{L} \\ 0 & -\frac{r+R}{L} & \frac{d}{L} & \frac{-1+d}{L} \\ \frac{1-d}{C} & -\frac{d}{C} & 0 & 0 \\ -\frac{d}{C} & \frac{1-d}{C} & 0 & 0 \end{bmatrix}, \quad G = \begin{bmatrix} \frac{(1-d)R}{L} & \frac{1}{L} \\ \frac{(1-d)R}{L} & 0 \\ \frac{-1+d}{C} & 0 \\ \frac{-1+d}{C} & 0 \end{bmatrix}.$$

The perturbations are introduced to the system variables to drive a small-signal model of the quasi-Z-source network needed for the controller design. Subsequently, we have the following expressions:

$$\frac{d\hat{x}(t)}{dt} = \tilde{F}(\bar{X} + \hat{x})(t) + \tilde{G}(\bar{U} + \hat{u})(t) \tag{5.8}$$

$$\hat{y}(t) = E\hat{x}(t) \tag{5.9}$$

where

$$(\bar{X} + \hat{x}) = \begin{bmatrix} \bar{I}_{L_1} + \hat{\imath}_{L_1} & \bar{I}_{L_2} + \hat{\imath}_{L_2} & \bar{V}_{C_1} + \hat{v}_{C_1} & \bar{V}_{C_2} + \hat{v}_{C_2} \end{bmatrix}^T \epsilon\, \mathbb{R}^4$$

and

$$(\bar{U} + \hat{u}) = [\bar{I}_{load} + \hat{\imath}_{load} \quad \bar{V}_{in} + \hat{v}_{in}]^T \epsilon\, \mathbb{R}^2.$$

The variables $\hat{x}$, $\hat{u}$, $\bar{X}$ and $\bar{U}$ represent the small disturbance and the average value of state variables, respectively.

$$\tilde{F}=\begin{bmatrix} -\frac{r+R}{L} & 0 & \frac{-1+\bar{D}+\hat{d}}{L} & \frac{\bar{D}+\hat{d}}{L} \\ 0 & -\frac{r+R}{L} & \frac{\bar{D}+\hat{d}}{L} & \frac{-1+\bar{D}+\hat{d}}{L} \\ \frac{1-\bar{D}-\hat{d}}{C} & -\frac{\bar{D}+\hat{d}}{C} & 0 & 0 \\ -\frac{\bar{D}+\hat{d}}{C} & \frac{1-\bar{D}-\hat{d}}{C} & 0 & 0 \end{bmatrix}, \qquad \tilde{G}=\begin{bmatrix} \frac{(1-\bar{D}-\hat{d})R}{L} & \frac{1}{L} \\ \frac{(1-\bar{D}-\hat{d})R}{L} & 0 \\ \frac{-1+\bar{D}+\hat{d}}{C} & 0 \\ \frac{-1+\bar{D}+\hat{d}}{C} & 0 \end{bmatrix}.$$

where, $\bar{D}$ and $\hat{d}$ represent the average values of the shoot-through duty cycle and the small signal value, respectively. By developing and rearranging the small-signal model equation (5.8), we obtain the following model:

$$\frac{d\hat{x}(t)}{dt}=\begin{bmatrix} -\frac{r+R}{L} & 0 & \frac{\bar{D}-1}{L} & \frac{\bar{D}}{L} \\ 0 & -\frac{r+R}{L} & \frac{\bar{D}}{L} & \frac{\bar{D}-1}{L} \\ \frac{1-\bar{D}}{C} & -\frac{\bar{D}}{C} & 0 & 0 \\ -\frac{\bar{D}}{C} & \frac{1-\bar{D}}{C} & 0 & 0 \end{bmatrix}\hat{x}(t)+\begin{bmatrix} \frac{\bar{V}_{C_1}+\bar{V}_{C_2}-R\bar{I}_{load}}{L} & \frac{1}{L} \\ \frac{\bar{V}_{C_1}+\bar{V}_{C_2}-R\bar{I}_{load}}{L} & 0 \\ \frac{\bar{I}_{load}-\bar{I}_{L_1}-\bar{I}_{L_2}}{C} & 0 \\ \frac{\bar{I}_{load}-\bar{I}_{L_1}-\bar{I}_{L_2}}{C} & 0 \end{bmatrix}\hat{d}+ \qquad (5.10)$$

$$\begin{bmatrix} \frac{1}{L} \\ 0 \\ 0 \\ 0 \end{bmatrix}\hat{v}_{in}+\begin{bmatrix} \frac{(1-\bar{D})R}{L} \\ \frac{(1-\bar{D})R}{L} \\ \frac{\bar{D}-1}{C} \\ \frac{\bar{D}-1}{C} \end{bmatrix}\hat{\imath}_{load}.$$

Subsequently, the small-signal transfer functions of the capacitor voltage and the inductor current with the shoot-through duty cycle can be expressed as

$$G_1(s)=\frac{\hat{v}_C(s)}{\hat{d}(s)}=\frac{(1-2\bar{D})(\bar{V}_{C_1}+\bar{V}_{C_2}-R\bar{I}_{load})+(Ls+r+R)(\bar{I}_{load}-\bar{I}_{L_1}-\bar{I}_{L_2})}{LCs^2+C(r+R)s+(1-2\bar{D})^2} \qquad (5.11)$$

$$G_2(s)=\frac{\hat{\imath}_L(s)}{\hat{d}(s)}=\frac{(\bar{V}_{C_1}+\bar{V}_{C_2}-R\bar{I}_{load})Cs+(2\bar{D}-1)(\bar{I}_{load}-\bar{I}_{L_1}-\bar{I}_{L_2})}{LCs^2+C(r+R)s+(1-2\bar{D})^2} \qquad (5.12)$$

Transfer functions (5.11) and (5.12) are used to design and tune the FOPI controller of the QZSI.

5.2.2.3 Steady State Analysis

The steady-state analysis has the advantage of developing a procedure, which can be used to design the proposed QZSI application. It helps to determine the important characteristics of the QZSI in steady state. During the steady state, the average voltages of the inductors and the average currents of the capacitors over one switching cycle T are zero. The average voltage and current equations can be derived by using (5.6) as follows:

$$\frac{d\bar{x}(t)}{dt} = Fx(t) + Gu(t) = 0 \tag{5.13}$$

where $\bar{x}$ the symbol denotes the average value of instantaneous variable x in the period T.

If we ignore the series resistance R and parasitic inductance r, the capacitor voltages and inductor currents are deduced from (5.13) as follows:

$$\begin{cases} v_{c_1} = \frac{1-D}{1-2D} v_{in} \\ v_{c_2} = \frac{D}{1-2D} v_{in} \end{cases} \tag{5.14}$$

$$i_{L_1} = i_{L_2} = \frac{1-D}{1-2D} i_{load} \tag{5.15}$$

The DC-link peak voltage $\hat{v}_{dc}$ can be derived from the sum of two capacitor voltages, $v_{c_1}$and v_{c_2}, by:

$$\hat{v}_{dc} = v_{c_1} + v_{c_2} = \frac{1}{1-2D} v_{in} = Bv_{in} \tag{5.16}$$

where $B \geq 1$ is the boost factor resulting from the shoot-through period. Regarding the AC side of the QZSI, the peak phase voltage can be written as

$$\hat{v}_o = m_c \frac{\hat{v}_{dc}}{2} = \frac{m_c}{1-2D} . \frac{v_{in}}{2} = G_c \frac{v_{in}}{2} \tag{5.17}$$

where m_c and G_c are the inverter modulation index and total voltage gain of the QZSI, respectively.

5.2.2.4 Simple Boost Control Method

Pulse width modulator (PWM) is a mechanism used to perform the modulation concept for controlling the QZSI switches. In this study, the simple boost control method (SBC) control scheme has been implemented in the PWM to generate the gate signals of the QZSI switches. This method consists in making the comparison between three sinusoidal reference signals and two constant voltage envelopes with the triangular carrier waveform [100]. Figure 5.3 shows the SBC technique with a switch S_7 drive signal. The triangular carrier waveform is compared with the two constant voltage envelopes (v_p and v_n) to generate the shoot-through states. When the triangular carrier waveform is greater or lower than v_p or v_n, respectively, the shoot-through pulses are produced. Otherwise, the triangular carrier waveform is compared with the three sinusoidal control voltages (v_a , v_b , and v_c) and the inverter operates in this case with the conventional active and zero states. The switch S_7 of QZSI contributes to a bidirectional power flow. It is operated to have a signal which will be complementary to the shoot-through signal of the inverter. When the inverter is operated in the shoot-through state, S_7 is open, which allows the voltage boost function. When the inverter operated in the non-shoot-through state, S_7 is closed, and a reverse current can flow through S_7 and provide the energy back to the DC source. The SBC technique is used because it enables to have a constant shoot-through duty cycle, which results in a lower inductor current ripple that needs lower inductance values, as demonstrated by Shen et *al*. [82].

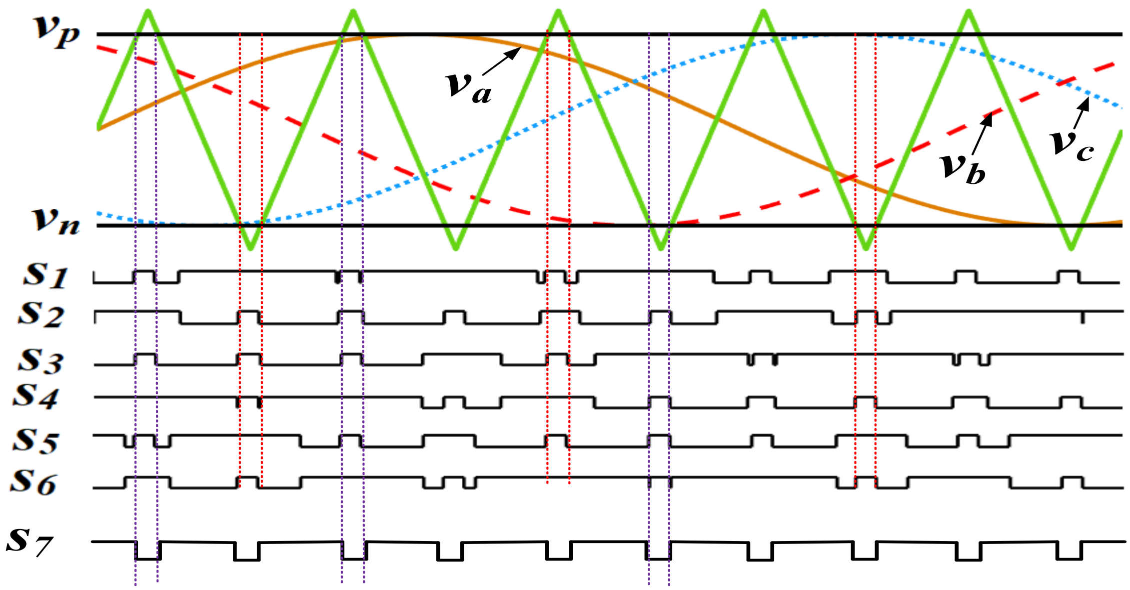

Figure 5.3: The wave-forms of SBC technique with a switch S_7 drive signal.

5.3 Fractional order PI Controller Design

The FOPI controller is known to provide the good step performance response [119]. The output feedback of the FOPI controller, K_{PI}, has the following form:

$$K_{PI}(s) = k_p + k_i \frac{1}{s^{\lambda}} \tag{5.18}$$

where k_p and k_i are the proportional and the integral gains respectively, and λ is the fractional integrator order, which provides an extra degree of freedom. The FOPI controller is implemented using FOMCON toolbox [120]. For the EV under study, the controller tuning is performed to obtain high performance in setpoint tracking, while considering battery aging.

Four controllers are needed: two for the DC side and two for the AC side of the QZSI. For the DC side, cascade FOPI controllers are designed to regulate the DC-link voltage and the inductor current of the QZSI using (5.13) and (5.14). The voltage and current closed-loop FOPI control filtered by a low-pass filter permits to obtain the shoot-through duty cycle d. The shoot-through duty cycle d and the modulation index m_c are delivered to the PWM block, which generates the switching signals. The voltage and current FOPI controller parameters are KpC, KiC, λ_C and $KpL1$, $KiL1$, λ_{L1}, respectively. For the AC side, FOPI controller is designed to control the speed and the motor current of the EV with the parameters Kpv, Kiv, λ_v and $Kpcm$, $Kicm$, λ_{cm}, respectively. The voltage and the current control schemes of the QZSI that fed the SPMSM traction system is presented in Section 5.2 based on Figure 5.2 a.

5.4 Tuning Methods and Algorithm of Optimization

This section describes the different tuning methods used to tune the FOPIDs, i.e. ZN, pole placement, and the ACO-NM algorithm. The tuning methods are compared based on the aging performance indexes values of the battery current.

5.4.1 Ziegler–Nichols Tuning Method

The ZN tuning method is a heuristic method for tuning P, PI and PID controllers [121]. This method attempts to reach good values for the three PID gain parameters. Usually, it is achieved by setting K_i and K_d gains to zero and by increasing K_p gain from zero until the output of the control loop reaches constant and stable oscillations; the K_u gain is therefore obtained. Then, K_u and the oscillation period P_u are used to determine the gains K_p, K_i and K_d according to the type of controller used as presented in Table 5.2.

Table 5.2: Ziegler-Nichols Tuning Formula

Type of controller	K_p	K_i	K_d
P	$K_u/2$		
PI	$K_u/2.2$	$P_u/1.2$	
PID	$K_u/1.7$	$P_u/2$	$P_u/8$
where $K_i = \frac{K_p}{T_i}$			

5.4.2 Pole Placement Tuning Method

The pole placement tuning method is an analytical method used in feedback control systems theory and is widely used with multiple inputs and outputs systems. The method uses the transfer function of the plant to determine the closed-loop denominator [122]. The main advantage of this method is its simplicity of use for a wide range of applications. The main drawback of the pole placement tuning method is the difficulty to select the best locations of poles to fulfill the dynamic performance requirements of the system.

5.4.3 ACO-NM algorithm as a controller tuning method

The subsection explains the ACO-NM algorithm. For details concerning the equations and parametrization, please refer to [117]. The ant colony crosses the combinatorial graph presented on Figure 5.4. Each ant selects according to a probabilistic rule a node in each column to build a solution x. Each variable to tune has its own node column, i.e., on Figure 5.4, $x(1)$ refers to the first variable, $x(2)$ to the second, and so on, until the last variable $x(n)$, where n is the number of variables to optimize. Each single node within a same column has a unique value ranging from the lower bound lb to the upper bound ub. Once the graph has been travelled by all ants, the objective function for each ant's solution is evaluated. A pheromone matrix mapping the optimization graph is employed as a memory to direct the colony for the next subsequent iteration. Ants are attracted to pheromone, which means that paths between two nodes with higher quantity of pheromone are more appealing to ants. Thus, pheromone quantities are deposited onto the pheromone matrix based on the objective function values; higher quantity of pheromone is deposited to paths leading to better solutions. The ant colony travels the graph until the ACO stop criterion is reached. Thereafter, the constrained NM algorithm takes precedence and starts optimizing. To start NM algorithm, the best ACO solution reached is used to create a simplex of $n + 1$ vertices. The algorithm makes the simplex shape change according to various steps [123] in order to explore the bounded search space. The NM algorithm stops once it reaches the NM stop criteria. If the simplex steps out of bounds, the procedure proposed in [117] brings the simplex into the search space. The simplified ACO algorithm followed by the constrained NM method is performed repeatedly until the ACO-NM stop criterion is reached.

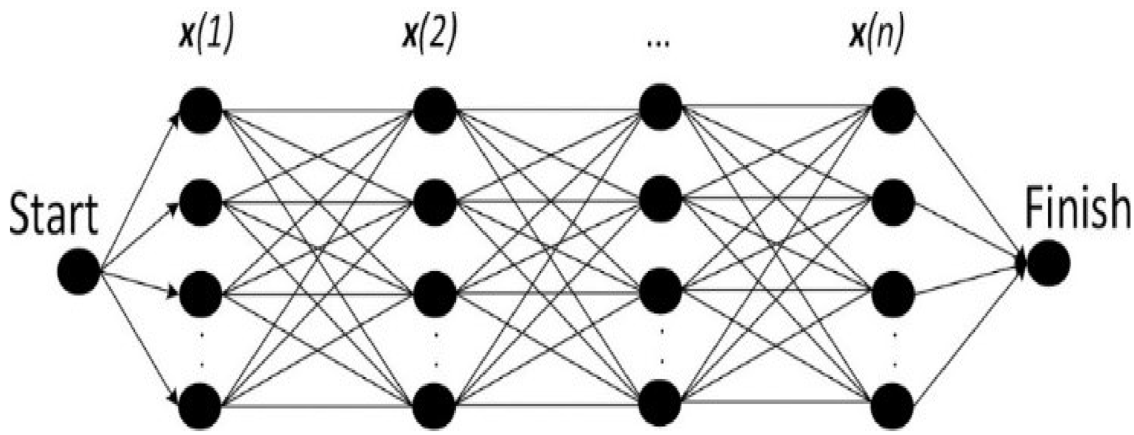

Figure 5.4: Combinatorial optimization graph for ACO algorithm [115].

To apply the ACO-NM algorithm, the FOPI tuning problem is modelled as the following optimization problem,

$$\min_{x} J(x)$$
$$\text{Subject to: } lb\big(x(j)\big) \leq x(j) \leq ub\big(x(j)\big), \quad j = 1, \ldots, n \tag{5.19}$$

where *n* is the number of controller parameters to tune, lb and ub refer to the lower and upper bounds of the search space respectively defined as represented in the Table 5.3.

Table 5.3: Parameters lower and upper bounds

FOPI structure	**Parameters**	**Lower and upper bounds**
Motor speed	Kpv	[1 to 50]
	Kiv	[1 to 100]
	λ_v	[0.25 to 2.5]
DC-Link current	$KpL1$	[1 to 50]
	$KiL1$	[10 to 200]
	λ_{L1}	[0.25 to 2.5]
DC-Link voltage	KpC	[1 to 50]
	KiC	[1 to 150]
	λ_C	[0.25 to 2.5]

Motor current	$Kpcm$	[1 to 50]
	$Kicm$	[100 to 300]
	λ_{Cm}	[0.25 to 2.5]

In this study the cost function, $J(x)$, is defined as follows

$$J(x) = \int_0^{T_{sim}} |e_{mot}|\, dt + \int_0^{T_{sim}} e_{cur}{}^2\, dt \tag{5.20}$$

where e_{mot} is the difference between the motor speed setpoint and the actual motor speed, e_{cur} is the difference between the current setpoint and the actual current and T_{sim} is the model simulation time. This cost function ensures that the optimized solution is suitable for the EV, i.e. the system limits are not violated.

5.5 Simulation Results and Discussion

5.5.1 Speed Step Response Comparison and Tracking Performance

For comparison purposes, simulation has been performed for a portion of ECE15 and Artemis driving cycles. The main parameters of the EV used for the simulations are presented in Table 5.1. i_{dref} is sometimes known as field weakening current and has been set to zero for this analysis, considering speeds under the base speed of the SPMSM. Table 5.4 presents the FOPI controller parameters computed by the different tuning methods.

Table 5.4: Parameters summary for different tuning methods

FOPI structure	**Controller Parameters**	**ZN tuning**	**Pole Placement tuning**	**ACO-NM tuning**
Motor speed	Kpv	4.2091	4.2091	24.1229
	Kiv	9.1007	9.1007	3.5456
	λ_v	1.1000	1.1000	0.6878
DC-Link current	$KpL1$	0.5088	0.2424	1.2169
	$KiL1$	174.9411	63.8710	29.3216
	λ_{L1}	0.9000	0.9000	0.6247
DC-Link voltage	KpC	0.1736	0.9070	1.1055
	KiC	59.6987	93.5538	68.3257

	λ_C	0.9000	0.9000	0.6515
Motor current	$Kpcm$	0.7276	0.7298	9.1064
	$Kicm$	250.1658	208.0763	233.9843
	λ_{Cm}	0.9000	0.9000	1.0969

Figure 5.5 shows acceleration responses based on the ECE15 driving cycle using FOPI-based controllers with the different tuning methods. The comparison among FOPI-based controllers in terms of performance measures, i.e. rise time, settling time, peak overshoot, delay time, and steady-state error, has been computed from the speed responses of Figure 5.5 and are presented in Table 5.5.

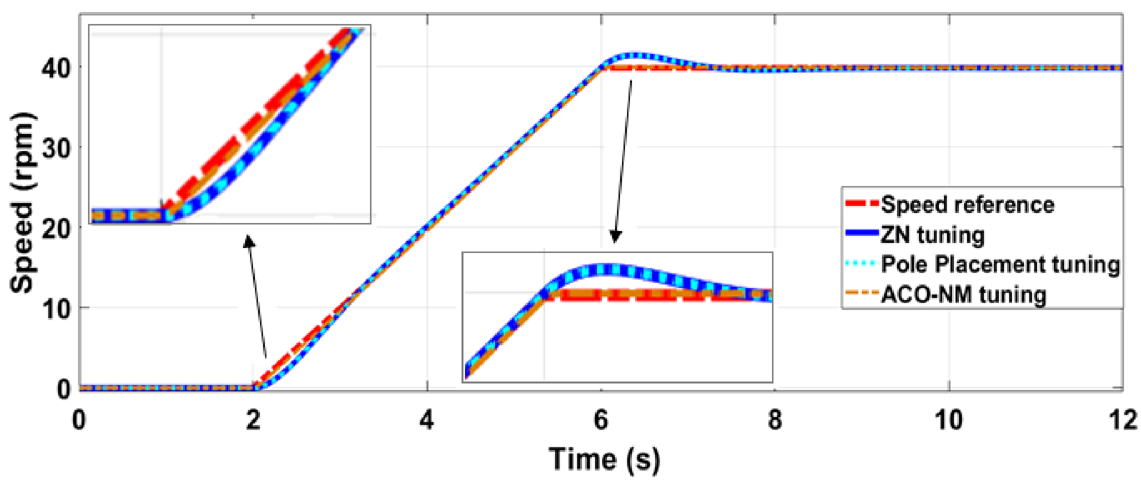

Figure 5.5: Speed responses using different tuning methods for FOPI-based.

Table 5.5: Performance comparison

Performance criteria	ZN tuning	Pole Placement tuning	ACO-NM tuning
Rise time t_r (s)	3.038	**3.035**	3.182
Settling time t_s (s)	9.068	9.073	**7.236**
Peak overshoot (%)	4.16%	4.16%	**0.15%**
Delay time (s)	4.009	**4.005**	4.045
Steady-state error	0	0	0

From Table 5.5, it can be concluded that speed step response using the FOPI-based ACO-NM algorithm achieves better performance compared to the other tuned controllers. The FOPI-based ACO-

NM algorithm provides minimum peak overshoot and minimum settling time. The steady-state error remains zero for all the tuning methods.

Simulations were also carried out for a portion of Artemis driving cycles to validate the model of the QZSI that feeds the motor using the FOPI controller-based and SBC technique, as presented in Figure 5.6 (a) to (d). These results are only based on the ACO-NM algorithm for all FOPI controllers. The acceptable peak-to-peak current ripple and peak-to-peak voltage ripple as 2.5% and 5%, respectively for the inductance and capacitance are chosen for the final design of QZSI. Figure 5.6 (a) and (b) show the speed and torque waveforms, respectively. The v_{dc} voltage and i_{L1} current and their references with FOPI controllers are presented in Figure 6 (c) and (d), respectively.

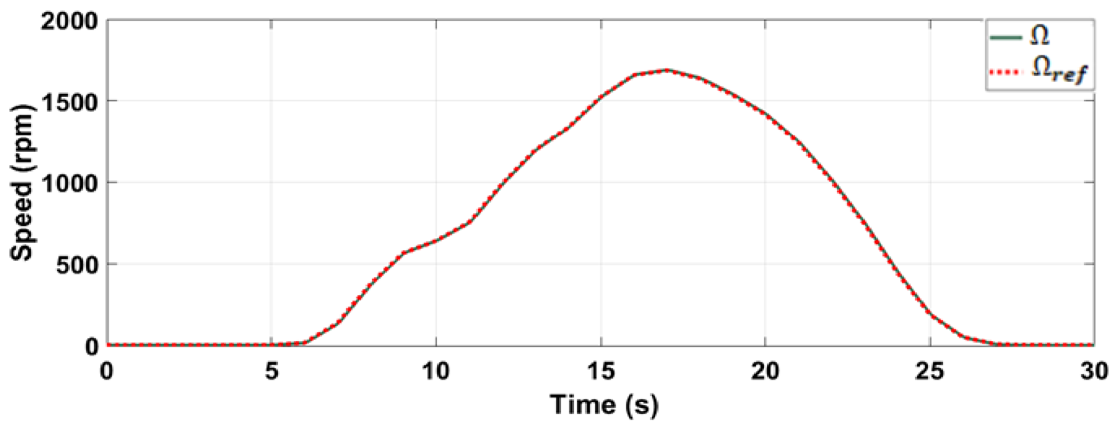

(a)

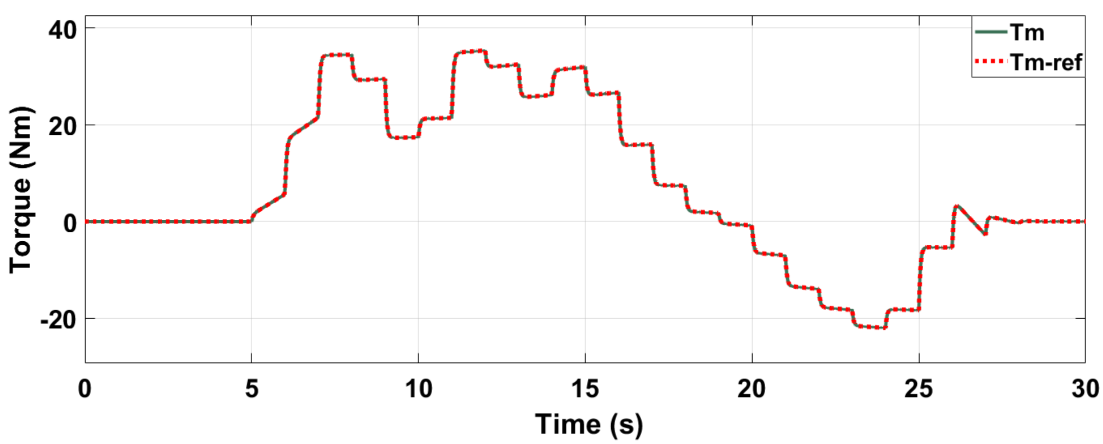

(b)

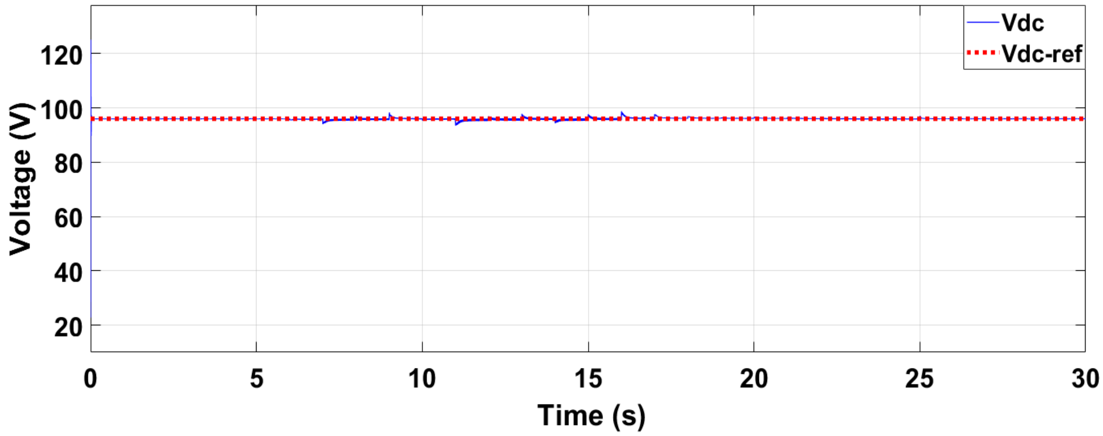

(c)

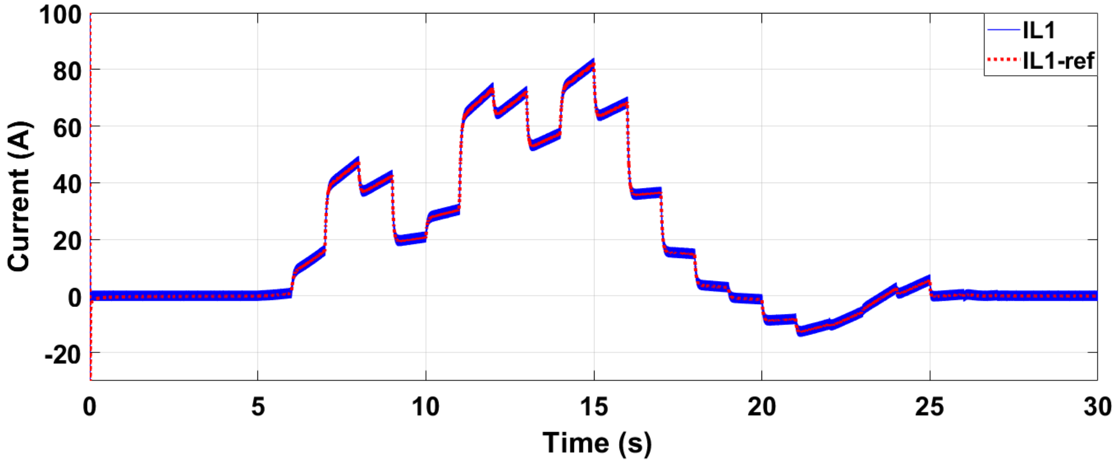

(d)

Figure 5.6: QZSI using the FOPI controllers and SBC technique: simulation results for a portion of Artemis driving cycles.

(a) Motor speed and reference (b) Motor torque and reference (c) The v_{dc} voltage and its reference (d) The i_{L1} current and its reference.

Figure 5.6 (a) shows that the speed has been controlled to track the driving cycle in a best-desired way. The different results point out the ability of the QZSI to give a quick response to the load with FOPI control using the ACO-NM algorithm.

5.5.2 Battery Aging index comparison

To compare the FOPI control strategy tuned by traditional methods and the ACO-NM algorithm, the aging performance indexes of the battery with these control methods are computed. The battery lifetime is affected by their usage mode. Their lifetime is highly reduced by the variations of large and frequent currents. The root-mean-square (RMS) value, the mean value (μ), the standard deviation (σ) of the cell current and the coefficient (c_v) characterizing the instantaneous current peaks over the driving profile constitutes the aging performance indexes of battery [124].

The RMS value of the cell current specifies the effective current. It can be written as:

$$RMS = \sqrt{\frac{1}{N}\sum_{i=1}^{N}\left(I_{B,cell}(i)\right)^2} \tag{5.21}$$

The mean value of the cell current indicates the long-term stress from losses and respective thermal effect on batteries. It can be expressed as:

$$\mu = \frac{1}{N}\sum_{i=1}^{N} I_{B,cell}(i) \tag{5.22}$$

The standard deviation defines the strong variation of C-rate of the batteries, and it is given by:

$$\sigma = \sqrt{\frac{1}{N}\sum_{i=1}^{N}\left(I_{B,cell}(i) - \mu\right)^2} \tag{5.23}$$

The variation coefficient characterizing the instantaneous current peak can be deduced by the following expression:

$$c_v = \frac{\sigma}{\mu} \tag{5.24}$$

The Figure 5.7 shows the performance comparison for the different FOPI tuning methods using the aging index of the battery to evaluate the indirect performance of the close loop structure. It also shows the battery aging index comparison between powertrain original configuration (inverter directly supplied by the battery) and QZSI considering the same on-board energy. Figure 5.7 illustrates that FOPI control tuned by the ACO-NM algorithm improves the computed aging index using a combination of two terms in the objective function, speed error and square current error.

The ACO-NM tuning method permit to reduce the RMS value and σ by 2% and 5% of the battery current regarding the ZN tuning method and the original configuration (battery and voltage source inverter), respectively. This tuning method also contributes to diminish the μ value and c_v of the current. FOPI control using the ACO-NM algorithm provides the best aging performance index values for the EV battery under study.

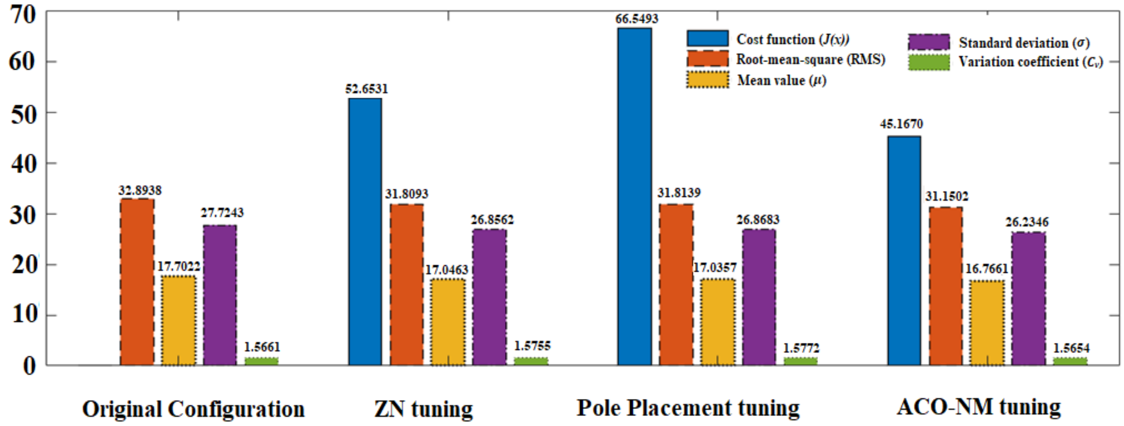

Figure 5.7: Aging index comparison using as reference the original powertrain configuration.

Therefore, tuning the FOPI with the ACO-NM algorithm can enhance the battery lifetime compared to other tuning methods. Figure 5.7 also shows that the QZSI produces the best aging performance index values in terms of the RMS, σ (average value) and μ (standard deviation) of the current for the battery than the original configuration. The use of QZSI for an EV can also increase the battery lifetime than the original configuration, which makes the QZSI more suitable in EV systems than the original configuration.

5.6 Conclusion

In this paper, the optimization of the FOPI controller for the bidirectional QZSI using for electric traction system has been presented. A small-signal model of the QZSI with an electric traction system has been designed. The ZN method with the relay, the pole placement method and the ACO-NM algorithm have optimized the FOPI parameter controller, and the results have been compared. The proposed tuning method is perfectly adapted to overcome the non-linearities and uncertainties of QZSI model and FOPI controller structure. The improvement in terms of peak overshoot reduction demonstrates superior capacity of the ACO-NM tuning method. The simulation results show that the best performance in terms of peak overshoot, settling time and steady-state error has been achieved by the ACO-NM algorithm. Moreover, the results prove that the FOPI controller designed with the ACO-NM algorithm provides more suitable aging performance index values for the battery of the studied EV. Also, the results point out the ability of the QZSI to give a quick response to the load. The comparative results also show that the QZSI can also contribute to increase the lifetime of the battery used for EV than the voltage source inverted directly supplied by the battery (original configuration). Therefore, QZSIs and FOPIs would benefit the next generation of EVs. Future works will consist of using this FOPI tuned by the ACO-NM algorithm for the QZSI applied to multi-source EV with experimental validations, including stability analysis.

5.7 Acknowledgment

This work was supported in part by Grant 950-230672 from Canada Research Chairs Program, in part by Grant RGPIN-2017-05924 from the Natural Sciences and Engineering Research Council of Canada, in part by the Postdoctoral research scholarship of Fonds de recherche du Québec - Nature et Technologies, in part by FCT-Portuguese Foundation for Science and Technology project UIDB/00308/2020, and by the European Regional Development Fund through the COMPETE 2020 Program within projects ESGRIDS (POCI-01-0145-FEDER-016434) and MAnAGER (POCI-01-0145-FEDER-028040).

Chapter 6 Multi-source Bidirectional Quasi-Z-source Inverter using Fractional Order PI Controller for Electric Traction System

Original Title: Multi-source Bidirectional Quasi-Z-source Inverter using Fractional Order PI Controller for Electric Traction System

Authors and affiliation :

- **Daouda Mande**: Ph.D. student, e-TESC Laboratory, Department of Electrical & Computer Engineering, University of Sherbrooke
- **João P. Trovão**: Professor, e-TESC Laboratory, Department of Electrical & Computer Engineering, University of Sherbrooke
- **Ruben Gonzalez Rubio**: Professor, eXit Laboratory, Department of Electrical & Computer Engineering, University of Sherbrooke
- **Minh C. Ta**: Professor, e-TESC Laboratory, Department of Electrical & Computer Engineering, University of Sherbrooke

Date of Acceptance: **25 April 2021**

State of acceptance: Published

Reference: 2021 IEEE Vehicle Power and Propulsion Conference (VPPC),

DOI: 10.1109/VPPC53923.2021.9699307

Summary

Content: This paper proposes a new control configuration of hybrid energy storage system (HESS) using a battery pack and a supercapacitor for electric vehicle (EV). The HESS is designed based on bidirectional quasi-Z-source inverter (QZSI) and a DC-DC converter. The HESS configuration with its modeling and major operation modes for EV are shown. The control scheme of the HESS using fractional order PI (FOPI) controller is presented. FOPI controller is also combined with a filtering technique to contribute to supercapacitor battery degradation mitigation. The flux-weakening method is applied to provide correct operation with the maximum available torque at any speed request within current and voltage limits. The simulation has been carried out to verify the performance and effectiveness of the HESS.

Results: The multi-source QZSI has the ability to respond quickly to mechanical load and provide constant DC bus voltage across the entire power demand profile. This HESS can successfully operate for traction and regenerative modes of EV motor. During these modes of operation, the control of HESS using FOPI controller for the EV motor functions well. These combinations of energy storage permit the EV to give good response during acceleration and the ability to recapture the energy during regenerative mode.

Contribution to this thesis: In this chapter, the topology of QZSI with these energy storages constitutes a veritable alternative for on-board energy management in multi-source EV. The multi-source bidirectional QZSI network provides independent power routines for the supercapacitor and the battery. The supercapacitor has a higher power density while battery has higher energy density. Then, this HESS performance can be increased in power and energy density by combining supercapacitor and battery. These combinations of energy storage enable the EV to give good response during acceleration. This HESS with these types of controllers and power distribution control system for management can globally enhance the performance of multi-source off-road EV. This performance improvement of the multi-source off-road EV can allow the efficient energy use of the battery for a longer distance coverage and extending its driving range.

Abstract

This paper proposes a new control configuration of hybrid energy storage system (HESS) using a battery pack and a supercapacitor for electric vehicle (EV). The HESS is designed based on bidirectional quasi-Z-source inverter (QZSI) and a DC-DC converter. The HESS configuration with its modeling is presented in this paper. The operation modes of HESS for EV and its control scheme using fractional order PI controller (FOPI) are presented. FOPI controller is combined with a filtering technique to contribute to battery degradation mitigation. The flux-weakening method is applied to provide correct operation with the maximum available torque at any speed request within current and voltage limits. The simulation results verify the performance and effectiveness of the HESS topology. The results also point out the ability of the inverter to give a fast response to the mechanical load and provide a DC bus constant voltage over the power-demand profile. The proposed HESS with these types of controllers and converter can globally enhance the performance of the EV by allowing the efficient energy use of the battery for a longer distance coverage and extending its driving range.

Keywords: Quasi-Z-source inverter, DC-DC converter, fractional order PI controller, electric vehicle, hybrid energy storage system, battery, supercapacitor.

6.1 Introduction

Electric vehicle production is gradually becoming more essential due to global concerns about environmental pollution, rapidly increasing fuel costs and depleting fossil fuel reserves. Nowadays, there is growing interest on electric vehicles (EVs) research in powertrain efficiency and battery lifetime. Various combinations of energy storage systems have been developed for EVs such as full EVs, hybrid EVs (HEVs) and EV plug-in HEVs. Among them, the hybrid energy storage system (HESS) which combines the battery, and the supercapacitor is widely used [125, 126, 127]. HESS has good characteristics in terms of power and energy density to extend EV driving range while improving its dynamic performance [128, 129]. The battery is generally able to provide a high energy density, while the supercapacitor has an advantage over the higher power density. Numerous configurations for the design of HESS have been proposed in the literature [125]. These configurations can be classified into the passive or active types. In the passive type, the battery and the supercapacitor are directly connected to the DC input of the inverter. Although this configuration has an advantage in terms of cost and power density, its lack of control negatively affects the system performance. In the active type, a DC-DC converter has been used and connected between the battery pack and the ultracapacitor [130, 131]. In this case, the DC-DC converter permits the control of the charge and discharge rates of the two sources. Then, this configuration enables to extend the battery lifetime and improves the efficiency of the system. The active type of HESS configuration realizes better performance as compared to passive HESS structures. However, the high cost, extra weight, large volume, the complexity of the circuitry and the control of the DC-DC converter usually limit their use in traction drive systems [128, 130].

Recently, the Z-source inverter (ZSI) has been used as replacement of conventional two-stage inverter in HESS with the idea to solve the aforementioned problems. The ZSI superiority compared to conventional two-stage inverter has been shown in [18]. ZSI has a unique characteristic of buck-boost capability which enables it to have wide voltage range. Many control strategies can be implemented with the dynamic model for Z-source network. In literature, the small-signal analyses and mathematical models have been used for the ZSI dynamic functioning study [9]. Thanks to the advantages of ZSI, these topologies are successfully used in fuel cell, battery, and other energy systems, such as solar energy systems. The configuration Z-source network using a fuel cell has been presented in [59]. ZSI applied to fuel cell vehicle has been compared with traditional voltage source inverter and conventional two-stage inverter in [60]. The results demonstrate that the ZSI has better efficiency, less switching devices, and more passive components requirement than the other types of inverters [98]. Hybrid ultracapacitor–battery energy storage system based on quasi-Z-source topology and enhanced frequency dividing coordinated control for EV has been studied in [64]. The results prove that the HESS can be integrated into the traction inverter system to obtain better performance and lower cost compared with conventional two-stage design. Moreover, the ZSI can also be applied to hybrid EV using fuel cell and battery with slight modification in its topology [65]. Nonetheless, this configuration has certain disadvantages with the necessity to use a high voltage battery and the fact that the DC link voltage is twice of the battery voltage during regenerative braking when the fuel cell is disconnected from ZSI input terminals. This disconnection could damage the switches of the inverter.

An effective control strategy must be designed to enhance the performance of HESS [132]. To regulate the power allocation, HESS for EV, stand-alone renewable energy power systems and wind power applications have been studied [133, 134]. The control strategies such as optimal control [135], neural network control [136] hierarchical control [137], model predictive control [138] have been also used. Most control strategies intend to deflect the power surge to supercapacitors feasibly using power flow regulation. In the last years, fractional order PI (FOPI) controller has been received a considerable attention both from academia and industry. FOPI controller provides greater flexibility in improving system performance comparatively to traditional PI controller through the presence of an additional tuning parameter [107]. This additional parameter which is the fractional integrator gain offers to the FOPI controllers additional features, such as flexibility on the system stability [107], robustness to plant uncertainties, high-frequency noise rejection, reduced sensitivity to load disturbances [139]. FOPI controller gives more adjustable time and frequency responses of the control system allowing fulfillment of better as well as robust performance.

This paper presents multi-source bidirectional QZSI using FOPI controllers for multiple sources EVs. FOPI controller is combined with a filtering technique for supercapacitor and battery degradation mitigation. The paper is organized as follows. Section 6.2 introduces the description of the proposed HESS configuration. The proposed HESS control design using FOPI as well as its effectiveness is discussed in the section 6.3. Section 6.4 presents the proposed HESS implemented using the Simscape™ Power Systems library of MATLAB/Simulink®. The simulations results are then presented and discussed. Conclusions are mentioned in Section 6.5.

6.2 Description of the proposed HESS

6.2.1 HESS configuration and its modeling

The complete configuration of the proposed HESS is shown in Figure 6.1. This configuration is based on the quasi-Z-source network consisting of capacitors C_1, C_2, inductors L_1, L_2 and the DC-DC converter. This DC-DC converter comprises inductor L, switches S_8, S_9 where C_1 represents its output capacitor. The DC-DC converter is used to control the absorbing and the releasing of battery power. The supercapacitor, battery and motor are the power sources and load, respectively, in this powertrain. The switches S_7 and S_8 contributes to a bidirectional power flow between energy storage devices and motor.

QZSI operating principles and features have been widely analyzed in [8]. During the steady state, the relationship of the capacitor voltages and the terminal voltages of the supercapacitor can be related to the shoot-through duty cycle D_H as follows:

$$\begin{cases} v_{c_1} = \dfrac{1 - D_H}{1 - 2D_H} v_{sc} \\ v_{c_2} = \dfrac{D_H}{1 - 2D_H} v_{sc} \end{cases} \tag{6.1}$$

The DC-link peak voltage $\hat{v}_{dc}$ can be derived from the sum of two capacitor voltages, v_{c_1} and v_{c_2}, by:

$$\hat{v}_{dc} = v_{c_1} + v_{c_2} = \frac{1}{1 - 2D_H} v_{sc} = B v_{sc} \tag{6.2}$$

where $B \geq 1$ is the boost factor resulting from the shoot-through period. Regarding the AC side of the QZSI, the peak phase voltage can be written as

$$\hat{v}_o = m_H \frac{\hat{v}_{dc}}{2} = \frac{m_H}{1 - 2D_H} . \frac{v_{sc}}{2} = G_H \frac{v_{sc}}{2} \tag{6.3}$$

where m_H and G_H are the inverter modulation index and total voltage gain of the QZSI, respectively.

The DC-DC converter used to control the power exchange of the battery can operate in two states as presented in [8]. The relationship of the battery and the capacitor C_1 voltage can be deduced as follows:

$$v_{c1} = \frac{1}{1 - d_C} v_{bat} \tag{6.4}$$

where d_C is the shoot-through duty cycle of the DC-DC converter.

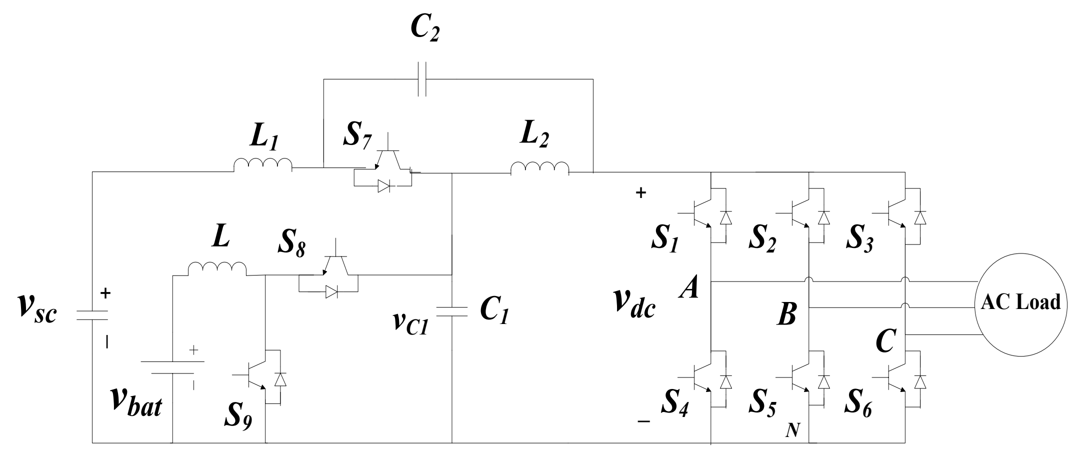

Figure 6.1: Configuration of the proposed HESS.

6.2.1 Operation mode of the proposed HESS

The proposed HESS can operate in three modes of operation: low power, high power [28, 80] and supercapacitor energy recovery mode. Each of these power modes can be used in traction or regenerative operation. In low power traction/regenerative mode, the total motor power demand is only provided by the battery pack and the supercapacitor has no power exchange with the battery and the motor. Also, the EV traction motor receives/stores energy in the battery via mode 1 and 2 as presented in Table 6.1.

In high-power traction/regenerative mode, the supercapacitor discharges or charge its power to support the battery pack to provide the motor power demand. During acceleration, the supercapacitor assists the battery to support the peak traction power and improves the EV response time for any acceleration request through mode 3 (Table 6.1). During deceleration or braking, considerable part of the regenerative power is stored in supercapacitor through mode 8 (Table 6.1). That will be contributed to increase the battery lifetime due to operation in a safe operating point.

In supercapacitor energy recovery mode, the supercapacitor is charged through mode 4 or 7 (Table 6.1) after releasing the power in order to conserve the energy storage level.

Table 6.1 summarizes the complete modes of operation where "O" and "I" mean releasing and absorbing the energy, respectively. Null represents the case where the supercapacitor is bypassed. Figure 6.2 shows the direction of power flow between the motor and energy storage devices during the high-power traction/regenerative mode operation of the HESS.

Table 6.1: HESS OPERATION MODES

	Supercapacitor	**Battery**	**Motor**
Mode 1	Null	O	I
Mode 2	Null	I	O
Mode 3	O	O	I
Mode 4	I	O	I
Mode 5	O	I	I
Mode 6	O	I	O
Mode 7	I	O	O
Mode 8	I	I	O

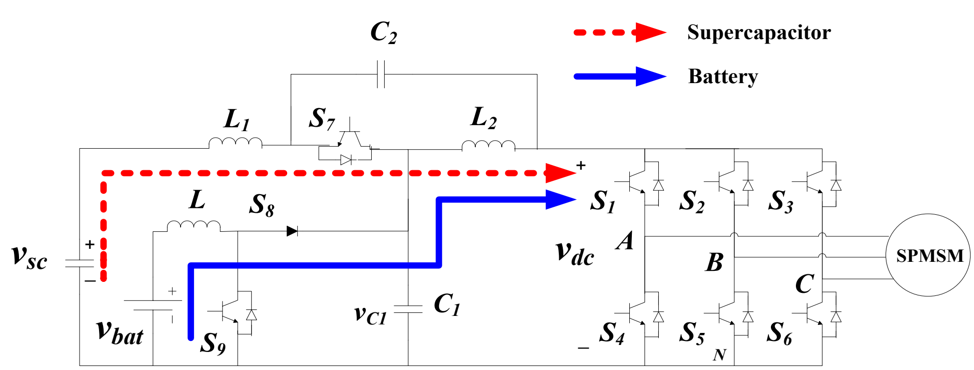

(a)

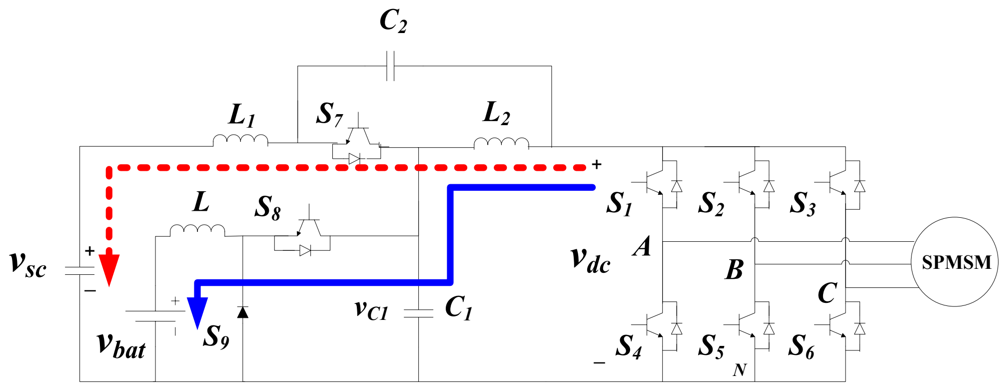

(b)

Figure 6.2: Direction of power flow during the high-power mode operation: (a) traction mode (b) regenerative mode.

6.3 Control of the proposed HESS system using FOPI

In our study, surface permanent magnet synchronous machine (SPMSM) is used as a traction electric motor. Its state space representation can be described as follows:

$$\begin{cases} L_d \frac{di_d}{dt} = -r_s\, i_d + v_d + p\Omega L_q i_q \\ L_q \frac{di_q}{dt} = -r_s\, i_q + v_q - p\Omega\left(L_d i_d + \psi_f\right) \\ J\frac{d\Omega}{dt} = T_e - \Gamma_{ch} - f\Omega \end{cases} \qquad (6.5)$$

$$T_e = \frac{3}{2}p(\psi_f i_q + (L_d - L_q)i_d i_q) \qquad (6.6)$$

where i_d and i_q are winding currents on the phases d and q, respectively [A], v_d and v_q are phase voltage [V] on the d and q axis, respectively, r_s is phase resistance [Ω] and L is phase inductance [H] and assumed to be constant, p is the number of pole pair, f is coefficient of viscous friction [kg.m^2/s], J is rotor inertia [kg.m^2], ψ_f is magnet flux linkage [Wb], Ω and Γ_{ch}.are rotor angular speed [rpm] and the load torque [N.m], respectively, T_e represents the developed motor torque [N.m].

Cascade FOPI controllers have been designed to accomplish the speed control and disturbance rejection. FOPI controller provides more adjustable time and frequency responses of the HESS control system to have robust performance as shown in [140]. The output feedback of the FOPI controller, K_{PI} , has the following form:

$$K_{PI}(s) = k_p + k_i \frac{1}{s^{\lambda}} \tag{6.7}$$

where k_p and k_i are the proportional and the integral gains respectively, and λ is the fractional integrator order, which gives an additional degree of freedom. FOMCON toolbox for MATLAB™ has been used for the implementation of FOPI controller [120].

The 3-phase stator currents of the SPMSM are measured and converted into i_d and i_q currents. The actual rotating speed is compared with the reference speed and the FOPI controller allows to obtain the reference current i_{qref}. The flux-weakening (FW) method is applied to provide correct operation with the maximum available torque at any speed within current and voltage limits. This method is achieved by considering the maximal allowable motor phase voltage and phase current. The constraints of maximum phase voltage and maximum phase current available can be expressed as follows:

$$i_d^{\,2} + i_q^{\,2} \leq i_{max}^{\,2} \tag{6.8}$$

$$v_d^{\,2} + v_q^{\,2} \leq v_{max}^{\,2} \tag{6.9}$$

where i_{max} and v_{max} represents the current and voltage limit, respectively. When the motor speed is lower than the base speed ($\Omega \leq \Omega_{base}$), the i_{dref} is set as zero in the constant torque region. In the FW region, where the motor speed is higher than the base speed ($\Omega > \Omega_{base}$), the FW strategy permits to obtain negative current reference i_{dref} based on following expression [141]:

$$I_d = \frac{\psi_f}{L_d}\left(\frac{\Omega_{base}}{\Omega} - 1\right) \tag{6.10}$$

where L_d indicates the phase d inductance of the SPMSM, ψ_f is the equivalent magnetic flux linkage of the SPMSM, and Ω and Ω_{base} denote the motor speed and the base speed, respectively.

The measured and reference currents are compared, and the FOPI controller allows to obtain the reference voltages $v_{dref},\ v_{qref}$.These voltages are also converted and permits to generate the voltages using maximum constant boost control (MCBC) technique [66]. FOPI controller is also used to regulate the DC-link voltage, the inductors current of the QZSI and the DC-DC converter. The voltage and current closed loop FOPI control filtered by a low-pass filter (LPF) enables to obtain the shoot-through duty cycle d_H. The use of this LPF contributes to reduce voltage and current ripple. The shoot-through duty cycle d_H and the modulation index m_H are delivered to the PWM block allowing to generate the switching signals. The switch S_7 of QZSI operates to a bidirectional power flow. It is controlled to have signal that is complementary with the shoot-through signal of the inverter. The proposed HESS powertrain control scheme is shown in Figure 6.3. In the control scheme, the I_{load} average current is filtered through a LPF with cut-off frequency *f*. A fraction of this filtered current amount represented by $\frac{1}{m_{S_8S_9}.\eta_{conv}^{k_{conv}}}$ is used as the battery reference current I_{batref} where $m_{S_8S_9}, \eta_{conv}^{k_{conv}}$, k_{conv} represent modulation index, efficiency and the coefficient depending on the power direction of the DC-DC converter, respectively. The average current is filtered in order to eliminate the noise and very high frequency ripple due to the switching operation. This current is used in bidirectional DC-DC converter to control the buck and boost operation of battery. This current control must permit to obtain acceptable charging and discharging of the battery current in response to the transient power change with better stability.

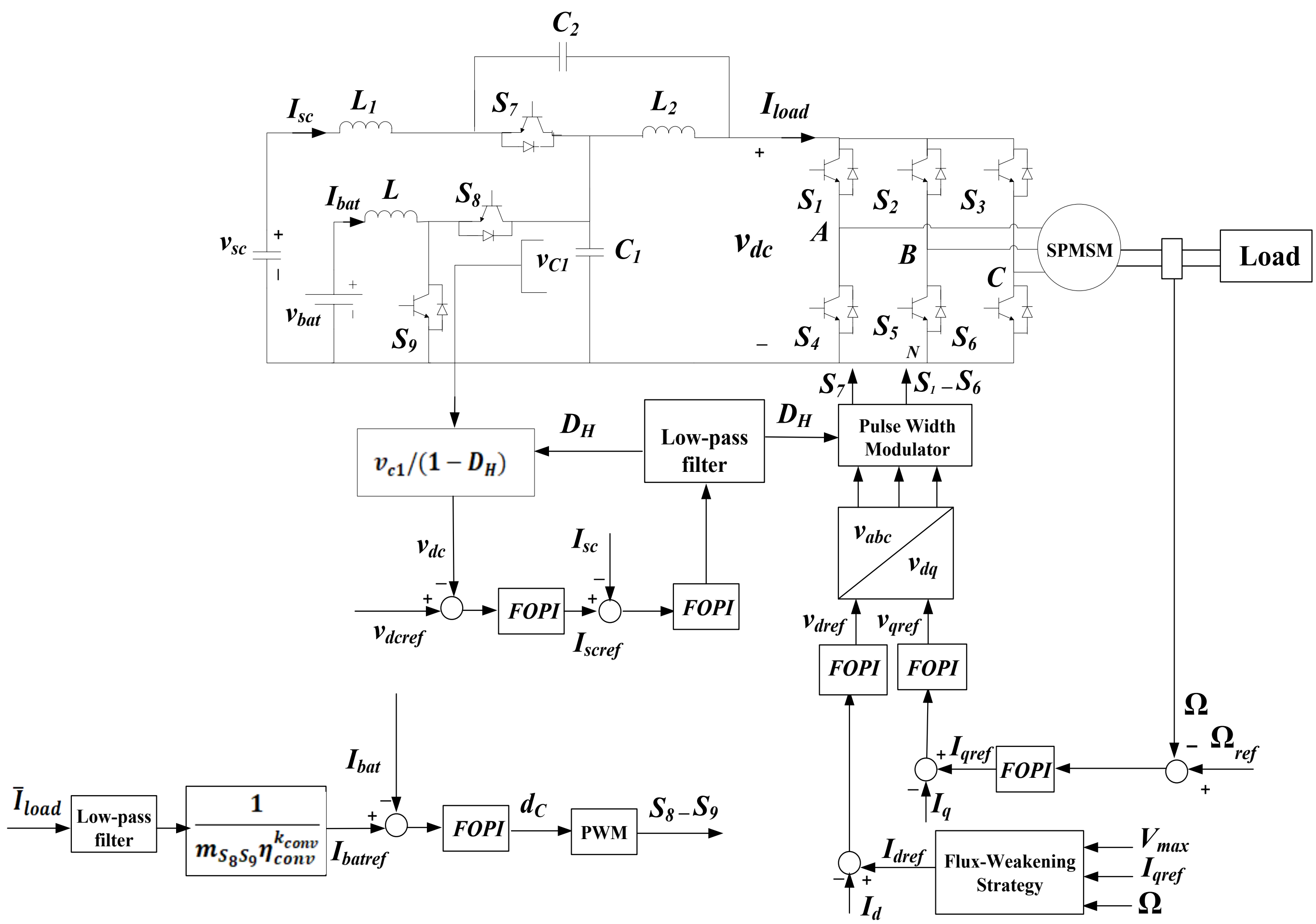

Figure 6.3: Speed control scheme based on FOPI controllers.

6.4 Simulation results

A simulation has been performed using the Simscape™ Power Systems library of MATLAB/Simulink® to verify the effectiveness of the proposed HESS for EV. The main parameters of the HESS for the simulations are presented in Table 6.2 [98, 140]. The SPMSM rated power is 15 kW. MCBC method as presented in [66] has been used to generate the gate signals of the QZSI switches. The speed and torque waveforms have been shown in Figure 6.4 and Figure 6.5, respectively. Figure 6.6 and Figure 6.7 show the currents i_q, i_d with their references, respectively. Figure 6.8 represents the v_{dc} voltage and its reference. The battery and supercapacitor current and its references have been represented in Figure 6.9 and Figure 6.10, respectively. Figures 6.11 and 6.12 show the battery and supercapacitor voltages, respectively.

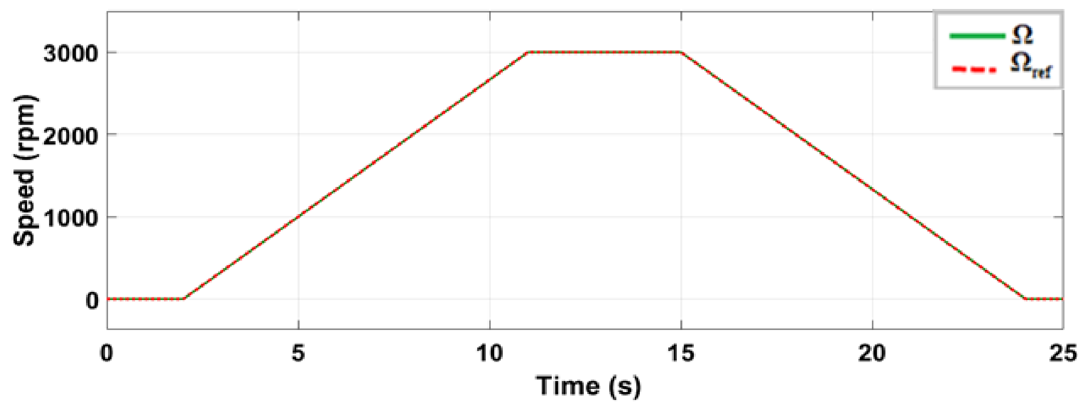

Figure 6.4: Motor speed and reference with multi-source bidirectional QZSI.

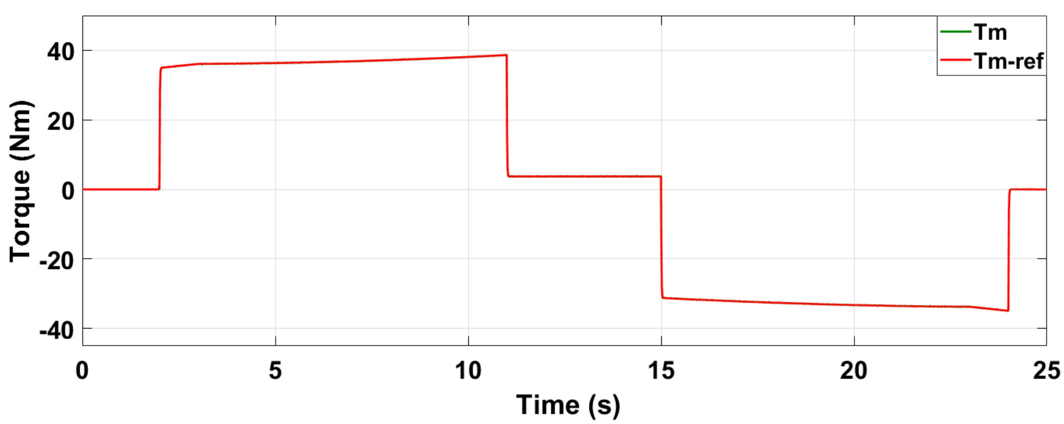

Figure 6.5: Motor torque and reference with multi-source bidirectional QZSI.

Table 6.2: EV PLATFORM PARAMETERS

Parameters	**Variable Name**	**Values**
Vehicle (e-Commander)		
Total mass of the EV	M_{veh}	857 kg
Aerodynamic standard	$c_x A$	1.3 m^2
Rolling coefficient	k_{roll}	0.035
Air density (at 20^O C)	ρ	1.223 kg/m^3
Motor to wheel transmission ratio	G_{tr}	20.5
Efficiency of the transmission	η_{tran}	0.87
Wheel radius	R_{wh}	0.3175 m
SPMSM parameters		
Phase inductance	L_d, L_q	1 mH
Phase resistance	r_s	0.08 Ω
Number of pole pair	p	2
Global inertia referred to the rotor	J	1 kg.m^2
Magnet flux linkage	ψ_f	0.1 Wb
Rated power	P_r	15 kW
Motor base speed	Ω_{base}	154 rad/s
Multi-source Quasi-Z-source inverter parameters		
Inductance	L_1, L_2	220 µH
Inductance	L	2.72 mH
Capacitance	C_1	2.3 mF
Capacitance	C_2	8.5 mF
Cut-off frequency	f	40 mHz
Switching frequency	f_s	10 kHz
Batteries (Lithium-ion valence battery cells)		
Cell capacity	$C_{batcell}$	40 Ah
Cell nominal voltage	$v_{batcellnom}$	12.8 V
Cell minimum voltage (at 20% SoC)	$v_{batcellmin}$	10 V
Cell equivalent serial resistance	$r_{batcell}$	15 $m\Omega$
Number of cells in series	$n_{batcellse}$	4
Number of branches in parallel	$n_{batcellpa}$	4
Supercapacitor		
Rated capacitance	C_{sc}	58 F
Nominal voltage	v_{scnom}	16 V
Number of series capacitors	$n_{sccellse}$	3
Number of parallels capacitors	$n_{sccellpa}$	3
Internal resistance	r_{sc}	2.2 mΩ

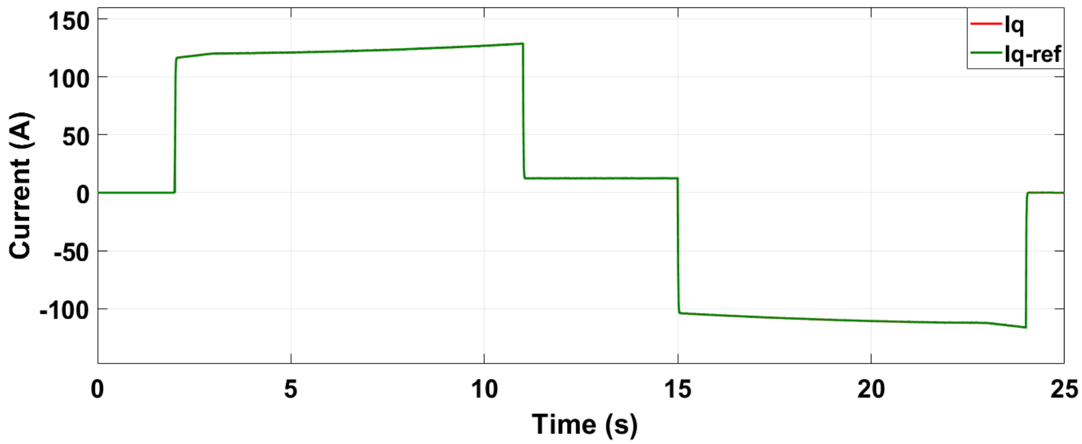

Figure 6.6: The i_q current and its reference.

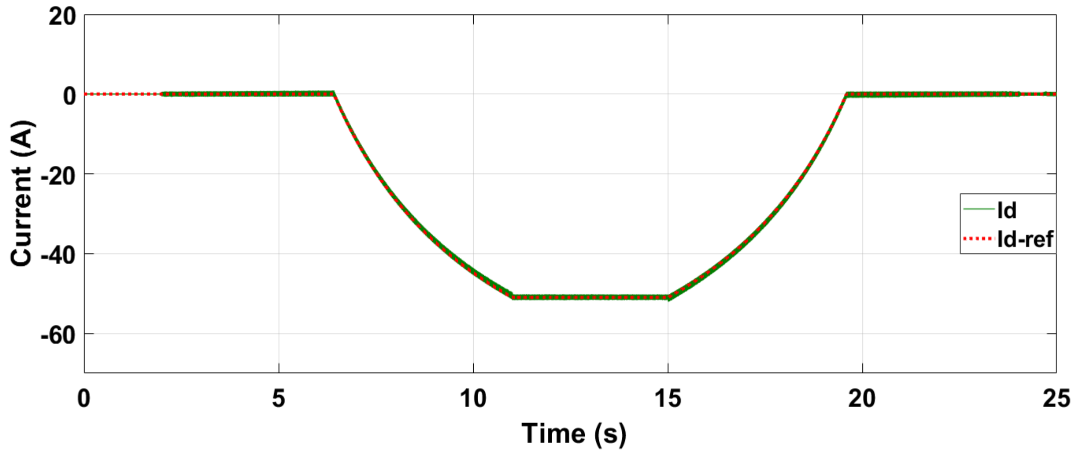

Figure 6.7: The i_d current and its reference.

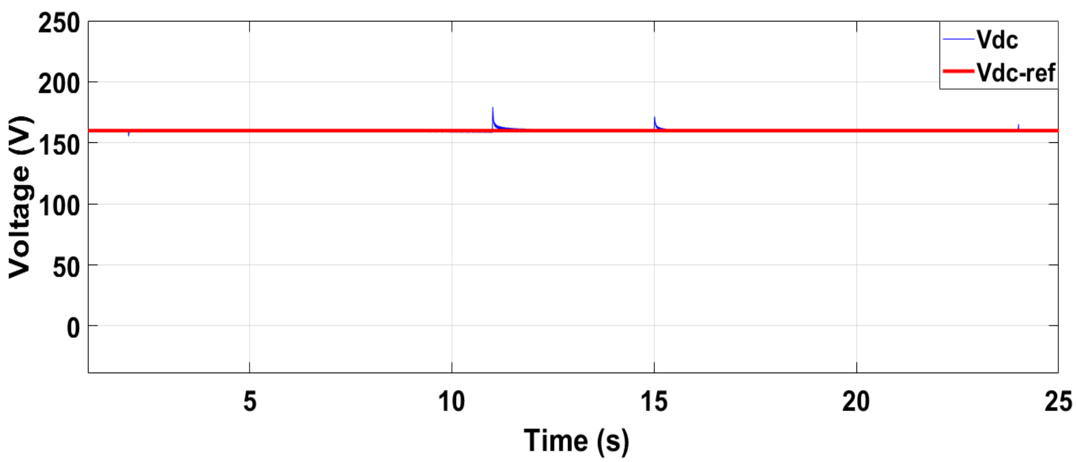

Figure 6.8: The v_{dc} voltage and its reference.

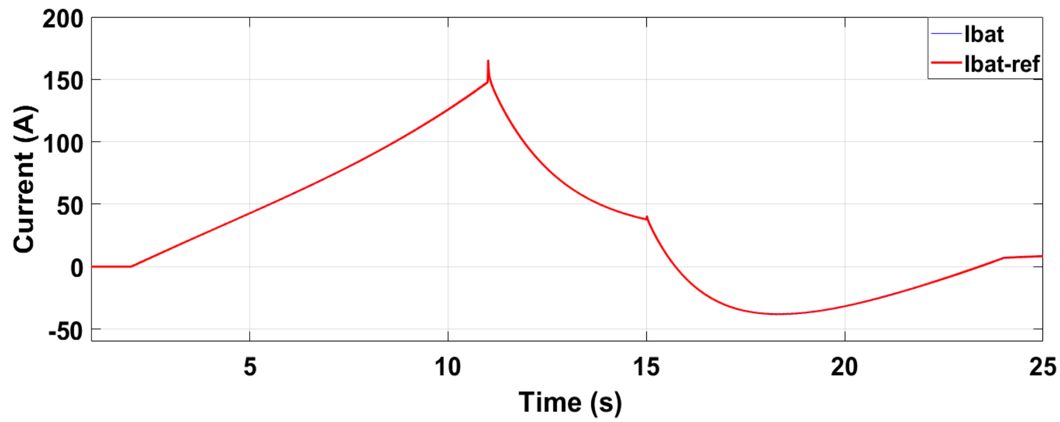

Figure 6.9: The battery current and its reference.

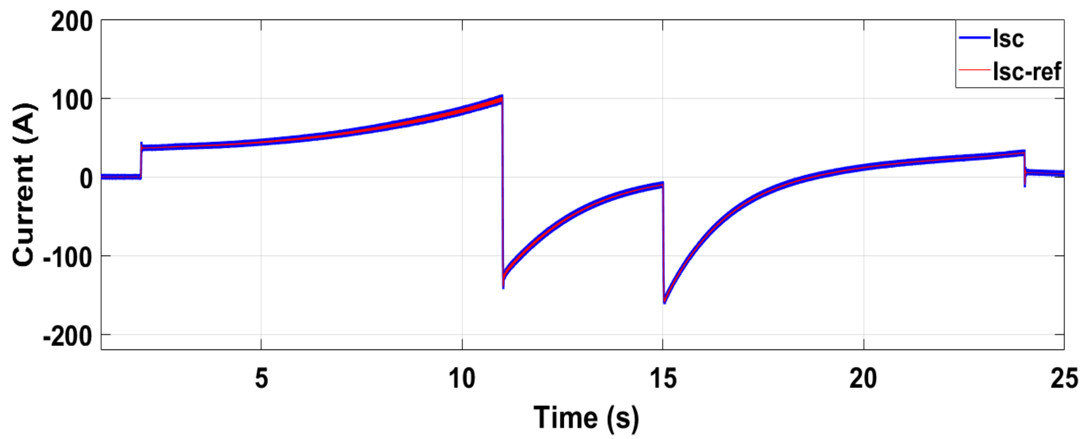

Figure 6.10: The supercapacitor current and its reference.

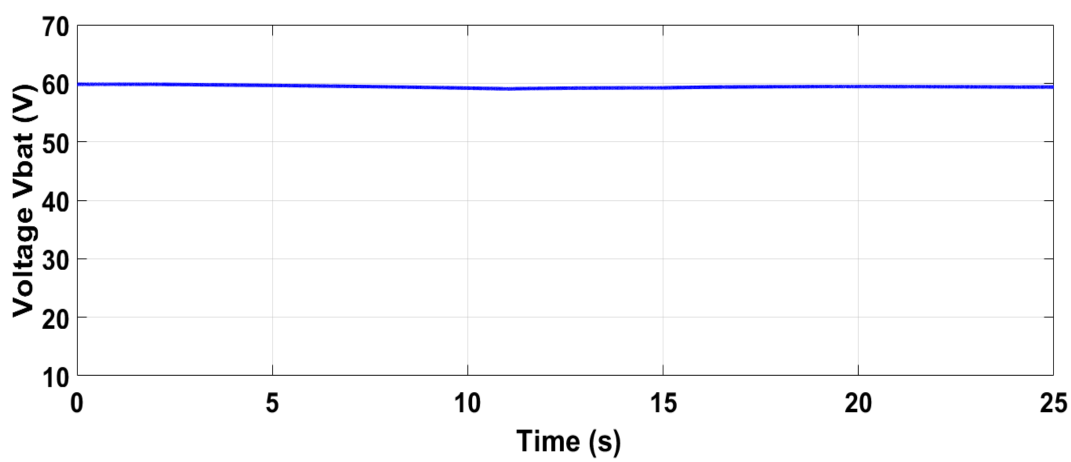

Figure 6.11: The battery voltage v_{bat}.

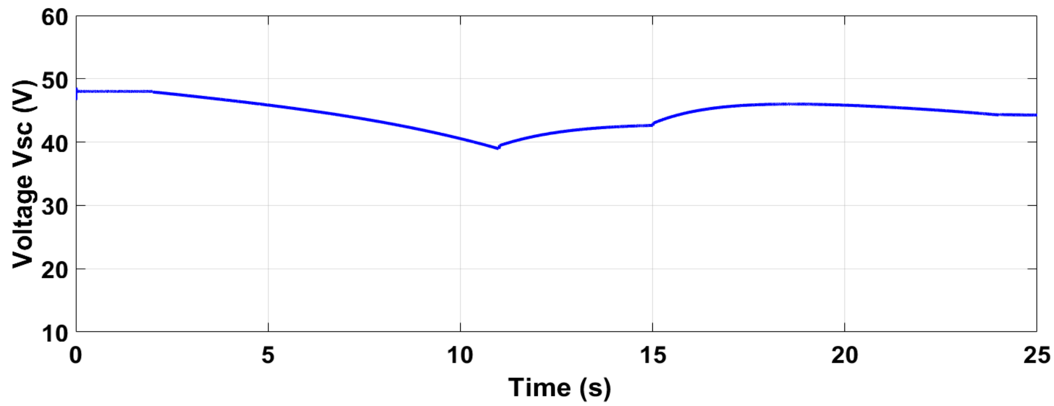

Figure 6.12: The supercapacitor voltage v_{sc}.

These figures show that the speed, the torque, the v_{dc} voltage, the battery and supercapacitor currents has been controlled using FOPI to track their references in a best desired way including in the FW operation. The results reveal the ability of the inverter to respond quickly to the mechanical load and provide a DC bus constant voltage over all the power-demand profile. Figure 6.13 shows battery, supercapacitor, and total power of the proposed HESS during EV motor traction and regenerative modes in high-power mode.

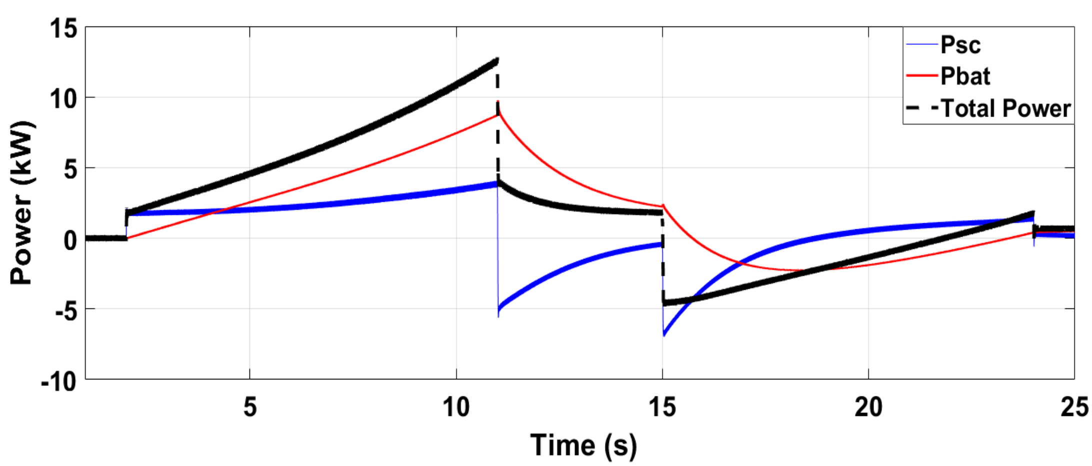

Figure 6.13: The battery and the supercapacitor power.

For t < 15 s, EV motor operates in traction mode and HESS operates in high power mode during 11 s. The battery pack and the supercapacitor are discharged. The supercapacitor discharges its power to support the battery to provide the motor power demand. During acceleration, supercapacitor assists the battery to provide the peak traction power and contributes to improve the EV response time for an acceleration request. For 11 to 15 s, the supercapacitor operates in recovery mode**.** For t > 15 s, EV motor operates in regenerative mode and the supercapacitor operates in recovery mode for the interval between 15 to 18 s. The battery gets charged for the interval between 16 to 18s. For 12 to 18 s, the battery is charged while the supercapacitor is discharged. During deceleration, the part of the regenerative power is stored in the supercapacitor. The above results of the proposed HESS prove that the addition of the supercapacitor can help the battery to cover the peak traction power demand of the EV. The supercapacitor can contribute to efficient energy use of the battery and extend the EV driving range. This HESS composed of a battery and supercapacitor using FOPI control enables to make full use of advantages in energy and power density, that can further enhance the performance of any EV**.**

6.5 Conclusion

This paper has proposed a new configuration of supercapacitor/battery HESS based on bidirectional QZSI for EV. The overall HESS configuration with its modeling is presented. The operation modes of HESS for EV are defined. The control scheme of the proposed HESS to meet the dynamic response requirements for energy storage devices using FOPI is also studied. The flux-weakening algorithm has been applied. The simulation results verify the performance and effectiveness of the proposed HESS. The multi-source bidirectional QZSI network provides independent power routines for the supercapacitor and the battery. The results have shown that the proposed HESS can successfully operate for traction and regenerative modes of EV motor. During these modes of operation, the control of HESS using FOPI for the EV motor functions well. The results highlight the ability of the inverter to respond quickly to mechanical load and provide constant DC bus voltage across the entire power demand profile. The buck/boost characteristic of the QZSI permits to achieve an efficient use of supercapacitor energy. This proposed HESS enables to improve the power and energy density using FOPI to control the energy storage devices voltage and current. The addition of supercapacitor can contribute to efficient energy use of the battery for a longer distance coverage, which permits to extend the EV driving range. Hence the future work is to use a power distribution control system for the enhancement of the energy management in a multi-source off-road EV.

6.6 Acknowledgment

This work was supported in part by Grant 950-230672 from Canada Research Chairs Program, in part by Grant RGPIN-2017-05924 from the Natural Sciences and Engineering Research Council of Canada, and in part by FCT-Portuguese Foundation for Science and Technology project

UIDB/00308/2020, and by the European Regional Development Fund through the COMPETE 2020 Program within project MAnAGER (POCI-01-0145-FEDER-028040).

Chapter 7 Dual-source Bidirectional Quasi-Z-source Inverter Development for Off-Road Electric Vehicles

Original Title: Dual-source Bidirectional Quasi-Z-source Inverter Development for Off-Road Electric Vehicles

Authors and affiliation :

- **Daouda Mande**: Ph.D. student, e-TESC Laboratory, Department of Electrical & Computer Engineering, University of Sherbrooke
- **João P. Trovão**: Professor, e-TESC Laboratory, Department of Electrical & Computer Engineering, University of Sherbrooke
- **Minh C. Ta**: Professor, e-TESC Laboratory, Department of Electrical & Computer Engineering, University of Sherbrooke
- **T. Van Do**: Ph.D. student, e-TESC Laboratory, Department of Electrical & Computer Engineering, University of Sherbrooke

Date of Acceptance: 17 September 2022

State of acceptance: Published

Reference: World Electric Vehicle Journal, DOI: 10.3390/wevj13090174

Summary

Content: In this chapter, battery pack and a supercapacitor bank hybrid energy storage system (HESS) with new control configuration is proposed for electric vehicles (EVs). Bidirectional quasi-Z-source inverter (Bq-ZSI) and a bidirectional DC-DC converter are used in the powertrain of the EV. The scheme of the control for the proposed HESS Bq-ZSI using finite control set model predictive control (FCS-MPC) is first deduced to enhance the dynamic performance. With the idea of managing to battery degradation mitigation, the fractional-order PI (FOPI) controller is then applied and associated with a filtering technique. The Opal-RT-based real-time simulation is next executed to verify the performance and effectiveness of the proposed HESS control strategy.

Results: The proposed HESS Bq-ZSI with this control scheme provides a quick response to the mechanical load and stable DC link voltage under the studied driving cycle. Moreover, the comparative results also show that the proposed HESS Bq-ZSI equipped with the new control configuration enables to reduce the root-mean-square value, the mean value, and the standard deviation by 57 %, 59 % and 27 %, respectively, of the battery current compared to the battery-based inverter. Thus, the proposed HESS Bq-ZSI using these types of controllers can help to improve the EV system performance.

Contribution to this thesis: In this chapter, the multi-source Bq-ZSI based on the SC/BAT HESS with this new control configuration represents a real alternative for on-board energy management in multi-source EV. The proposed HESS Bq-ZSI can be well operated for different modes of EV motor, in which independent power routines for the supercapacitor and the battery can be accomplished by the multi-source Bq-ZSI. The control enhancement of the dual-source Bq-ZSI enables to improve efficacy and dynamic performance for dual-source EV. The proposed HESS which combines these types of power electronic converters and controllers including power distribution control system for management can overall enhance the performance of multi-source off-road EV. This performance enhancement of the multi-source off-road EV permits to efficient use of battery energy, enabling longer distance coverage, thus extending the driving range of EV.

Abstract

In this paper, a battery pack and a supercapacitor bank hybrid energy storage system (HESS) with a new control configuration is proposed for electric vehicles (EVs). A bidirectional quasi-Z-source inverter (Bq-ZSI) and a bidirectional DC-DC converter are used in the powertrain of the EV. The scheme of the control for the proposed HESS Bq-ZSI using finite control set model predictive control (FCS-MPC) is first deduced to enhance the dynamic performance. With the idea of managing battery degradation mitigation, the fractional-order PI (FOPI) controller is then applied and associated with a filtering technique. The Opal-RT-based real-time simulation is next executed to verify the performance and effectiveness of the proposed HESS control strategy. As a result, the proposed HESS Bq-ZSI with this control scheme provides a quick response to the mechanical load and stable DC link voltage under the studied driving cycle. Moreover, the comparative results also show that the proposed HESS Bq-ZSI equipped with the new control configuration enables the reduction of the root-mean-square value, the mean value, and the standard deviation by 57%, 59%, and 27%, respectively, of the battery current compared to the battery-based inverter. Thus, the proposed HESS Bq-ZSI using these types of controllers can help to improve the EV system performance.

Keywords: quasi-Z-source inverter; DC-DC converter; finite control set model predictive controller; real-time simulation; hybrid energy storage system; battery; supercapacitor; electric vehicle.

7.1 Introduction

Electric vehicles (EV) are becoming an increasingly important part of the automotive landscape due to concerns about environmental pollution, rapidly rising fuel costs, and the depletion of fossil fuel reserves. In the last decades, there has been growing interest in EV research. Several combinations of energy storage systems (ESSs) for EVs such as full EV, hybrid EV, and EV plug-in have been developed. The hybrid energy storage system (HESS) combining the battery (BAT) and the supercapacitor (SC) is widely used [125, 126, 127]. It constitutes an attractive solution for the EV energy storage system. The HESS exhibits good characteristics in terms of the power and energy density to extend the EV driving range while enhancing its dynamic performance [129, 141]. The battery is generally capable of delivering high energy density, while the supercapacitor has an advantage of higher power density. Various configurations for the design of the HESS have been proposed in the literature [125]. These configurations can be classified into the passive or active types. In the passive type, the battery and the supercapacitor are directly connected via the DC input of the inverter. This topology has an advantage in terms of cost and power density; however, its lack of control negatively affects the system performance, which might have a negative impact on the battery lifetime. In this respect, the usage mode of the battery highly affects its lifetime [90]. Variations of large and frequent currents greatly stress the battery [91]. The cycle life of the battery deteriorates over time as it is affected by cycling conditions and multiple degradation mechanisms [142]. Moreover, the control method of the battery current and its behavior can seriously impact the long-term performance of the battery. In [93], the aging index of the battery was used to evaluate the performance of fractional-order PI control using the ant colony optimization Nelder–Mead algorithm. In the active type, DC-DC converters are commonly used to couple the DC link with the ESSs [130,131]. The rates of charge and discharge control of the two sources are achieved through the DC-DC converters. This leads to increasing the lifetime of the battery and improving the system efficiency. Consequently, this kind of HESS configuration can provide better performance over the passive one. However, the use of DC-DC converters in traction drive systems is generally limited due to their large volume, extra weight, high cost, and complexity of control [130,141].

In order to solve the aforementioned problems, utilizing single-stage converters based on the Z-Source inverter (ZSI) and quasi-ZSI (qZSI) has come under attention to replace the conventional two-stage inverters. Their superiorities compared to the conventional ones have been shown by Peng [8, 97], who showed that these topologies present a unique buck-boost capability characteristic, allowing them to have a wide range of voltage variations. To promote their application to the EV power electronics system, numerous studies have been implemented. The dynamic operation of the qZSI system has been investigated using the small-signal analyses and mathematical models in the literature [9]. The ZSI and the qZSI are widely used with different ESSs due to their advantages. Z-source network (ZSN) configuration based on the qZSI using a fuel cell has been shown in [59]. A comparison between the ZSI and the conventional two-stage inverter in fuel cell vehicles has been presented in [60]. As pointed out, using the ZSI results in improved system efficiency and reduced system size and volume for this vehicle. However, the adoption of the ZSI in the EV system is still under restriction since the ZSI experiences discontinuous input/high inrush currents, resulting in a reduction in the lifetime of the ESS. Recently, the SC/BAT HESS ZSI has been studied for the EV in [64]. This converter integrates the BAT into its ZSN without adding an extra DC-DC converter. That enables the obtention of a lower cost and better performance compared to the conventional two-stage inverter. Nonetheless, this integration could lead to the damaging of the BAT because of its rush discharging/charging currents exiting in a short time, which might be beyond its controller's bandwidth. Moreover, the BAT's lifetime is strongly influenced by these rush currents. In this paper, the dual-source Bq-ZSI is used in the EV powertrain to overcome these issues mentioned above. This impedance source inverter is obtained by coupling the BAT with the ZSN of the Bq-ZSI through a bidirectional DC-DC converter. The HESS Bq-ZSI is considered as a non-minimum phase system with right-half plane (RHP) zeros. This results in restraints in the controller's bandwidth and the system's slow dynamic response for the DC-link controller. It is well understood that the RHP zero results in an undershoot as well as an overshoot in the transient response. Moreover, the field-oriented control (FOC) of motor drives with PI controllers also has limitations in fast and smooth performances over a broad range of motor speeds. Thus, to enhance the dynamic performance of the HESS Bq-ZSI, designing an effective control strategy is extremely important to deal with rapid input and load changes. Various control schemes have recently been studied to manage the power distribution for stand-alone renewable energy power systems, wind power systems, and EV applications [134, 135, 136, 143, 144, 145, 146]. Among these schemes, the finite control set model predictive control (FCS-MPC) has been found to be a promising control scheme in power electronics [147]. This controller examines only a finite set of possible switching states of power converters, solves the cost function for each of them, and chooses a switching state that minimizes the cost function. Thus, it possesses a simple nature, nonlinearities in the control design, an easy implementation, and a fast dynamic response in tracking the reference values of the controlled variables [148-151]. As a result, this controller is used in this study for improving the dynamic performance of the proposed HESS Bq-ZSI. For conducting experiments more safely and decreasing the development cycle and costs, the control schemes of the EV power electronics converters can first be carried out by offline simulation tools, such as MATLAB/Simulink, PSIM, PSCAD, etc. However, the goal of these tools is to attain simulation results quickly, and their computing time can be shorter or longer than the response time of the real system. Furthermore, they may struggle to interface with real hardware and controllers. This makes them not suitable for controlling the industrial complex powertrains. By contrast, the real-time simulation in which the computing time is shorter than the time-step is a considerable platform for tackling these issues, owing to its extremely high security and repeatability. Therefore, it is applied in this study to implement more precisely for EV power electronics systems. A literature survey reveals that there is a lack of studies on control methods to enhance the dynamic performance of EV systems based on the HESS ZSI topology. To fill this gap, this paper presents the control enhancement of the dual-source Bq-ZSI for an off-road EV. In this respect, the FCS-MPC controller is used for the Bq-ZSI deployment, while the fractional-order PI (FOPI) controller is integrated with a filtering technique to mitigate the degradation of the battery. Compared to the traditional PI controller, the FOPI controller provides greater flexibility in improving system performance due to the presence of fractional integrator gain. This additional tuning parameter gives the FOPI controllers more features, such as robustness regarding plant uncertainties, flexibility regarding the system stability, high-frequency noise rejection, and reduced sensitivity to load disturbances [139]. Thus, the main contributions of the paper are as follows:

- It provides a novel control configuration of SC/BAT HESS Bq-ZSI for EV systems.
- It improves the SC/BAT HESS EV in terms of the dynamic performance and the battery lifetime.

To verify the proposed control method, an Opal-RT-based real-time simulation is used to evaluate the dynamic performance of the SC/BAT HESS Bq-ZSI. This paper is organized as follows. Section 7.2 introduces the configuration of the HESS. In Section 7.3, the design of the proposed HESS control using FCS-MPC and its effectiveness are discussed. The real-time simulation results and the comparison of different architectures and control methods in terms of the aging performance indexes of the battery are presented in Section 7.4. A conclusion is drawn in Section 7.5.

7.2 Hybrid Energy Storage System Configuration and Modeling

Figure 7.1 shows the configuration of the proposed HESS Bq-ZSI. This configuration is based on the ZSN of the Bq-ZSI composed of capacitors (C_1, C_2) and inductors (L_1, L_2) and the bidirectional DC-DC converter. This DC-DC converter is composed of C_1, which represents its output capacitor, the inductor L, and the switches (S_8, S_9). Since the shoot-through state of the Bq-ZSI could solely be altered in a zero state, its practical boost factor is commonly restricted. This may limit its applications in the EV, where the high-voltage gain is required for the ESS. To tackle this issue, the higher voltage of the battery is necessary for the Bq-ZSI; however, it might increase the EV cost, the system size, and the volume. Thus, in this study, the battery is connected to the bidirectional DC-DC converter to supply the required power for the electric motor, while the supercapacitor coupled to the qZSI network is used as backup energy storage to provide/absorb transient power during acceleration/braking operations. Moreover, the battery-absorbed and -released power are controlled in bidirectional power flows by the DC-DC converter through its switches S_7 and S_8.

The Bq-ZSI operating principles have been largely examined in [8]. The relationship between the capacitor voltages and the supercapacitor terminal voltages during the steady state can be deduced with the shoot-through duty cycle D_H by:

$$\begin{cases} v_{c_1} = \dfrac{1 - D_H}{1 - 2D_H} v_{sc} \\ v_{c_2} = \dfrac{D_H}{1 - 2D_H} v_{sc} \end{cases} \tag{7.1}$$

The DC-link peak voltage $\hat{v}_{dc}$ can be derived from the sum of two capacitor voltages, v_{c_1} and v_{c_2}, by:

$$\hat{v}_{dc} = v_{c_1} + v_{c_2} = \frac{1}{1 - 2D_H} v_{sc} = B v_{sc} \tag{7.1}$$

where $\boldsymbol{B} \geq 1$ is the boost factor resulting from the shoot-through period. Regarding the AC side of the Bq-ZSI, the peak phase voltage can be written as follows:

$$\hat{v}_o = m_H \frac{\hat{v}_{dc}}{2} = \frac{m_H}{1 - 2D_H} \cdot \frac{v_{sc}}{2} = G_H \frac{v_{sc}}{2} \tag{7.2}$$

in which $\boldsymbol{m_H}$ and $\boldsymbol{G_H}$ denote the inverter modulation index and the total voltage gain of the Bq-ZSI, respectively.

The battery power exchange is controlled by the DC-DC converter, which can operate in two states, as shown in [8]. The relationship between the capacitor $\boldsymbol{C_1}$ and the battery voltage can be expressed as:

$$v_{c1} = \frac{1}{1 - d_C} v_{bat} \tag{7.3}$$

where $\boldsymbol{d_C}$ is the duty cycle of the DC-DC converter.

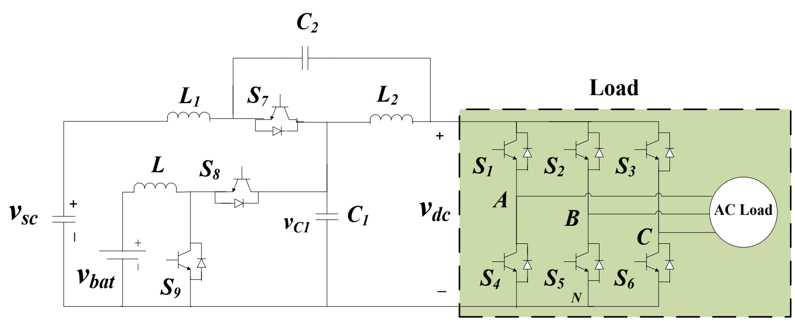

Figure 7.1: Proposed HESS Bq-ZSI configuration.

In general, the proposed HESS operation modes can be categorized into low-power, high-power [28, 80], and supercapacitor energy recovery modes. In traction or regenerative operation, each of these power modes can be used. In the low-power traction/regenerative mode, the battery pack only offers the total motor power demand. In this case, there is no power exchange for the supercapacitor with the battery and the motor. Additionally, the EV traction motor receives/stores energy in the battery through modes 1 and 2, as shown in Table 7.1.

In the high-power traction/regenerative mode, the supercapacitor power can be discharged or charged. Its power is used to assist the battery pack to afford the motor power demand. During acceleration, the supercapacitor helps the battery to sustain the maximum traction power via mode 3 (Table 7.1). This enhances the response time of the EV for a request of acceleration. The major part of the regenerative power is stored in the supercapacitor during braking or deceleration through mode 8 (Table 7.1). This will help to extend the lifetime of the battery due to operation within a safe operating point.

The supercapacitor is charged in the supercapacitor energy recovery mode after releasing the power to maintain the energy storage level via mode 4 or 7 (Table 7.1).

The complete modes of HESS operation are listed in Table 7.1 where positive and negative denote releasing and absorbing the energy, respectively. Null indicates that the supercapacitor is bypassed. Figure 7.2 presents the power flow between the motor and the energy storage device in the HESS high-power traction/regenerative mode.

Table 7.1: Operation modes of the HESS

	Supercapacitor	**Battery**	**Motor**
Mode 1	Null	+	−
Mode 2	Null	−	+
Mode 3	+	+	−
Mode 4	−	+	−
Mode 5	+	−	−
Mode 6	+	−	+
Mode 7	−	+	+
Mode 8	−	−	+

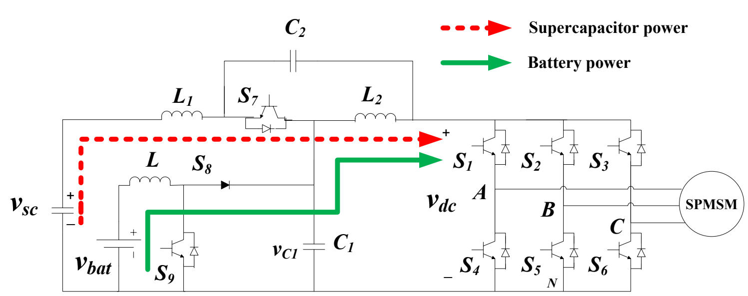

(a)

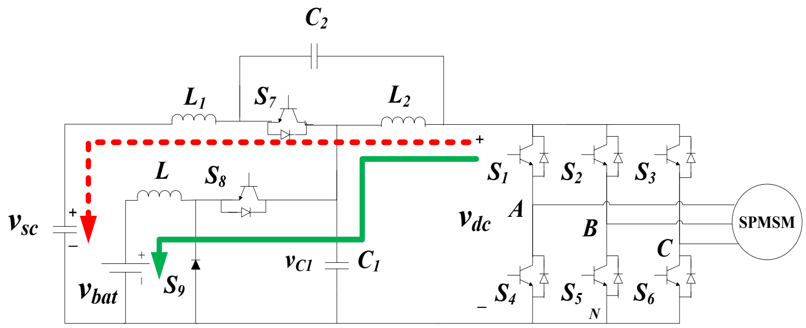

(b)

Figure 7.2: Power flow direction during the high-power mode operation: (a) traction mode (b) regenerative mode.

7.3 Finite Control Set Model Predictive Controller

In this study, a surface permanent magnet synchronous machine (SPMSM) is used as a traction electric motor. Its state space representation can be described as presented in [8]. The FCS-MPC and FOPI controllers are designed to improve the dynamic performance for the speed control and disturbance rejection. The FCS-MPC is an optimal control technique which provides the easy handling of constraints and fast dynamic performance [152]. In this respect, the cost function of the FCS-MPC is used for the enhanced performance, considering some parameters of the system. The FCS-MPC control technique is adopted based on the model of SPMSM. From the SPMSM side, the feedback signals are the rotor speed and the three-phase stator currents i_{abc}. The i_d and i_q currents are obtained from the measured and converted three-phase stator currents of the SPMSM. The FOPI controller is designed to achieve the speed control. It also allows for the determination of the reference current i_{qref}. With the idea of ensuring correct operation with the maximum available torque within current and voltage limits at any speed, the flux weakening (FW) strategy is applied. This strategy is realized by taking into consideration the motor's maximum allowable phase voltage and phase current. The available maximum phase voltage and maximum phase current constraints can be deduced as follows:

$$i_d{}^2 + i_q{}^2 \leq i_{max}{}^2 \tag{7.4}$$

$$v_d{}^2 + v_q{}^2 \leq v_{max}{}^2 \tag{7.5}$$

where v_{max} and i_{max} denote the voltage and current limitations, respectively. In the constant torque region, where the motor speed is smaller than the base speed ($\Omega \leq \Omega_{base}$), the i_{dref} is set as zero. When the motor speed is greater than the base speed ($\Omega > \Omega_{base}$), the FW strategy allows for the obtention of the negative current reference i_{dref} in the FW region. The i_{dref} is determined from the following expression [140].

$$I_d = \frac{\psi_f}{L_d}\left(\frac{\Omega_{base}}{\Omega} - 1\right) \tag{7.6}$$

where L_d is the phase d inductance of the SPMSM, ψ_f represents the equivalent magnetic flux linkage of the SPMSM, and Ω and Ω_{base} are the motor speed and the base speed, respectively.

According to the discrete time model obtained with the backward Euler method, as shown in [153], the state variables $i_{sc}(k+1)$, $v_{c1}(k+1)$, $v_{c2}(k+1)$, $i_d(k+1)$, and $i_q(k+1)$ are predicted for the $(k+1)$th time instant. They are also used to evaluate the predetermined cost function. The cost functions are established with the aim of minimizing the tracking error between the measured currents and the reference currents. The cost function g_1 for the SPMSM control system can be given as:

$$g_1 = \left(i_{dref}(k+1) - i_d(k+1)\right)^2 + \left(i_{qref}(k+1) - i_q(k+1)\right)^2 + f_{lim}$$

with

$$f_{lim} = \begin{cases} \infty \; if \; |i_d(k+1)| \; or \; |i_q(k+1)| \geq i_{max} \\ 0 \; if \; |i_d(k+1)| \; or \; |i_q(k+1)| \leq i_{max} \end{cases} \tag{7.7}$$

From the Bq-ZSI side, the cost function g_2 can be expressed as:

$$g_2 = (i_{scref}(k+1) - i_{sc}(k+1))^2 + \lambda(v_{c1}(k+1) - v_{c2}(k+1))^2 \tag{7.8}$$

where λ is the weighting factor adjusted according to the desired performance. It is used for the DC-link capacitor voltages balancing control. f_{lim} is a hard constraint function which limits the current output magnitude and represents a safety future. The optimal switching state associated with the minimum values of g_1 and g_2 is selected and applied to the qZSI and the SPMSM at the beginning of the next sampling time.

The inductor currents of the DC-DC converter and DC-link voltage are controlled using the FOPI controller. The bidirectional power flow is operated by the switch S_7 of the Bq-ZSI. The pulse width modulation (PWM) technique is used to control the switch S_7. It has a signal that is complementary with the shoot-through signal of the inverter. Figure 7.3 shows the control scheme of the proposed HESS. As shown in the control scheme, the low-pass filter (LPF) allows for the filtering of the average current. The filtering strategy is used to distribute the power. This strategy is formulated based on the different frequency characteristics of energy storages [154]. The low pass filter (LPF) ensures that the battery supports a low frequency power to reduce the current stress and extend the battery lifetime [155]. The filtering strategy can be achieved by using the following expression:

$$I_{bat_{ref}} = \frac{1}{m_{S_8 S_9} \eta_{conv}^{k_{conv}}} \left(\frac{1}{\tau_{LPF} s + 1} \right) I_{load} \tag{7.9}$$

where I_{load} denotes the load current. A fraction of the load average current filtered amount represented by $\frac{1}{m_{S_8 S_9} \eta_{conv}^{k_{conv}}}$ is used as the battery reference current $I_{bat_{ref}}$, where $m_{S_8 S_9}$, $\eta_{conv}^{k_{conv}}$, and k_{conv} indicate the modulation index, the efficiency, and the coefficient which depend on the DC-DC converter power direction, respectively. τ_{LPF} represents the time constant of the LPF and is deduced by $\tau_{LPF} = \frac{1}{2\pi f_{LPF}}$, where f_{LPF} is the cut-off frequency. The average current is combined with the filter to reduce the very high frequency ripple and the noise that is caused by the switching operation. The buck and boost operation of the battery are controlled through this current that is used in the bidirectional DC-DC converter. The control of this current must achieve suitable charging and discharging currents of the battery with better stability in response to the transient power variation.

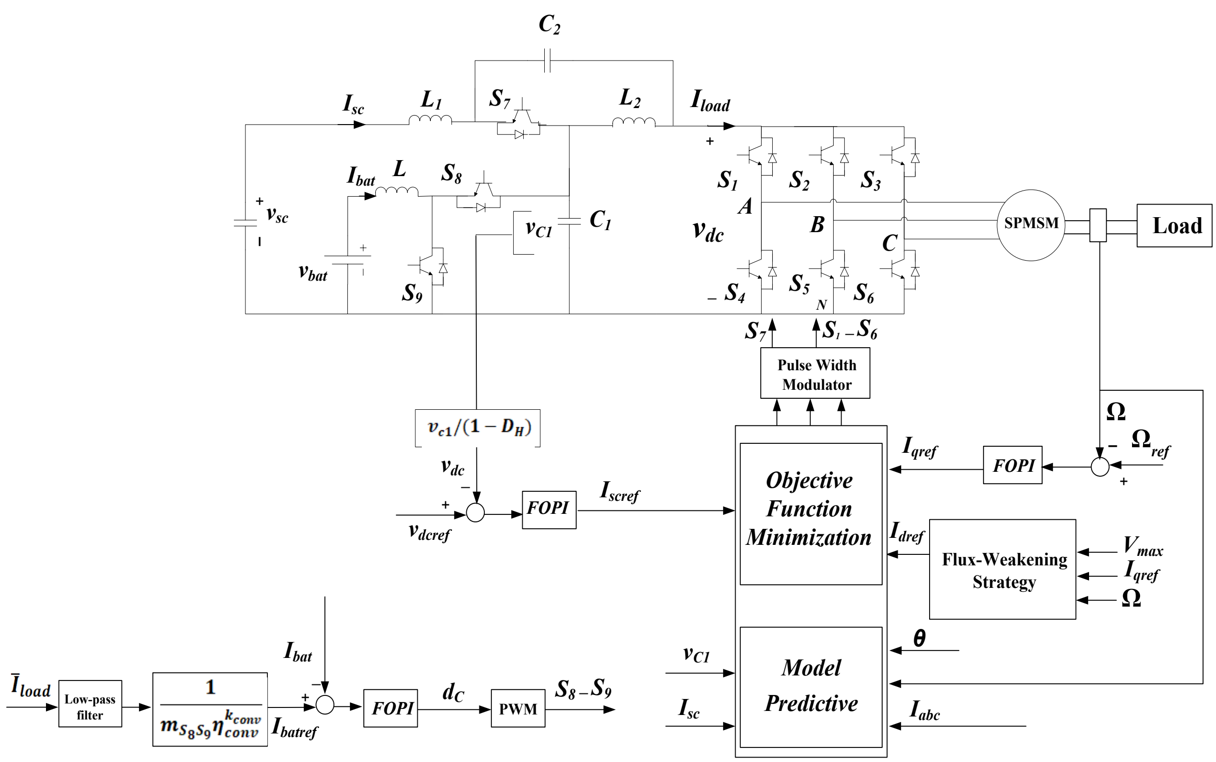

Figure 7.3: The control scheme for multi-source Bq-ZSI.

7.4 Real-time Simulation

7.4.1 Real-time Simulation Results

The OP4510-based real-time simulation from Opal-RT is performed to verify the real-time operation of the proposed control method for the SC/BAT HESS Bq-ZSI under the Artemis driving cycles with the main parameters in Table 7.2. In this respect, the reference EV used in this study is the e-TESC 4W platform, as presented in Figure 7.4. It is an off-road EV supplied by a battery pack of lithium-ion LG Chem ICR2 cells and a supercapacitor bank of Maxwell BMOD0058 E016 B02. Figure 7.5 shows the real-time simulation setup. The proposed HESS Bq-ZSI is first implemented on the OP4510 FPGA-based Electric Hardware Solver, and the control algorithm in Figure 7.3 is then executed on the OP4510 CPU, in which the controller parameters of the FOPI are presented in Table 7.3.

The real-time simulation results of the speed and torque waveforms are shown in Figure 7.6 and Figure 7.7, respectively. The currents i_q and i_d, with their references, are represented in Figure 7.8 and Figure 7.9, respectively, while the v_{dc} voltage and its reference are shown in Figure 7.10. Figures 7.11 and 7.12 represent the battery and supercapacitor currents and their references, respectively. The battery and supercapacitor voltages are represented in Figure 7.13 and Figure 7.14, respectively.

Figure 7.4: e-TESC 4W platform (adapted from BRP e-Commander vehicle).

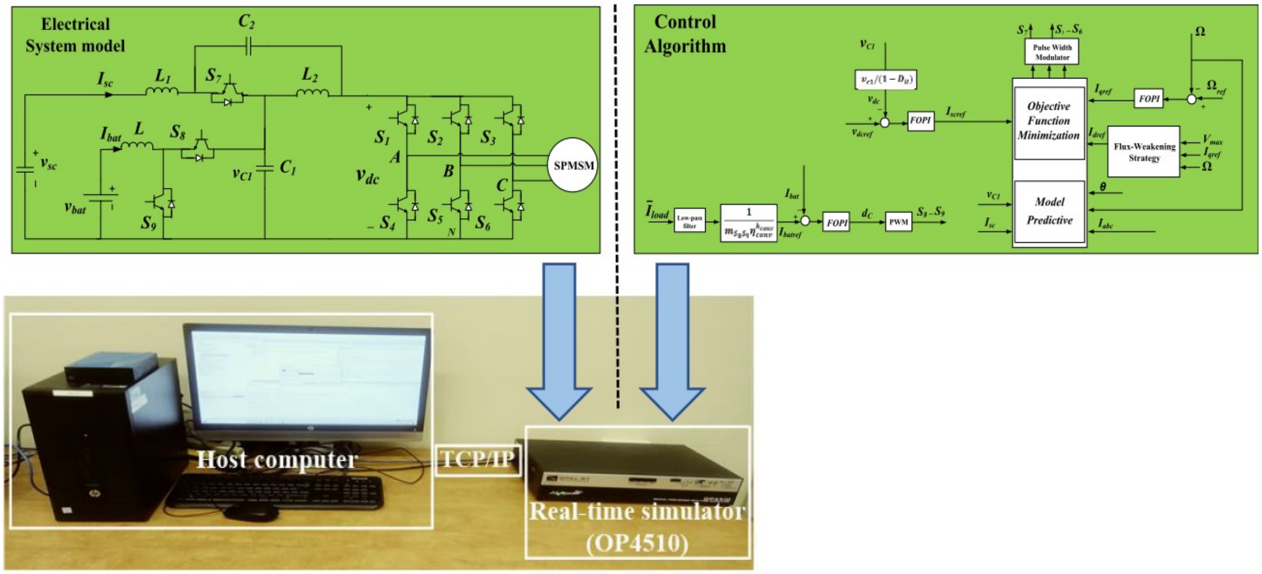

Figure 7.5: Real-time simulation setup.

Table 7.2: Parameters of EV platform

Parameters	Variable Name	Values
Vehicle (e-Commander)		
Total mass of the EV		857 kg
Aerodynamic standard	A	1.3
Rolling coefficient		0.035
Air density (at 20 °C)	ρ	1.223 kg/m^3
Motor-to-wheel-transmission ratio		20.5
Efficiency of the transmission		0.87
Wheel radius		0.3175 m
Parameters of SPMSM		
Phase inductance	L_d, L_q	1 mH
Phase resistance	r_s	0.08 Ω
Number of pole pairs	p	2
Global inertia referred to the rotor	J	1 kg.m^2
Equivalent magnetic flux linkage	ψ_f	0.1 Wb
Rated power	P_r	15 kW
Motor base speed	Ω_{base}	154 rad/s
Parameters of original configuration		
Inductance	L	2.5 µH
Capacitance	C	4.5 mF
Switching frequency	f_s	10 kHz
Parameters of multi-source Bq-ZSI parameters		
Inductance	L_1, L_2	660 µH
Inductance	L	2.72 mH
Capacitance	C_1	4.9 mF
Capacitance	C_2	8.9 mF
Cut-off frequency of LPF	f_{LPF}	40 mHz
Switching frequency	f_s	10 kHz
Batteries (Lithium-ion LG Chem ICR2 cell)		
Cell capacitance	$C_{batcell}$	2500 mAh
Cell maximum voltage	$v_{cellmax}$	4.2 V
Number of cells in series	N_s	12
Number of branches in parallel	N_p	48
Supercapacitor (Maxwell BMOD0058 E016 B02)		
Rated capacitance	C_{sc}	58 F
Nominal voltage	v_{scnom}	16 V
Number of series capacitors	N_s	4
Number of parallels capacitors	N_p	4
Internal resistance	r_{sc}	22 mΩ

Table 5.3: FOPI controller parameters summary

Parameters	Kpv	Kiv	λ_v	KpL	KiL	λ_L	KpC	KiC	λ_C
FOPI Structure	**Motor Speed**			**Battery Current**			**DC-Link Voltage**		
Value	0.2086	3.4246	0.1000	0.1075	15.9137	0.7500	0.0231	22.9688	0.7000

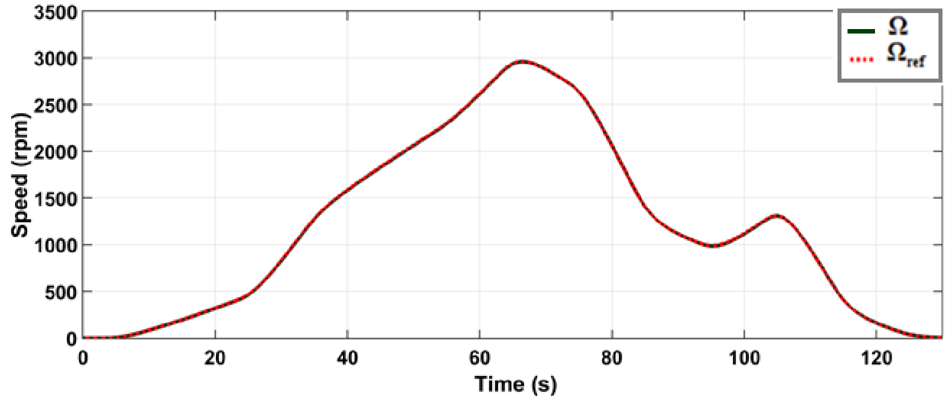

Figure 7.6: Motor speed and reference.

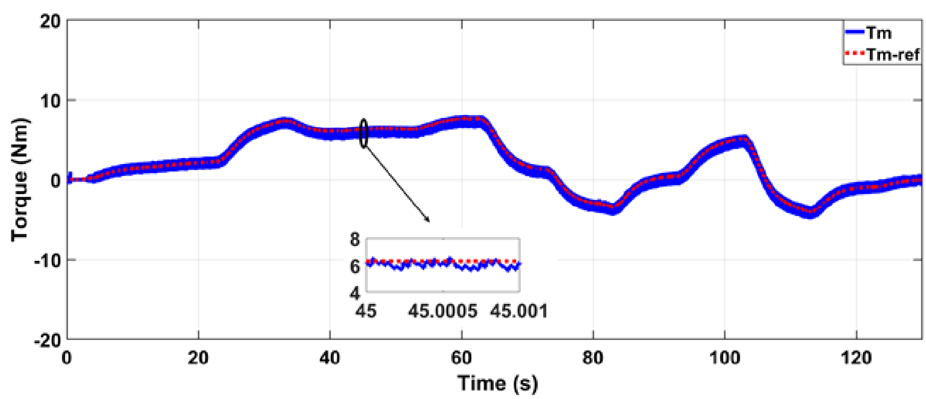

Figure 7.7: Motor torque and reference.

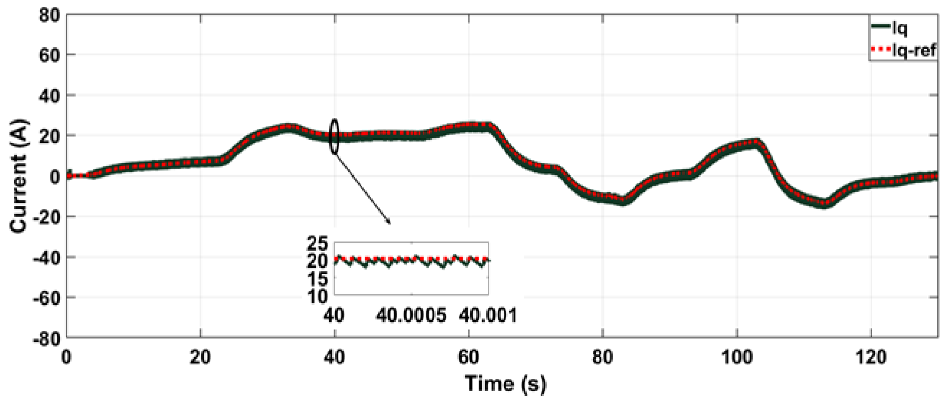

Figure 7. 8: i_q current and reference.

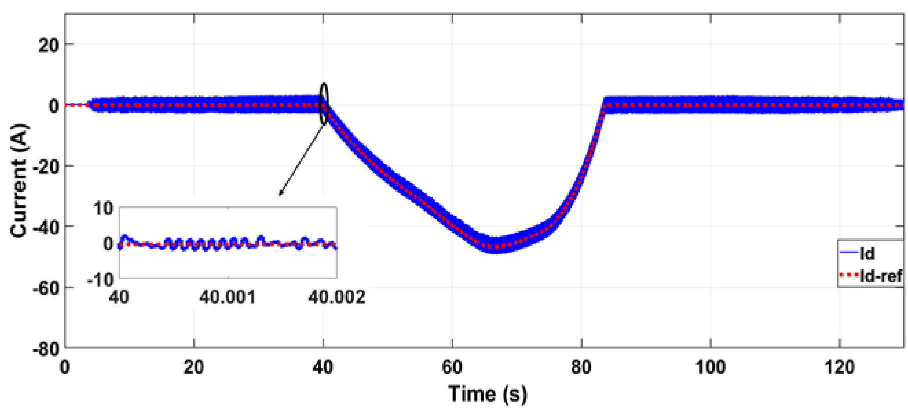

Figure 7.9: i_d current and reference.

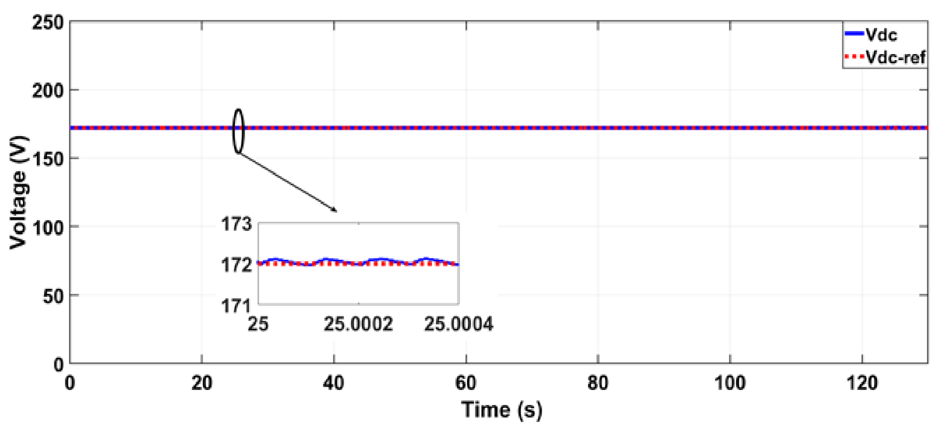

Figure 7.10: v_{dc} voltage and reference.

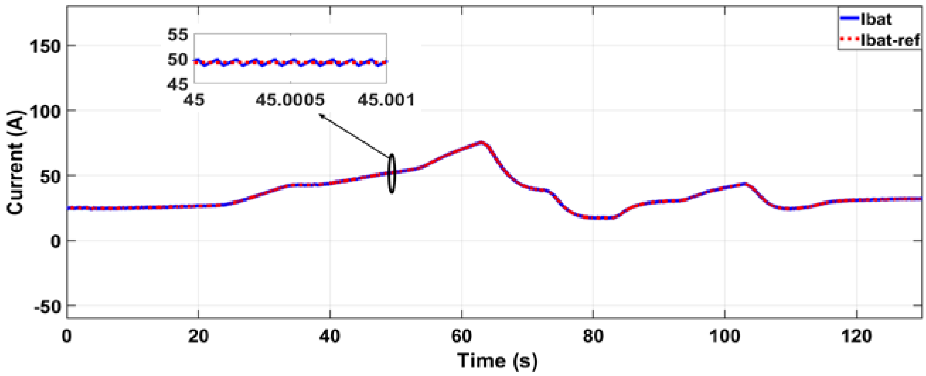

Figure 7.11: Battery current and reference.

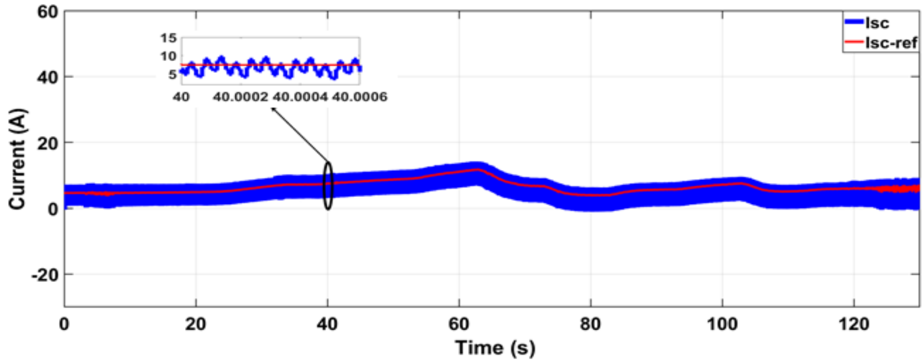

Figure 7.12: Supercapacitor current and reference.

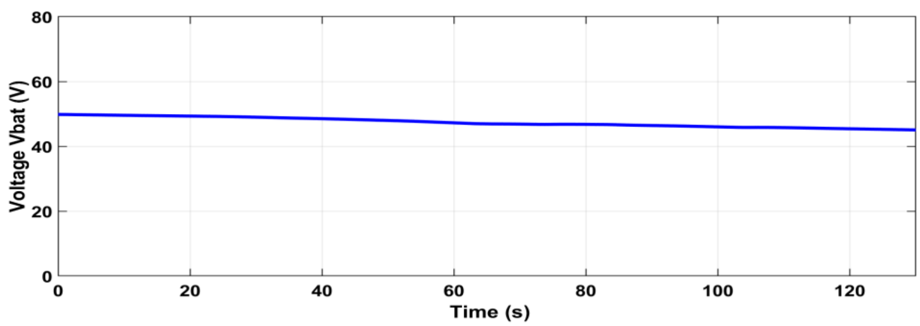

Figure 7.13: Battery voltage v_{bat}.

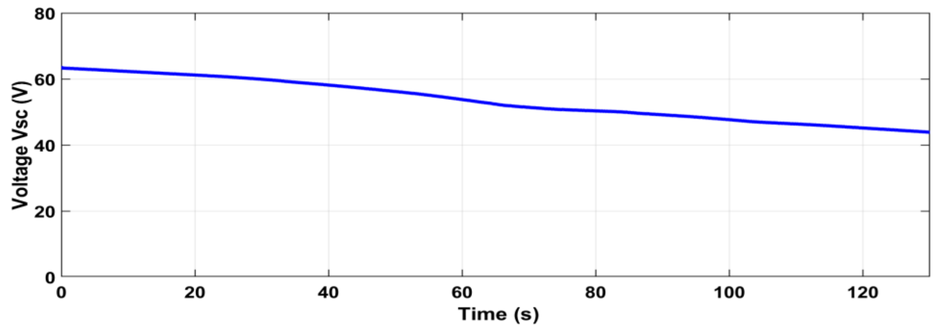

Figure 7.14: Supercapacitor voltage v_{sc}.

In Figures 7.6 and 7.10, the proposed HESS Bq-ZSI shows the quick responses to the mechanical load and provides a constant DC-link voltage over the power-demand profile. The battery, the supercapacitor, and the total power of the proposed HESS during EV motor traction in the high-power mode are presented in Figure 7.15.

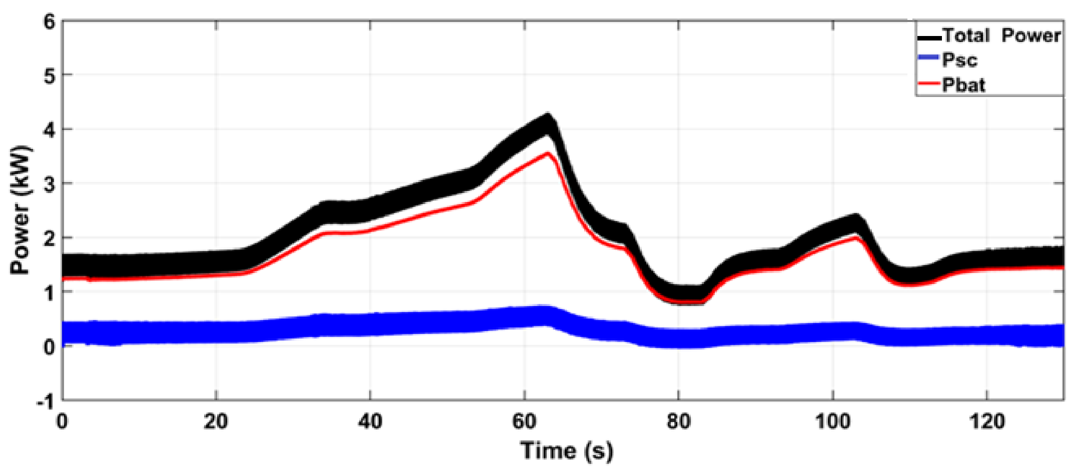

Figure 7.15: Power of the battery and the supercapacitor.

For time t < 75 s, the EV motor operates in the traction mode, while the proposed HESS conducts in the high-power mode. Both the battery pack and the supercapacitor are discharged. In this condition, the supercapacitor transfers its power to help the battery afford the motor power demand. During acceleration, the supercapacitor helps the battery offer the maximum traction power and enables the enhancement of the response time of the EV for a request of acceleration. From 75 s to 85 s, the EV motor works in the regenerative mode, and the supercapacitor implements in the recovery mode. The major part of the regenerative power is stored in the supercapacitor during the deceleration. The EV motor also operates in the traction mode, while the proposed HESS works in the high-power mode for time 85 s to 105 s. The supercapacitor affords its power to assist the battery for the required motor power. From 105 s to 130 s, the EV motor also performs in the regenerative mode, whereas the supercapacitor operates in the recovery mode. From the above-mentioned results obtained, it can be inferred that integrating the supercapacitor can help the battery to provide the maximum traction power demand of the EV. Therefore, it contributes to the efficient use of battery energy to obtain a longer distance coverage.

7.4.2 Battery Aging Index Comparison

The aging performance indexes of the battery are determined to compare the proposed HESS Bq-ZSI using the new control configuration and powertrain original configuration (inverter directly supplied by the battery). The battery lifetime is strongly influenced by their usage mode, in which the sudden changes in large and frequent currents may result in decreasing its lifetime. The value of the root-mean-square (RMS), the mean value (μ), the standard deviation (σ) of the cell current, and the coefficient (c_v) characterizing the instantaneous current peaks over the driving cycle illustrate the aging performance indexes of the battery [124].

The RMS value of the cell current indicates the effective current. It can be expressed as:

$$RMS = \sqrt{\frac{1}{N}\sum_{i=1}^{N}\left(I_{B,cell}(i)\right)^2} \tag{7.10}$$

The mean value of the cell current specifies the long-term stress from losses and the respective thermal effect on batteries. It can be written as:

$$\mu = \frac{1}{N}\sum_{i=1}^{N} I_{B,cell}(i) \tag{7.11}$$

The standard deviation defines the strong variation of the C-rate of the batteries and can be deduced by the following expression:

$$\sigma = \sqrt{\frac{1}{N}\sum_{i=1}^{N}\left(I_{B,cell}(i) - \mu\right)^2} \tag{7.12}$$

The variation coefficient illustrating the instantaneous current peak can be determined as follows:

$$c_v = \frac{\sigma}{\mu} \tag{7.13}$$

Figure 7.16 presents the performance comparison utilizing the aging index of the battery branches for these two topologies under the same driving cycle. As is observed, the multi-source Bq-ZSI using the proposed control configuration provides better aging indexes in terms of the RMS and the average values of the battery current. It helps to reduce the RMS, μ, and σ values by 57%, 59%, and 27%, respectively, as compared to the original ones. Moreover, using the FCS-MPC for the multi-source Bq-ZSI leads to improved aging indexes compared to only using the FOPI controllers. Based on these results, it could be concluded that using the FCS-MPC-based multi-source Bq-ZSI for the e-TESC 4W EV leads to an improvement in the battery lifetime over the original inverter and the FOPI-based multi-source Bq-ZSI, which makes it more suitable in EV systems than the original configuration.

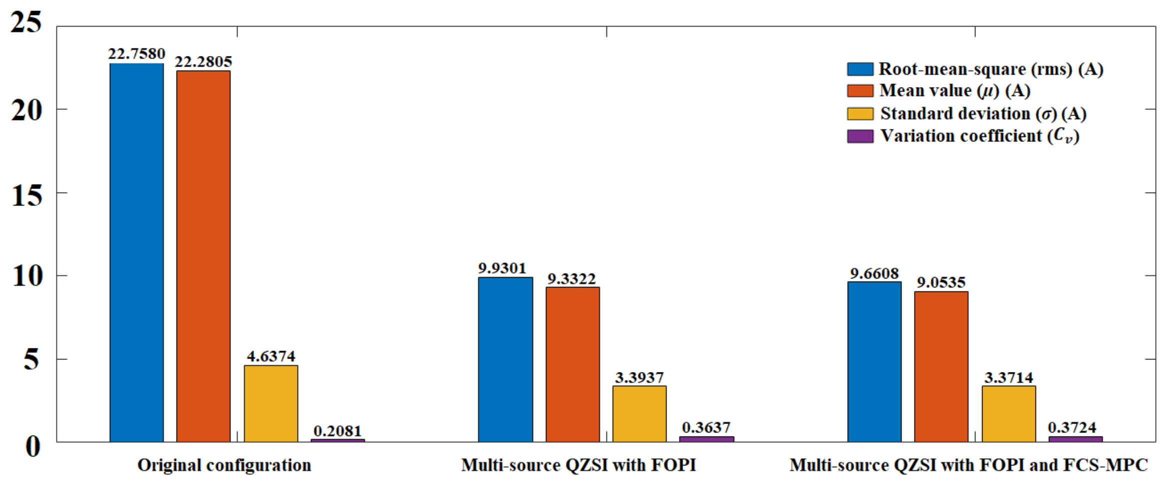

Figure 7.16: Performance comparison using ageing index factors.

7.5 Conclusions

This paper has proposed a new control configuration for multi-source Bq-ZSI based on the SC/BAT HESS for the EV. To overcome the problems of the battery rush discharging/charging currents, the bidirectional DC-DC converter is employed to connect the battery, while the ZSN of the Bq-ZSI is used to couple the supercapacitor. The proposed HESS Bq-ZSI control scheme using the FCS-MPC and the FOPI was first investigated to achieve the dynamic response that is required for energy storage devices. The real-time simulation based on Opal-RT was then implemented to validate the effectiveness of the proposed HESS control strategy. The results have proved that the proposed HESS can be well operated for different modes of the EV motor, in which independent power routines for the supercapacitor and the battery can be accomplished by the multi-source Bq-ZSI. The proposed HESS Bq-ZSI control using the FCS-MPC has shown good dynamic responses and stable DC-link voltages under the studied driving cycle. In comparison with the original configuration, the battery lifetime can be improved by using the proposed HESS Bq-ZSI with the new control structure.

Moreover, the multi-source Bq-ZSI using the FCS-MPC also provided improved aging performance index values for the battery of the studied EV compared to only using the FOPI controllers.

These results indicate that the proposed HESS Bq-ZSI using the FCS-MPC improves the EV system performance. The integration of the supercapacitor into the proposed HESS allows for the efficient use of battery energy, enabling longer distance coverage and thus extending the driving range of the EV. Future work will consist of proposing a power distribution strategy in multi-source off-road EVs with a signal-hardware-in-the-loop experimental test, including a stability analysis.

Author Contributions: Conceptualization, D.M. and J.P.T.; Data curation, D.M., T.V.D., and J.P.T; Funding acquisition, J.P.T.; Methodology, J.P.T. and M.C.T; Project administration, J.P.T; Validation, J.P.T and M.C.T; Writing—original draft, D.M.; Writing—review & editing, J.P.T. and M.C.T. All authors have read and agreed to the published version of the manuscript.

Funding: This work was supported in part by Grant 950-230672 from Canada Research Chairs Program, in part by Grant RGPIN-2017-05924 from the Natural Sciences and Engineering Research Council of Canada, and in part by FCT-Portuguese Foundation for Science and Technology project UIDB/00308/2020.

Conflicts of Interest: The authors declare no conflict of interest.

Chapter 8 Conclusions and Future Directions

8.1 Conclusions

In this thesis, multi-source power electronic converter was proposed for overall performance enhancement of multi-source EV traction system. To this end, efficient power electronic converter was selected. The QZSI topology represents an alternative inverter for EV. Its study, control and management approach were developed for performance improvement of EV traction system. The methodology consisted of making a concise review of the main existing topologies of impedance source inverters and comparative studies to determine the QZSI as a good candidate for multi-source EV system. After that, optimization of FOPI controller and the finite control set model predictive controller (FCS-MPC) for bidirectional QZSI have been applied for the multi-source EV with management approaches. These techniques of control for QZSI globally help to enhance the performance of the multi-source EV by optimizing the electric power consumption and extending its driving range.

Then, the comprehensive review on main topologies of impedance source inverter used in EV applications was studied in chapter 2. The appropriate values were used for QZSI topology parameters design. These values were the critical values of the inductances and the capacitances. This review enables to determine suitable impedance source inverter for EV. The topology of QZSI is the promising architecture which can be used in EV with better performance and reliability. In the chapter 3, the comparative study between the bidirectional QZSI and bidirectional conventional two-stage-inverter for electric traction system was contributed to prove and choose QZSI as an attractive alternative power converter for EV applications. Furthermore, the comparative study between different powertrain topologies regarding batteries aging index factors for an off-road EV application was permitted to select the QZSI as a good candidate to be used in a multi-source EV system (chapter 4). The topology of QZSI can contribute to increase the lifetime of the battery used for EV traction purpose.

Furthermore, the efficacy of the control technique structure with the QZSI can globally enhance the performance of the EV by optimizing the electric power consumption and extending its driving range. Subsequently, in the chapter 5, an ACO-NM algorithm is used for the optimization of the FOPI controller parameters for bidirectional QZSI and applied to an off-road EV. FOPI controller designed with the ACO-NM algorithm provides more suitable aging performance indexes values for the battery of the EV. The ACO-NM algorithm reduces the root-mean-square value and the standard deviation by 2 % and 5% of the battery current compared to the ZN tuning method and direct battery supply topology, respectively. This optimized method contributes to increase the lifetime of the battery used for off-road EV.

With the idea to develop multi-source EV with management approach, HESS composed of battery packs and supercapacitors for electric vehicle was proposed in chapter 7. The optimization of FOPI controller and the FCS-MPC for bidirectional QZSI was also applied for the EV with the management approaches. Management approaches consisted of developing strategies to control the energy flows through the HESS for efficient use of battery energy allowing a longer distance coverage. The optimal control technique of FCS-MPC enables to provide easy handling of constrains and fast dynamic performance of multi-source EV. The flux-weakening controller was also designed to provide correct operation with the maximum available torque at any speed within current and voltage limits. The proposed control scheme of the HESS contributes to reduce the root-mean-square value, the mean value, and the standard deviation value by 57%, 59%, 27%, respectively as compared to the battery-only based inverter. The addition of supercapacitor enhances the performance of the EV and enables an efficient energy use of the battery for a longer distance coverage, which permits to extend the EV driving range.

In this thesis, the comprehensive review on main topologies of impedance source inverter has served to select the QZSI topology as promising architectures for multi-source EVs application. Also, the comparative studies have permitted to examine and choose the QZSI as a good candidate to be used in multi-source EV system regarding batteries aging index factors for an off-road EV. Furthermore, optimized method using FOPI controller has contributed to obtain more suitable aging performance index values for the battery. Finally, the control configuration using FOPI controller and FCS-MPC for bidirectional QZSI has helped to enhance efficacy and dynamic performance for multi-source EV. The effectiveness of the proposed HESS control strategy has been validated using Opal-RT-based real-time simulation. An improved power distribution control system for energy management will enhance the proposed HESS performance.

8.2 Conclusions (FR)

Dans cette thèse, un convertisseur d'électronique de puissance multi-source a été proposé pour l'amélioration des performances globales du système de traction du véhicule électrique (VE) multi-source. À cette fin, un convertisseur d'électronique de puissance efficace a été sélectionné. La topologie de l'onduleur à quasi-Z-source (QZS) représente un onduleur alternatif pour le VE. Les études, le contrôle et une approche de gestion d'énergie ont été développés pour améliorer les performances du système de traction du VE. La méthodologie consistait à faire un examen concis des principales topologies existantes d'onduleurs à sources impédantes et des études comparatives pour déterminer l'onduleur QZS comme un bon candidat à utiliser dans un système de VE multi-source. Ensuite, l'optimisation du contrôleur PI d'ordre fractionnaire (PIOF) et du contrôleur par modèle prédictif d'ensemble de contrôle fini (CMP-ECF) pour l'onduleur QZS bidirectionnel a été appliqué au VE multi-source avec des approches de gestion. Les approches de gestion consistaient à développer des stratégies pour contrôler les flux d'énergie à travers le système de stockage d'énergie hybride (SSEH) permettant une utilisation efficace de l'énergie de la batterie pour une couverture de distance plus longue. Ces techniques de contrôle pour l'onduleur QZS contribuent globalement à améliorer les performances du VE multi-source en optimisant la consommation de l'énergie électrique et en étendant son autonomie.

Ainsi, une revue compréhensive des principales topologies des onduleurs à sources impédantes utilisées dans les applications du VE a été menée au chapitre 2. Des valeurs appropriées ont été utilisées pour la conception des paramètres de la topologie de l'onduleur à QZS. Ces valeurs étaient les valeurs critiques des inductances et des capacitances. Cette revue a permis de déterminer un onduleur à source impédante la plus convenable pour le VE. Ainsi, la topologie de l'onduleur QZS présente une architecture prometteuse qui peut être utilisée dans le VE avec de meilleures performances et de fiabilité. Dans le chapitre 3, l'étude comparative entre l'onduleur QZS bidirectionnel et l'onduleur bidirectionnel conventionnel à deux étages pour un système de traction électrique a été apportée pour prouver et choisir l'onduleur QZS comme convertisseur de puissance alternatif attrayant pour les applications dans les véhicules électriques. De plus, l'étude comparative entre différentes topologies de groupes motopropulseurs concernant les facteurs d'indice de vieillissement des batteries pour une application du VE tout-terrain a permis de sélectionner l'onduleur QZS comme bon candidat à utiliser dans un système de VE à source multiple (chapitre 4). La topologie de l'onduleur QZS peut contribuer à augmenter la durée de vie de la batterie utilisée à des fins de traction du VE.

Par ailleurs, l'efficacité de la structure de la technique de contrôle avec l'onduleur QZS peut globalement améliorer les performances du VE en optimisant la consommation de l'énergie électrique et en étendant son autonomie. Ainsi, dans le chapitre 5, un algorithme de colonies de fourmis (ACO-NM) est utilisé pour l'optimisation des paramètres du contrôleur PIOF pour l'onduleur QZS bidirectionnel et appliqué pour le VE tout-terrain. Le contrôleur PIOF conçu avec l'algorithme ACO-NM fournit des valeurs d'indices de performance de vieillissement plus appropriées pour la batterie du VE. L'algorithme ACO-NM réduit la valeur quadratique moyenne et l'écart type de 2% et 5% du courant de la batterie par rapport à la méthode de réglage de Ziegler-Nichols (ZN) et à la topologie connectée directement à la batterie, respectivement. Cette méthode optimisée contribue à augmenter la durée de vie de la batterie utilisée pour les VEs tout-terrain.

Avec l'idée de développer des VEs multi-sources avec une approche de gestion, un SSEH composé d'une batterie et d'un supercondensateur pour le VE a été proposé au chapitre 6. L'optimisation du contrôleur PIOF et du CMP-ECF pour l'onduleur QZS bidirectionnel a également été appliqué pour le VE avec des approches de gestion. La technique de contrôle optimale du CMP-ECF permet une gestion aisée des contraintes et des performances dynamiques rapides des VEs multi-sources. Le contrôleur d'affaiblissement du flux magnétique du moteur a également été conçu pour fournir un fonctionnement correct avec le couple maximum disponible à n'importe quelle vitesse dans les limites de courant et de tension. Le schéma de contrôle proposé du SSEH contribue à réduire la valeur moyenne quadratique, la valeur moyenne et la valeur d'écart type de 57%, 59%, 27%, respectivement, par rapport à l'onduleur connecté directement à la batterie. L'ajout d'un supercondensateur améliore les performances du VE et permet une utilisation efficace de l'énergie de la batterie pour une couverture de distance plus longue, ce qui permet d'étendre l'autonomie du VE.

Dans cette thèse, l'examen complet des principales topologies d'onduleur à sources impédantes a servi à sélectionner la topologie d'onduleur QZS comme architecture prometteuse pour l'application des VEs multi-sources. De plus, les études comparatives ont permis d'examiner et de choisir l'onduleur QZS comme un bon candidat à utiliser dans un système de VE multi-source hors route. Ces études ont été effectuées en prenant en considération les facteurs d'indice de vieillissement de la batterie. Par la suite, une méthode optimisée utilisant le contrôleur PIOF a contribué à obtenir des valeurs d'indice de performance de vieillissement plus appropriées pour la batterie. Enfin, la configuration de contrôle utilisant les contrôleurs PIOF et CMP-ECF pour l'onduleur QZS bidirectionnel a contribué à améliorer l'efficacité et les performances dynamiques du VE multi-source. L'efficacité de la stratégie de contrôle du SSEH proposée a été validée à l'aide d'une simulation en temps réel basée sur l'Opal-RT. Un système de contrôle amélioré pour la distribution de l'énergie pourra augmenter les performances du SSEH proposé.

8.3 Future Directions

This thesis has presented the importance of the use of the proposed topology of multi-source QZSI for EV performance enhancement. Some methods of study and control with management approach were developed for electric vehicle traction systems. Nevertheless, there are many areas in which this research work can be examined. Some of these include:

The management approaches have been provided in this thesis. A power distribution with optimized control system for management will have a great impact for multi-source off-road EV. This optimized control system enables to achieve the energy management in multi-source off-road EV. The areas in which this study can be further explored are: power distribution control strategy based on fuzzy logic control combining linear quadratic regulator control or adaptive optimal control. Frequency dividing coordinated control method can also be proposed for energy management to exploit supercapacitor and battery advantages.

Moreover, the impedance source inverter studied in this thesis has components which can be minimized to the proper value. The use of new power electronics devices such as the SiC and GaN can enhance the performance of impedance source inverter since they have high switching frequency, high temperature capacity and expected low cost. That can reduce the volume and the cost of the proposed topology for electric vehicle traction system.

In the present thesis, the proposed HESS using QZSI topology with optimized control techniques has been applied to an off-road EV. However, the multi-source QZSI topology can be of interest in the innovation of many HESS for applications with avionics, marine, renewable energy resources, and other propulsion systems applications.

Finally, this thesis has shown that QZSI is promising power electronic converter for on-board energy management in multi-source off-road EV with flux-weakening control technique of SPMSM. Then, hardware-in-the-loop validation and a full-scale experimental prototype of QZSI applied to multi-source EVs are appreciated for realizing more realistic validations of the proposed approach. This validation was envisaged in this work. But it could not be realized because of the shortage of semiconductors and capacity to implement PCB board during the pandemic situation. The implementation of the system control algorithm is more convenient on a PCB board using FPGA.

References

[1] P. Friedlingstein et al., “Global Carbon Budget 2021,” Earth Syst. Sci. Data, vol. 14, Issue 4, pp. 1917–2005, 26 Apr 2022.

[2] Energy Technology Perspectives - Energy Post [online]. Available: https://energypost.eu [Accessed 27-October-2020].

[3] The Global Electric Vehicle Market In 2020 – Virta. [Online]. Available: https://www.virta.global/global-electric-vehicle-market. [Accessed 07-October-2020].

[4] Lamoussa J. Kere, Sousso Kelouwani, Kodjo Agbossou, Yves Dubé, Nilson Henao, Raymond Courteau, “Tracking maximum efficiency of hydrogen genset used as electric vehicle range extender,” International Journal of Hydrogen Energy, vol 39, pp. 3433-3443, February 2014.

[5] Thanh Vo-Duy, Minh C. Ta, Bảo-Huy Nguyễn and João Pedro F. Trovão, “Experimental Platform for Evaluation of On-Board Real-Time Motion Controllers for Electric Vehicles”, Energies, vol. 13, EISSN: 1996-1073, 6 December 2020

[6] L. Situ, “Electric vehicle development: the past, present & future,” 3rd International Conference on Power Electronics Systems and Applications PESA, pp. 1-3, 2009.

[7] Electric Vehicle Technology Explained. pp. 183 – 195, John Wiley & Sons, Ltd., ISBN 0-470-85163-5, UK, 2003.

[8] Mande, D., Trovão, J. P., Rubio, R. G and Minh C. Ta, “Comparison of bidirectional quasi-Z-source inverter and bidirectional conventional two-stage inverter for electric traction system,” IEEE Vehicle Power and Propulsion Conf., Chicago, IL, USA, August 2018.

[9] Liu, Y.; Ge, B.; Ferreira, F.J.T.E.; de Almeida, A.T.; Rub, A.A, “Modeling and SVPWM control of quasi-Z-source inverter,” In Proceedings of the 11th IEEE International Conference on Electrical Power Quality and Utilisation, Lisbon, Portugal, pp. 1–7, 17–19 October 2011.

[10] Gajanayake, C.J.; Vilathgamuwa, D.M.; Loh, P.C, “Development of a Comprehensive Model and a Multiloop Controller for Z-Source Inverter DG Systems,” IEEE Trans. Ind. Electron, 54, pp. 2352–2359, 2007.

[11] Gupta, A.K.; Ahmad, A.; Samuel, P, “HDL Co-Simulation of Single-Phase Z-Source Inverter,” In Proceedings of the IEEE Student Conference on Engineering and System SCES, Allahabad, India, 12–14 April 2013.

[12] Peng, F.Z.; Shen, M.; Qian, Z, “Maximum boost control of the Z-source inverter,” IEEE Trans. Power Electron, 20, pp. 833–838, 2005.

[13] Shen, M.; Peng, F.Z, "Operation Modes and Characteristics of the Z-Source Inverter with Small Inductance or Low Power Factor," IEEE Trans. Ind. Electron, 55, pp. 89–96, 2008.

[14] Rostami, H.; Khaburi, D.A, "Voltage gain comparison of different control methods of the Z-source inverter," International Conference on Electrical and Electronics Engineering - ELECO, Bursa, Turkey, 05-08 November 2009.

[15] P. Codani, P. L. Le Portz, P. Claverie, Y. Perez and M. Petit, "Coupling local renewable energy production with electric vehicle charging: a survey of the French case," World Electric Vehicle Journal, vol. 7, ISSN 2032-6653, 28 December 2015

[16] I. Colak, E. Kabalci and R. Bayindir, "Review of multilevel voltage source inverter topologies and control schemes," Energy Conversion and Management, vol. 52, no. 2, pp. 1114–1128, 2011.

[17] F. Z. Peng, "Z-Source Inverter," IEEE Transaction on Industry Applications, vol. 39, no. 2, pp. 504-510, 2003.

[18] Y. P. Siwakoti, F. Z. Peng, and F. Blaabjerg, "Impedance-source networks for electric power conversion part I: a topological review," IEEE Transactions on Power Electronics, vol. 30, no. 2, pp. 699–716, 2015.

[19] F. Z. Peng, A. Joseph, J. Wang, M. Shen, L. Chen, Z. Pan, E. Ortiz-Rivera and Y. Huang "Z-Source Inverter for Motor Drives," IEEE Transactions on Power Electronics, vol. 20, no. 4, pp. 857 – 863, 2005.

[20] D. Cao, Q. Lei and F. Z. Peng, "Development of high efficiency current-fed quasi-Z-source inverter for HEV motor drive," IEEE Applied Power Electronics Conference and Exposition (APEC), pp. 157–164, 2013.

[21] V. Vijay, K. J. Shruthi, P. G. Kini, C. Viswanatha and M. S. Bhatt, "Modified Z-Source Inverter Based Three Phase Induction Motor Drive for Solar PV Applications," 2014 International Conference on Power Signals Control and Computations, Thrissur, 2014.

[22] P. Cortés, G. Ortiz, J. I. Yuz, J. Rodríguez, S. Vazquez and L. G. Franquelo, "Model Predictive Control of an Inverter with Output LC Filter for UPS Applications," IEEE Transaction on Industrial Electronics, vol. 56, no. 6, pp. 1875-1883, 2009.

[23] Y. Yu, Q. Zhang, B. Liang, X. Liu, and S. Cui, "Analysis of a Single-Phase Z-Source Inverter for Battery Discharging in Vehicle to Grid Applications," Energies 2011, no. 12, vol. 4, pp. 2224-2235, 2011.

[24] C. J. Gajanayake, D. M. Vilathgamuwa, P. C. Loh, R. Teodorescu and F. Blaabjerg, F. "Z-Source-Inverter-Based Flexible Distributed Generation System Solution for Grid Power Quality Improvement," IEEE Transactions on Energy Conversion, vol. 24, no. 3, pp. 695-704, 2009.

[25] A. Shahinpour, J. S. Moghani, G. B. Gharehpetian and B. Abdi, "High Gain High-Voltage Z-Source Converter for Offshore Wind Energy Systems," The 5th Annual International Power Electronics, Drive Systems and Technologies Conference, Tehran, pp. 5-6, February 2014.

[26] R. Bharanikumar, R. Senthilkumar and A. Nirmal Kumar, "Impedance source inverter for wind turbine driven permanent magnet generator," 2008 Joint International Conference on Power System Technology and IEEE Power India Conference, pp.1-7, 2008.

[27] F. Z. Peng, X. Yuan, X. Fang and Z. Qian, "Z-source inverter for adjustable speed drives," IEEE Power Electronics Letters, vol. 1, no. 2, pp. 33-35, 2003.

[28] S. M. Dehghan, M. Mohamadian and A. Yazdian, "Hybrid electric vehicle based on bidirectional Z-source nine-switch inverter," IEEE Transactions on Vehicular Technology, vol. 59, no. 6, pp. 2641-2653, 2010.

[29] M. Hanif, M. Basu and K. Gaughan, "Understanding the Operation of a Z-source inverter for photovoltaic application with a design example," IET Power Electronics, vol. 4, no. 3, pp. 278-287, 2011.

[30] Y. P. Siwakoti, P.C. Loh, F. Blaabjerg, and G. E. Town, "Y-Source Impedance Network," IEEE Transactions on Power Electronics, vol. 29, no. 7, pp. 3250-3254, 2014.

[31] P. C. Loh, D. Li, and F. Blaabjerg, "Γ-Z-Source Inverters," IEEE Transactions on Power Electronics, vol. 28, no.11, pp. 4880-4884, 2013.

[32] M. Adamowicz, "LCCT-Z-Source Inverters," 2011 10th International Conference on Environment and Electrical Engineering, pp. 1-6, 2011.

[33] M. Zhu, K. Yu, and F. L. Luo, "Switched Inductor Z-Source Inverter," IEEE Transactions on Power Electronics, vol. 25, no. 8, pp. 2150-2158, 2010.

[34] M. K. Nguyen, Y. C. Lim and G. B. Cho, "Switched-inductor quasi-Z-source inverter," IEEE Transactions on Power Electronics, vol. 26, no. 11, pp. 3183-3191, November 2011.

[35] C. S. Singh and R. K. Tripathi, "Maximum Constant Boost Control of Switch Inductor Quasi-Z-Source Inverter," IEEE Student conference on Engineering and System, SCES 2013, pp. 12-14, 2013.

[36] J. Anderson and F. Z. Peng, "Four Quasi-Z-Source Inverters", 2008 IEEE Power Electronics Specialists Conference, vol. 58, no. 1, pp. 2743-2749, 2008.

[37] F. Guo, L. Fu, C. H. Lin, C. Li, W. Choi and J. Wang, "Development of an 85-kW Bidirectional Quasi-Z-Source Inverter With DC-Link Feed-Forward Compensation for Electric Vehicle Applications," IEEE Transactions on Power Electronics, vol. 28, no. 12, pp. 5477-5488, 2003.

[38] P. C. Loh, F. Gao and F. Blaabjerg, "Embedded EZ-Source Inverters", IEEE Transactions on Industry Applications, vol. 46, no. 1, pp. 256-267, 2010.

[39] A. Ho, Ji-Suk Hyun, T. Chun and H. Lee, "Embedded quasi-Z-source inverters based on active switched-capacitor structure," IECON 2016 - 42nd Annual Conference of the IEEE Industrial Electronics Society, Florence, pp. 3384-3389, 2016.

[40] K. C. R. Nisha, "PV powered generalized multicell switched-inductor embedded quasi-Z-source inverter using MSP-430 controller," 2016 International Conference on Circuit, Power and Computing Technologies (ICCPCT), Nagercoil, pp. 1-6, 2016.

[41] W. Qian, F. Z. Peng and H. Cha, "Trans-Z-source inverters," IEEE Transactions on Power Electronics, vol. 26, no. 12, pp. 3453-3463, 2011.

[42] Mehran Moslehi Bajestan, Mahdi Shahparasti and Davood Arab Khaburi, "Application of trans Z-source inverter in photovoltaic systems," 21st Iranian Conference on Electrical Engineering (ICEE), May 2013.

[43] Y. P. Siwakoti, P. C. Loh, F. Blaabjerg and G. E. Town, "Effects of Leakage Inductances on Magnetically Coupled Y-Source Network," IEEE Transactions on Power Electronics, vol. 29, no. 11, pp. 5662-5666, Nov. 2014.

[44] M. Adamowicz, R. Strzelecki, F. Z. Peng, J. Guzinski, and H. A. Rub, "High step-up continuous input current LCCT-Z-source inverters for fuel cells," IEEE Energy Conversion Congress and Exposition, pp. 2276-2282, Sep 2011.

[45] M. Adamowicz, R. Strzelecki, F. Z. Peng, J. Guzinski and H. A. Rub, "New type LCCT-Z-source inverters," in Proc. European Conference on Power Electronics and Applications (EPE), pp. 1-10, Sept. 2011.

[46] O. Ellabban, J. V. Mierlo, P. Lataire and P. V. den Bossche, "Z-Source Inverter for Vehicular Applications," IEEE Vehicle Power and Propulsion Conference, pp. 1938-8756, 2011.

[47] A. Pattanaphol, S. Khomfoi and P.Paisuwanna, "Z-Source Grid-Connected Inverter for Solving the photovoltaic cell Shading problem," International Conference on Electrical

Engineering/Electronics, Computer, Telecommunications and Information Technology, May 2010.

[48] N. Michael Hernández, G. Jaqueline Cardoso, José L. Azcue-Puma, José A. Torrico A and Alfeu J. Sguarezi Filho, "Z-Source Inverter Applied to Wind Power System With Battery Energy Storage System," IEEE International Conference on Industry Applications, Nov 2016.

[49] K. Beer and B. Piepenbreie, "Properties and Advantages of the Quasi-Z-Source Inverter for DC-AC Conversion for Electric Vehicle Applications," IEEE conference on Emobility-Electrical Power Train, pp. 1-6, November 2010.

[50] Y. Zhang, Q. Liu, J. Li and M. Sumner, "A Common Ground Switched-Quasi-Z -Source Bidirectional DC–DC Converter with Wide-Voltage-Gain Range for EVs With Hybrid Energy Sources," IEEE Transactions on Industrial Electronics, vol. 65, no. 6, pp. 5188-5200, June 2018.

[51] J. H. Park, H. G. Kim, E. C. Nho and T-W. Chun, J. Choi, "Grid-connected PV System Using a Quasi-Z-source Inverter," IEEE Applied Power Electronics Conference and Exposition, pp. 925-929, Feb 2009.

[52] S. Khani, L. Mohammadian, S. H. Hosseini and S. Ghasemzadeh, "Design and Control of Fully Parallel Embedded Z-Source Inverters Based Flexible Photovoltaic Systems for Grid Power Quality Improvement under Distorted Condition," IEEE 21st Iranian Conference on Electrical Engineering (ICEE), pp. 1-7, May 2013.

[53] S. Jiang and F. Z. Peng, "Modular Single-Phase Trans-Z-Source Inverter for Multi-Input Renewable Energy System," IEEE Applied Power Electronics Conference and Exposition (APEC), pp. 2107-2114, Feb 2012.

[54] E. G. Shehata, "Predictive control of a new configuration of bidirectional quasi Y-source inverter fed IPMSM for electric vehicle applications," IEEE Nineteenth International Middle East Power Systems Conference (MEPCON), pp. 287-292, Dec 2017.

[55] M. Forouzesh, A. Baghramian and N. Salavati, "Improved Y-Source Inverter for Distributed Power Generation," IEEE 23rd Iranian Conference on Electrical Engineering (ICEE), pp. 1677-1681, May 2015.

[56] F. Khoshkhati, S. Toofan and B. Asaei, "Modeling and control of asymmetric γ-source inverters for photovoltaic applications," International Journal on Technical and Physical Problems of Engineering" (IJTPE), Iss. 19, vol. 6, no. 2, June 2014.

[57] B. A. Welchko, J. M. Nagashima, G. S. Smith, S. Chakrabarti, M. Perisic and G. John, "Double ended inverter system with an impedance source inverter subsystem," United States Patent US7956569, June/July 2011.

[58] V. Vasanthi and S. Ashok, "Performance evaluation of Z-source inverter fed locomotive drives with different control topologies," IEEE International Conference on Power Electronics, Drives and Energy Systems, pp.1-4, December 2012.

[59] J. Jung and A. Keyhani, "Control of a Fuel Cell Based Z-Source Converter," IEEE Transaction on Energy Conversion, vol. 22, no. 2, pp. 467-476, 2007.

[60] M. Shen, A. Joseph, J. Wang, F. Z. Peng and D. J. Adams, "Comparison of traditional inverters and Z-source inverter for fuel cell vehicles," IEEE Transaction on Power Electronics, vol. 22, no. 4, pp.1453-1463, July 2007.

[61] João P. Trovão, Victor D. N. Santos, Paulo G. Pereirinha, Humberto M. Jorge and Carlos Henggeler Antunes, "Comparative Study of Different Energy Management Strategies for Dual-Source Electric Vehicles," World Electric Vehicle Journal, vol. 6, ISSN 2032-6653, 27 September 2013.

[62] Emil B. Iversen, Juan M. Morales and Henrik Madsen, "Optimal charging of an electric vehicle using a Markov decision process," Applied Energy 123, pp. 1-12, 2014.

[63] Fengqi Zhang, Xiaosong Hu, Reza Langari and Dongpu Cao, "Energy management strategies of connected HEVs and PHEVs: Recent progress and outlook," Elsevier Progress in Energy and Combustion Science, vol. 73, pp. 235-256, July 2019.

[64] S. Hu, Z. Liang, and X. He, "Ultracapacitor-Battery Hybrid Energy Storage System Based on the Asymmetric Bidirectional Z-Source Topology for EV," IEEE Transaction on Power Electronics, vol. 31, no. 11, pp. 7489-7498, November 2016.

[65] Omar Ellabban, Joeri Van Mierlo and Philippe Lataire, "Control of A High-Performance Z-Source Inverter for Fuel Cell/ Supercapacitor Hybrid Electric Vehicles," World Electric Vehicle Journal, vol. 4, ISSN 2032-6653, 24 September 2010.

[66] Daouda Mande, João P. Trovão, Ruben Gonzalez Rubio and Minh C. Ta, "Comparison of Different Power Train Topologies for an Off-Road Electric Vehicle," IEEE Vehicle Power and Propulsion Conference, October 2019.

[67] Naga Kishore Godavarthi, P. Sri Rama Lakshmi and V. T. Sree Devi, "Comparative analysis of PWM methods of Quasi-Z source Inverter," IEEE conferences International Conference on

Renewable Energy and Sustainable Energy (ICRESE), pp. 86-90, 2013.

[68] Tie SF, Tan CW, “A review of energy sources and energy management system in electric vehicles,” Renewable and Sustainable Energy Reviews, vol. 20, pp. 82-102, April 2013.

[69] Wuhua L, Xiangning H, “Review of nonisolated high-step-up DC/DC converters in photovoltaic grid-connected applications,” IEEE Trans Ind Electron, vol. 58, pp. 1239-50, 2011.

[70] Chen W, Huang AQ, Li C, Wang G, Gu W, “Analysis and comparison of medium voltage high power DC/DC converters for offshore wind energy systems,” IEEE Trans Power Electron, vol. 28, pp. 2014-2023, 2013.

[71] Luth T, Merlin MMC, Green TC, Hassan F, Barker CD, “High-Frequency Operation of a DC/AC/DC System for HVDC Applications,” IEEE Trans Power Electron, vol. 29, pp. 4107-4015, 2014.

[72] Ratanapanachote S, Ju C Han, Enjeti PN, “A digitally controlled switch mode power supply based on matrix converter,” IEEE Trans Power Electron, vol. 21, pp. 124-30, 2006.

[73] Sulligoi G, Bosich D, Giadrossi G, Lin Z, Cupelli M, Monti A, “Multiconverter medium voltage DC power systems on ships: constant-power loads instability solution using linearization via state feedback control,” IEEE Transactions on Smart Grid, vol. 5, pp. 2543-52, 2014.

[74] de Sousa GJ, Heldwein ML, “Three-phase unidirectional modular multilevel converter,” Proceedings of the 15th European conference on power electronics and applications (EPE), pp. 1-10, 2013.

[75] Yu T, Dongjin F, Ting W, Zhiwei X, “Hybrid switched-inductor converters for high step-up conversion,” IEEE Trans Ind Electron, vol. 62, no. 3, pp. 1480-1490, 2015.

[76] M.H. Taghvaee, et al., “A current and future study on non-isolated DC-DC converters for photovoltaic applications,” Renewable and Sustainable Energy Reviews, vol. 17, pp. 216-227, Oct. 2012.

[77] S. Choi, et al., “Analysis, design and experimental results of a floating-output interleaved input boost-derived DC-DC high-gain transformer-less converter,” IET Power Electron., vol. 4, iss. 1, pp. 168-180, Jan. 2011.

[78] C. J. Gajanayake, D. M. Vilathgamuwa, and Poh Chiang Loh, “Development of a Comprehensive Model and a Multiloop Controller for Z-Source Inverter DG Systems,” IEEE

Transactions on Industrial Electronics, vol. 54, no. 4, pp. 2352-2359, 2007.

[79] Y. Huang, M. Shen and F. Z. Peng, “A Z-Source Inverter for Residential Photovoltaic Systems,” IEEE Transactions on Power Electronics, vol. 21, no. 6, pp. 1776-1782, 2006

[80] Peng, F. Z., M. S. Shen, & K. Holland, “Application of Z-source inverter for traction drive of fuel cell-battery hybrid electric vehicles,” IEEE Trans. Power Electron., vol. 22, no. 3, 1054-1061, 2007.

[81] Florescu A., Stocklosa O., Teodorescu M, “The advantages, limitations and disadvantages of Z-source inverter,” International Semiconductor Conference, IEEE, vol. 2, pp. 483-486, 2010.

[82] M. Shen, J. Wang, A. Joseph, F. Z. Peng, L. M. Tolbert, and D. J. Adams,“Constant boost control of the Z-source inverter to minimize current ripple and voltage stress,” IEEE Transaction on Industry Applications, vol. 42, no. 3, pp. 770-778, 2006.

[83] Y. Liu, G. Baoming, H. Abu-Rub, and F. Z. Peng, “Overview of Space Vector Modulations for Three-Phase Z-Source/Quasi-ZSource Inverters,” IEEE Transactions on Power Electronics, vol. 29, no. 4, pp. 2098-2108, 2014.

[84] Anderson J, Peng F, “Four quasi-Z-source inverters,” Proceedings of IEEE Power Electronics Specialist Conference; pp. 2743-2749, Jun 2008.

[85] Feng Guo, Lixing Fu, Chien-Hui Lin, Cong Li, Woongchul Choi, Jin Wang, “Development ofan 85-kW Bidirectional Quasi-Z-Source Inverter With DC-Link Feed-Forward Compensation for Electric Vehicle Applications[J],” IEEE Transactions on power electronics, vol. 28, no. 12, pp. 5477-5488, 2003.

[86] H. Abu-Rub, A. Iqbal, Sk. Moin Ahmed, F. Z. Peng, Y. Li, and G. Baoming, “Quasi-Z-source inverter-based photovoltaic generation system with maximum power tracking control using ANFIS,” IEEE Trans. Sustainable Energy, vol. 4, no. 1, pp. 11-20, Jan. 2013.

[87] B. Ismail, S. T, “Development of a Single Phase SPWM Microcontroller-Based Inverter,” First International Power and Energy Conference PEC, Putrajaya, Malaysia, pp. 437-440, Nov 2006.

[88] L. Tan, B. Wu, S. Rivera and V. Yaramasu, "Comprehensive DC Power Balance Management in High-Power Three-Level DC–DC Converter for Electric Vehicle Fast Charging," IEEE Transactions on Power Electronics, Vol. 31, Issue 1, pp. 89-100, Jan 2016.

[89] K. Holland, M. Shen and F. Z. Peng, "Z-source inverter control for traction drive of fuel cell - battery hybrid vehicles," Fourtieth IAS Annual Meeting. Conference Record of the 2005 Industry Applications Conference, 2005., Kowloon, Hong Kong, 2005, pp. 1651-1656, vol. 3.

[90] Mohamed Abdel Monem, Khiem Trad, Noshin Omar, Omar Hegazy, Bart Mantels, Grietus Mulder, Peter Van den Bossche and Joeri Van Mierlo, "Lithium-ion batteries: evaluation study of different charging methodologies based on aging process," Applied Energy, vol. 152, pp. 143-155, August 2015.

[91] E. Sarasketa-Zabala, I. Gandiaga, E. Martinez-Laserna, L. M. Rodriguez-Martinez, and I. Villarreal, "Cycle ageing analysis of a LiFePO 4 /graphite cell with dynamic model validations: Towards realistic lifetime predictions," Journal of Power Sources, vol. 275, pp. 573-587, Feb. 2015.

[92] Yang Gao, Jiuchun Jiang, Caiping Zhang, Weige Zhang, Zeyu Ma and Yan Jiang, "Lithium-ion battery aging mechanisms and life model under different charging stresses," Journal of Power Sources, vol. 356, pp. 103-114, July 2017.

[93] O. Gomozov, J. P. F. Trovão, X. Kestelyn and M. R. Dubois, "Adaptive Energy Management System Based on a Real-Time Model Predictive Control With Nonuniform Sampling Time for Multiple Energy Storage Electric Vehicle," in IEEE Transactions on Vehicular Technology, vol. 66, no. 7, pp. 5520-5530, July 2017.

[94] K. A. Chinmaya and G. K. Singh, “Integrated onboard single-stage battery charger for PEVs incorporating asymmetrical six-phase induction machine,” in IET Electrical Systems in Transportation, vol. 9, no. 1, pp. 8-15, March 2019

[95] A. K. Singh and M. K. Pathak, “Single-stage ZETA-SEPIC-based multifunctional integrated converter for plug-in electric vehicles,” in IET Electrical Systems in Transportation, vol. 8, no. 2, pp. 101-111, June 2018.

[96] Trovão, J. P.; Silva, M.; Antunes, C. H.; Dubois, M. R, “Stability Enhancement of the Motor Drive DC Input Voltage of an Electric Vehicle Using On-Board Hybrid Energy Storage Systems,” Elsevier Appl. Energy, 205, 244-259, Nov 2017.

[97] O. Ellabban and H. Abu-Rub, “Z-source inverter: topology improvements review,” IEEE Industrial Electronics Magazine, vol. 10, no. 1, pp. 6-24, 2016.

[98] Mande, D.; Trovão, J.P.; Ta, M.C. Comprehensive Review on Main Topologies of Impedance Source Inverter Used in Electric Vehicle Applications. World Electr. Veh. J. 2020, 11, 37.

[99] P. C. Loh, D. M. Vilathgamuwa, C. J. Gajanayake, Y. R. Lim, and C.W. Teo, “Transient modelling and analysis of pulse-width modulated Z-source inverter,” IEEE Transactions on Power Electronics, vol. 22, no. 2, pp. 498-507, Mar. 2007.

[100] M. Amirbande, M.S. Zarbil, A. Vadehi and M. Rivera, “Simple boost control of a new 83 Z-source inverter,” IEEE Annual Power Electronics, Drives Systems and Technologies Conference, pp. 169-173, 2018.

[101] K. Choobdari Omran and A. Mosallanejad, “SMES/battery hybrid energy storage system based on bidirectional Z-source inverter for electric vehicles,” in IET Electrical Systems in Transportation, vol. 8, no. 4, pp. 215-220, December 2018.

[102] C.A. Monje, Y. Chen, B.M. Vinagre, D. Xue and V. Feliu-Batlle, Fractional-order systems and controls: fundamentals and applications, Springer Science & Business Media, 2010.

[103] I. Podlubny, “Fractional-order systems and PI λDμ controllers,” IEEE Transactions on Automatic Control, vol. 44, no. 1, pp. 208-214, 1999.

[104] I. Podlubny, L. Dorčák, and I. Kostial, “On fractional derivatives, fractional-order dynamic systems and PI λDμ controllers,” IEEE Proceedings of the 36th IEEE Conference on Decision and Control, pp. 4985-4990, Dec 1997.

[105] F. A. de Castro, N. D. Bernardes, M. A. de S. L. Cuadros, G. M. de Almeida, “Comparison of fractional and integer PID controllers tuned by genetic algorithm,” IEEE International Conference on Industry Applications, March 2017.

[106] M. E. M. Essa, M. A. S. Aboelela, M. A. M. Hassan, “A comparative study between ordinary and fractional order pid controllers for modelling and control of an industrial system based on Genetic Algorithm,” IEEE International Conference on Modern Circuits and Systems Technologies, May 2017.

[107] Y. Q. Chen, I. Petras and D. Xue, “Fractional order control - A tutorial,” IEEE American Control Conference, pp. 1397-1411, June 2009.

[108] Aleksei Tepljakov, “Fractional-order modeling and control of dynamic systems”, Springer: Tallinn, Estonia, February 2017.

[109] Hafiz M. Usman; Habibur Rehman; Shayok Mukhopadhyay, “Performance enhancement of electric vehicle traction system using FO-PI controller,” IET Electrical Systems in Transportation, Volume 9, Issue 4, p. 206-214, December 2019.

[110] Z. Miao, T. Han, J. Dang and M. Ju, “FOPI/PI controller parameters optimization using PSO with different performance criteria,” 2017 IEEE 2nd Information Technology, Networking, Electronic and Automation Control Conference (ITNEC), Chengdu, 2017, pp. 250-255, doi: 10.1109/ITNEC.2017.8284946.

[111] C. C. Hang, K. J. Astrom, W. K. Ho, “Refinements of the Ziegler–Nichols tuning formula,” IEEE Proceedings D - Control Theory and Applications, vol. 138, no. 2, pp. 111-118, March 1991.

[112] Blondin, M.J and Trovão, J. P, “Soft-computing techniques for cruise controller tuning for an off-road electric vehicle,” IET Electrical Systems in Transportation, Volume 9, Issue 4, p. 196-205, June 2019

[113] T. H. Kim, I. Maruta, T. Sugie, “Particle swarm optimization based robust PID controller tuning scheme,” IEEE Conference on Decision and Control, pp. 200-205, Dec 2007.

[114] M. Korkmaz, Ö. Aydoğdu, H. Doğan, “Design and performance comparison of variable parameter nonlinear PID controller and genetic algorithm based PID controller,” IEEE International Symposium on Innovations in Intelligent Systems and Applications, July 2012.

[115] M. Siva Ramakrishna, L. Ravi Srinivas, “Differential Evolution Based Tuning of PID Controller for an Automatic Voltage Regulator System”, International Journal of Industrial Electronics and Electrical Engineering, vol. 4, ISSN: 2347-6982, issue 8, Aug 2016.

[116] O. Bendjeghaba, S. Ishak Boushaki, N. Zemmour, “Firefly algorithm for optimal tuning of PID controller parameters,” IEEE International Conference on Power Engineering, Energy and Electrical Drives, pp. 1293-1296, May 2013.

[117] Blondin, M. J., Sanchis, J., Sicard, P., & Herrero, J. M, “New optimal controller tuning method for an AVR system using a simplified Ant Colony Optimization with a new constrained Nelder–Mead algorithm,” Applied Soft Computing, vol. 62, pp. 216-229, January 2018.

[118] F. Z. Peng, “Z-Source Inverter,” IEEE Transaction on Industry Applications, vol. 39, no. 2, pp. 504-510, 2003.

[119] Ali Yüce, Nusret Tan and Derek P. Atherton, “Fraction al Order PI Controller Design for Time Delay Systems,” International Federation of Automatic Control, vol. 49, no. 10, pp. 94-99, 2016.

[120] Aleksei Tepljakov (2020). FOMCON Toolbox for MATLAB (https://www.github.com/AlekseiTepljakov/fomcon-matlab), GitHub. Retrieved June 14, 2020.

[121] G. Mallesham, “Ziegler-Nichols based controller parameters tuning for load frequency control in a microgrid,” IEEE International Conference on Energy on Automation and Signal, Dec. 2011.

[122] K. Vaneková, M. Bakošová, R. Matušů, R. Prokop and J. Závacká, "Robust PI controller design for a laboratory time delay process," IEEE 18th Mediterranean Conference on Control and Automation, pp. 1000-1005, June 2010.

[123] Lagarias JC, Reeds JA, Wright MH, Wright PE, "Convergence properties of the Nelder--Mead simplex method in low dimensions," SIAM Journal on optimization, vol. 9, no. 1, pp. 112-147, 1998.

[124] Goussian, A., LeBel, F.A., Trovão, J.P. and Boulon, L, "Passive hybrid energy storage system based on lithium-ion capacitor for an electric motorcycle. Journal of Energy Storage, 25, p.100884, 2019.

[125] E. Chemali, M. Preindl, P. Malysz, A. Emadi, "Electrochemical and electrostatic energy storage and management systems for electric drive vehicles: state-of-the-Art review and future trends," IEEE Journal of Emerging and Selected Topics in Power Electronics, vol. 4, no. 3, pp. 1117-1134, September 2016.

[126] T. Zimmermann, P. Keil, M. Hofmann, M.F. Horsche, S. Pichlmaier, A. Jossen, "Review of system topologies for hybrid electrical energy storage systems," Journal of Energy Storage, vol. 8, pp. 78-90, November 2016.

[127] R. Hemmati, H. Saboori, "Emergence of hybrid energy storage systems in renewable energy and transport applications – a review," Renewable and Sustainable Energy Reviews, vol. 65, pp. 11-23, November 2016.

[128] F. Liu, J. Liu, H. Zhang, and D. Xue, "Stability issues of Z+Z type cascade system in hybrid energy storage system (HESS)," IEEE Transaction on Power Electronics, vol. 29, no. 11, pp. 5846-5859, November 2014.

[129] Y. Y. Chia, L. H. Lee, N. Shafiabady, and D. Isa, "A load predictive energy management system for supercapacitor–battery hybrid energy storage system in solar application using the support vector machine," Applied Energy, vol. 137, pp. 588-602, January 2015.

[130] A. Kuperman, I. Aharon, S. Malki, and A. Kara, "Design of a semiactive battery-ultracapacitor hybrid energy source," IEEE Transactions on Power Electronics, vol. 28, no. 2, pp. 806-815, June 2013.

[131] E. Chemali, L. McCurlie, B. Howey, T. Stiene, M. M. Rahman, M. Preindl, R. Ahmed, and A. Emadi, "Minimizing battery wear in a hybrid energy storage system using a linear quadratic regulator," in 41st Annual Conference of the IEEE Industrial Electronics Society (IECON),

Yokohama, Japan, pp. 3265-3270, November. 2015.

[132] A. K. Podder, O. Chakraborty, S. Islam, N. M. Kumar, H. H. Alhel, "Control Strategies of Different Hybrid Energy Storage Systems for Electric Vehicles Applications," IEEE Access., vol. 9, pp. 51865-51895, March 2021.

[133] A. M. Gee, F. V. Robinson, and R. W. Dunn, "Analysis of battery lifetime extension in a small-scale wind-energy system using supercapacitors," IEEE Transactions on Energy Conversion, vol. 28, no. 1, pp. 24-33, March 2013.

[134] L. W. Chong, Y. W. Wong, R. K. Rajkumar, Rajpartiban Kumar Rajkumar, D. Isa, "Hybrid energy storage systems and control strategies for stand-alone renewable energy power systems," Renewable and Sustainable Energy Reviews, vol. 66, pp. 174-189, December 2016.

[135] P. Wang, J. Xiao, and L. Setyawan, "Hierarchical control of hybrid energy storage system in DC microgrids," IEEE Transactions on Industrial Electronics, vol. 62, no. 8, pp. 4915-4924, August 2015.

[136] M. Ortúzar, J. Moreno, and J. Dixon, "Ultracapacitor-based auxiliary energy system for an electric vehicle: Implementation and evaluation," IEEE Trans. Ind. Electron., vol. 54, no. 4, pp. 2147-2156, August 2007.

[137] B. Hredzak, V. G. Agelidis, and M. Jang, "A model predictive control system for a hybrid battery–ultracapacitor power source," IEEE Transaction on Power Electronics, vol. 29, no. 3, pp. 1469-1479, March 2014.

[138] C. A. Monje, B. M. Vinagre, V. Feliu, Y. Q. Chen, "Tuning and auto-tuning of fractional order controllers for industry applications," Control Engineering Practice, vol. 16, issue 7, pp. 798-812, July 2008.

[139] Daouda Mande, Maude Blondin, João P. Trovão, "Optimization of Fractional Order PI Controller for Bidirectional Quasi-Z-Source Inverter Used for Electric Traction System," IET Electrical Systems in Transportation, vol. 10, Issue 4, pp. 376-384, December 2020

[140] L. Sepulchre, M. Fadel, M. Pietrzak-David, and G. Porte, "Flux-weakening strategy for high speed PMSM for vehicle application," IEEE 2016 International Conference on Electrical Systems for Aircraft, Railway, Ship Propulsion and Road Vehicles & International Transportation Electrification Conference, pp. 1-7, 4 November 2016

[141] Immanuel N. Jiya, Nicoloy Gurusinghe and Rupert Gouws, "Combination of LiCs and EDLCs with Batteries: A New Paradigm of Hybrid Energy Storage for Application in EVs", World Electric Vehicle Journal, vol. 9, ISSN 2032-665, 19 November 2018

[142] Y. Preger, H. M. Barkholtz, A. Fresquez, D. L. Campbell, B. W. Juba, J. Romàn-Kustas, S. R. Ferreira, and B. Chalamala "Degradation of Commercial Lithium-Ion Cells as a Function of Chemistry and Cycling Conditions," Journal of The Electrochemical Society, vol. 167, no. 12, ISSN 1945-7111, September 2020.

[143] Ahmed Aljanad, Azah Mohamed, Tamer Khatib, Afida Ayob and Hussain Shareef, "A Novel Charging and Discharging Algorithm of Plug-in Hybrid Electric Vehicles Considering Vehicle-to-Grid and Photovoltaic Generation", World Electric Vehicle Journal, vol. 10, ISSN 2032-6653, 27 September 2019

[144] G. Wang, M. Ciobotaru, and V. G. Agelidis, "Power smoothing of large solar PV plant using hybrid energy storage," IEEE Transactions on Sustainable Energy, vol. 5, no. 3, pp. 834-842, July 2014.

[145] Jie Yu, Fachao Jiang, Weiwei Kong and Yugong Luo, "A Distributed and Hierarchical Optimal Control Method for Intelligent Connected Vehicles in Multi-Intersection Road Networks", World Electric Vehicle Journal, vol. 13, ISSN 2032-6653, 4 February 2022

[146] K. Nosrati, H. R. Mansouri and H. Saboori, "Fractional-order PID controller design of frequency deviation in a hybrid renewable energy generation and storage system," IET International Conference & Exhibition on Electricity Distribution, pp. 1148-1152, June 2017.

[147] V. Yaramasu, B. Wu, M. Rivera, and J. Rodriguez, "Enhanced model predictive voltage control of four-leg inverters with switching frequency reduction for standalone power systems," IEEE 15th International Power Electronics and Motion Control Conference, Novi Sad, Serbia, September 2012.

[148] D. K. Choi and K. B. Lee, "Dynamic performance improvement of ac/dc converter using model predictive direct power control with finite control set," IEEE Transactions on Power Electronics, vol. 62, no. 2, pp. 757-767, February 2015.

[149] Abhishek Murali, Razia Sultana Wahab, Chandra Sekhar Reddy Gade, Chitra Annamalai and Umashankar Subramaniam, "Assessing Finite Control Set Model Predictive Speed Controlled PMSM Performance for Deployment in Electric Vehicles", World Electric Vehicle Journal, vol. 12, ISSN 2032-6653, 11 March 2021

[150] R. Mendez, D. Sbarbaro, J. Espinoza and C. Rojas, "Finite Control Set Model Predictive Control Assisted by a Linear Controller for True Parameter Uncertainty Compensation," IEEE Energy conversion congress and exposition, Cincinnati, USA, pp. 4964–4970, October 2017.

[151] A. Bakeer, M. A. Ismeil and M. Orabi, “A powerful finite control set-model predictive control algorithm for quasi z-source inverter,” IEEE Transactions on Industrial Informatics, vol. 12, no. 4, pp. 1371-1379, August 2016.

[152] P. Cortes, G. Ortiz, J. I. Yuz, J. Rodriguez, S.Vazquez and L.G. Franquelo, “Model predictive control of an inverter with output LC filter for UPS applications,” IEEE Transactions on Power Electronics, vol. 56, no. 6, pp. 1875-1883, June 2009.

[153] Y. Liu, H. Abu-Rub, Y. Xue and F. Tao, “A Discrete-Time Average Model-Based Predictive Control for a Quasi-Z-Source Inverter,” IEEE Transactions on Industrial Electronics, vol. 65, no. 8, pp. 6044-6054, August 2018.

[154] P. Thounthong and S. Rael, “The benefits of hybridization,” IEEE Industrial Electronics Magazine, vol. 3, no. 3, pp. 25-37, September 2009.

[155] Z. Song, H. Hofmann, J. Li, J. Hou, X. Han, M. Ouyang, “Energy management strategies comparison for electric vehicles with hybrid energy storage system,” Applied Energy, vol. 134, pp. 321-331, December 2014.